Development of a Software for the Design of Adhesive Joints

Ricardo Filipe Tavares Lima

MSc Thesis

Supervisor: Lucas Filipe Martins da Silva

FEUP

Faculty of Engineering of the University of Porto

MSc degree in Mechanical Engineering

February 2009

Dedico esta dissertação aos meus queridos pais que sempre acreditaram em mim e que inúmeras horas da sua vida despenderam comigo, educando-me, protegendo-me e orientando-me. Obrigado por todo o esforço, empenho e dedicação com que suportaram o meu percurso académico, sabendo que vocês abdicaram de muitos sonhos para que eu pudesse-se viver o meu…

O Autor

"Deus quer, o Homem sonha, a obra nasce."

Fernando Pessoa (1888-1935)

Resumo

Desenvolvimento de um software para projectar juntas adesivas

O principal objectivo deste trabalho foi o desenvolvimento de um software para projectar juntas adesivas. Realizou-se uma pesquisa bibliográfica entre vários modelos analíticos para o cálculo das tensões instaladas numa junta adesiva. Analisando os diferentes modelos, observou-se que cada modelo estava adequado para uma dada geometria e um dado comportamento mecânico dos aderentes e do adesivo. Desses modelos, seleccionaram-se os mais relevantes para o software tendo em conta as geometrias mais usadas na indústria e as considerações por eles assumidos quanto ao comportamento dos aderentes e adesivo. Esses modelos matemáticos foram implementados num software, com um conjunto de interfaces acessíveis e simples para o utilizador. Embora já existam alguns softwares que permitam obter previsões das tensões instaladas ao longo do comprimento de sobreposição da junta, eles apresentam geralmente um único modelo analítico de cálculo, que normalmente resulta de adaptações de modelos já existentes, limitando o utilizador à utilização do mesmo método para todos os casos de análise. No software apresentado, utilizando uma compilação de modelos analíticos disponíveis para diferentes tipos de análise, dá-se ao utilizador uma maior flexibilidade, permitindo que o utilizador escolha o método que mais se adapta a um caso específico. A análise de materiais compósitos também foi incluída, permitindo a análise de juntas adesivas com substratos compósitos laminados, alargando assim o campo de aplicação do software.

Para complementar o trabalho, alguns ensaios experimentais foram conduzidos para verificação e comparação dos resultados obtidos através do software.

Com este trabalho pode-se concluir que a previsão dos esforços numa junta evita muitos testes experimentais, servindo desta forma para uma primeira análise das tensões presentes no tipo de junta a projectar. Não possuindo num único método de cálculo, o utilizador pode escolher o que se mais adapta ao seu caso permitindo assim obter valores mais próximos dos reais.

Palavras-Chave: *Juntas adesivas; Projecto de juntas adesivas; Software; Distribuição de Tensões; Modelos analíticos; Epóxidos.*

Abstract

The main objective of this work was the development of a software for the design of adhesive joints. After conducting a literature research, several analytical models to predict the stresses in different joints geometries under different efforts were identified. Looking at the different models it was observed that each model is suitable for a given geometry and mechanical behaviour of adherends and adhesive. The most relevant models were selected for the software, taking into account the geometries used in the industry and the adherends/adhesive behaviour considerations. These mathematical models were implemented in a software application, with a set of interfaces accessible and simple for the user. Although there is already some software that can produce stress predictions along the overlap length , they generally include a single analytical model, which usually results from adaptations of some existing models, limiting the user to the same approach to all analysis cases. In the present software, the use of a collection of analytical models available for different types of joints and analysis, gives the user greater flexibility, allowing the choice of the method that best suits a given case. The analysis of composite materials was also included, allowing the analysis of adhesive joints with laminated composite adherends, extending the scope of the software.

To complement the work, some experimental tests were conducted to verify and compare results obtained with the software.

With this work, we can conclude that the prediction of joint stresses can avoid many experimental tests, serving as a first analysis for the stresses supported by the joints. Without being forced to use a single method, the user can chose the model best suited for the intended analysis.

Keywords: *Adhesive joints; Adhesive joints design; Software; Stresses distribution; Closed-form models; Epoxy.*

Acknowledgments

I would like to thank:

Prof. Lucas Filipe Martins da Silva for his supervision throughout this dissertation and for his patience and friendship.

Eng. Mariana Banea, Eng. Eduardo Marques and Eng. Filipe Chaves who provided advice and assistance in my first experimental activities.

Eng. Miguel Figueiredo, Eng. Rui Silva and Mr. José Francisco Moreira who provided assistance in my experimental activities.

Prof. José Dias Rodrigues and Dr. César Vasques who provided assistance in the MATLAB programming process.

D. Emilia Soares who was always available to help me in my experimental activities.

Eng. Daniel Peixoto and Mr. Luís Teixeira for the photos taken during the preparation of the experimental procedures.

Dr. Peter Davies and Dr. Jean-Yves Cognard for all the support given in the experimental tests in IFREMER.

LITEBUS (Modular Lightweight Sandwich Bus Concept), a INEGI (Institute of Mechanical Engineering and Industrial Management) project which partially funded the research presented.

Research in pre-graduation, project IPG96/2007 of the University of Porto which partially funded the research presented.

IFREMER (French Research Institute for Exploitation of the Sea) - Brest centre, for the financial and technical support in the experimental tests.

And all those who always supported me long this work mostly to my girlfriend Ana.

Acronyms

AY	Adherend Yielding
BVP	Boundary Values Problem
CEMUP	Materials Centre of the University of Porto
DLJ	Double Lap Joint
ESEM	Environment Scanning Electron Microscope
FEA	Finite Elements Analysis
GUI	Guide User Interface
GY	Adhesive Global Yielding
IFREMER	French Research Institute for Exploitation of the Sea
SLJ	Single Lap Joint
PABST	Primary Adhesively Bonded Structure Technology
PC	Personal Computer
XPS	X-ray Photoelectron Spectroscopy

Nomenclature

b	Joint Width
c	Half of the Overlap
D	Adherend Bending Stiffness
E	Adherend Young's Modulus
E_a	Adhesive Young's Modulus
E_s	Adhesive Secant Modulus
G	Adhesive Shear Modulus
k	Bending Moment Factor
k'	Transverse Force Factor
l	Overlap Length
M	Bending Moment
P	Applied Tensile Load
$\bar{P}$	Applied Tensile Load per Unit Width

x	Longitudinal Co-ordinate
t	Adherend Thickness
t_a	Adhesive Thickness
u	Horizontal Displacement
w	Vertical Displacement
y	Transverse Co-ordinate (Thickness Direction)
γ	Adhesive Shear Strain
γ_p	Adhesive Plastic Shear Stress
γ_{xy}	Adhesive Shear Stress in x-y Plane
ε_e	Adhesive Equivalent Strain (von Mises)
ε_x	Adhesive Strain in x Co-ordinate
ε_y	Adhesive Strain in y Co-ordinate
ε_r	Adhesive Tensile Failure Strain
λ	Adhesive Ratio of the Yield Stress in Compression to the Yield Stress in Tension
ν	Adherend Poisson's Ratio
ν_p	Adhesive Plastic Poisson's Ratio
ν_a	Adhesive Poisson's Ratio
σ	Adhesive Peel Stress
σ_y	Adhesive Tensile Yield Stress
σ_r	Adhesive Tensile Failure Stress
τ	Adhesive Shear Stress
τ_y	Adhesive Shear Yield Stress
τ_r	Adhesive Shear Failure Stress

Index

Figure Index

Table Index

Chapter 1

Introduction

The first adhesives were natural gums and other plant resins or saps. Neanderthals were the first to use them 50,000 years ago.

Since the adhesives began to be used industrially, adhesive and subsequently adhesive joints were increasingly used. Adhesive applications are increasing due to improvements in adhesive properties over the years such as flexibility, toughness, curing rate, and chemical resistance.

Therefore, it is important to have tools that help the designer engineer to design different types of adhesive joints. One precious tool is the prediction of stress distributions along the joint, which can give a large number of information about the adhesive joint, for example if a certain type of joint can support the applied effort or with a certain effort applied in the joint know if the adhesive is in the elastic or plastic field.

Along the years, many closed-form models were created for the determination of the stress distribution of adhesive joints, but they are dispersed in the literature and if the user wants to use the model, he will probably have to implement the model in a software, a process that can be very hard and slow. Several weeks of work are required for the most complicated models until they are ready to use.

A previous literature review was done about the closed-form models available, followed by a selection of those that best suit some pre-conditions established, such as the level of complexity of software implementation, the type of joint covered or the adhesive plasticity field consideration. Various software builders were analyzed to choose the one that has the best properties for building the software. Several aspects were considered, giving a greater importance to the interface creation aspect and calculus robustness, numeric and symbolic.

Various models were implemented in the chosen software builder, creating an independent software that allows the user to choose different types of joints and different closed-form models. The user can select the model that best suits the analysis conditions.

A comparison was done between the different models implemented in the software, analyzing the results. Another comparison was done between experimental results and software results, doing in this case an evaluation of the models that best predict the joint strength from linear to non-linear cases.

Next is showed a Gantt diagram (see Figure 1) of the work presented:

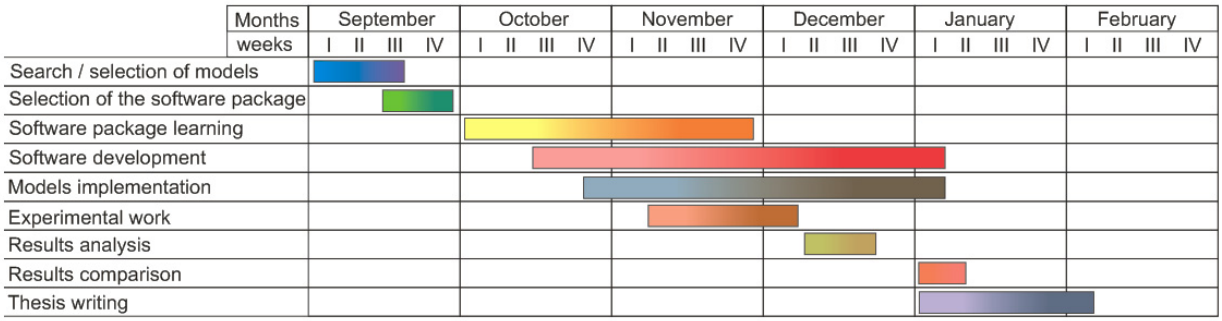

Figure 1 - Gantt diagram of the thesis.

1.1 State of the Art

Techniques for stress analysis of an adhesive joint generally fall into two main categories: closed-form methods and finite element methods. Closed-form methods are generally quicker and easier-to-use, but are only suitable for some geometries. These methods, due to their simple nature, cannot fully account the complete stress and strain conditions within the adhesive joint. Finite element methods cover almost any geometrical shape in their analysis and are capable of more accurate analysis of stress and strain distributions. The disadvantages of these methods are that the analyses are expensive and specialist knowledge is required. An ideal method would be an accessible yet accurate stress analysis technique.

In this section FEA will be reviewed as well as analytical based software developed for the analysis and design of adhesive joints.

Finite elements analysis [1]

Numerical analysis techniques, such as FEA, are used extensively in the design and stress analysis of adhesive joints. These techniques offer solutions to complex problems that are too difficult or impossible to resolve using closed-form solutions. Numerous FEA codes are available (see Annex A). These codes provide in-built constitutive models for simulating the behaviour of most adhesives, allowing non-uniform stress-strain distributions, geometric non-linearity, hygrothermal effects, elastic-plastic and visco-elastic behaviour, static and dynamic analysis, and strain rate dependence. Orthotropic element types include two-dimensional (2-D) solid plane-stress or plain-strain elements, axisymmetric shell or solid elements, three-dimensional (3-D) solid or "brick" elements and crack-tip elements. A number of automatic mesh generators are available with post-processing capabilities.

Although numerical methods are able to accommodate complex geometries, loadings, material properties and boundary conditions, the solutions generated are only approximations of the actual solution. It is important that the designer/analyst is aware of the limitations of the numerical techniques being applied and has a fundamental understanding of the mechanics of adhesive joints (i.e. stresses and failure mechanisms).

Closed-form analysis [1]

In the literature, there are many examples of closed-form solutions for obtaining stress and strain distributions. Many closed-form models are based on modified shear-lag equations **[2].** Aside from the shear-lag analysis technique, other workers have carried out stress analyses using a variety of other methods, such as those based on Hashin's variational analysis using the principle of minimum complementary energy **[3]**. Reviews of these closed-form theories and their assumptions can be found in **[4-7].**

As the analytical equations have become more complex (including factors such as stress variation through the adhesive thickness, plasticity, thermal effects, etc.), there is a greater requirement to use computing power to solve for the stresses. Hart-Smith **[8-13]** had a great influence on the methods used for stress analysis of adhesive joints and much of his work is evident in the Primary Adhesively Bonded Structure Technology (PABST) programme. Versions of this method have been prepared as FORTRAN programmes and have been used extensively in the aerospace industry. Other analyses have been implemented in spreadsheets or as a programme for personal computers.

Although simplified analytical procedures for designing adhesively bonded joints are available in the form of PC compatible software **[14]**, these packages are limited in number and scope. As with all design tools, the effectiveness of the analysis is directly related to the users knowledge, and therefore it is advisable that the user has a good understanding of engineering design and material behaviour. The software packages are there to assist in the design of efficient joints. A brief overview of commercial PC based analysis/design software packages is given in the Table 1. The main features of each software package are identified.

As it is shown in Table 1, the existing software packages are very specific and most of them only cover one or two joints geometries. Not all software packages can work with isotropic and anisotropic adherends, or include adhesive plasticity. Therefore the creation of the new software that gives the possibility of working with a set of different joint geometries, with composite adherends, adhesive and adherend plasticity and thermal effect would be very useful for the design engineer.

To satisfy that need, a software was created taking into account the aspects mentioned above, to better assist the design engineers in designing adhesive joints.

Table 1 - PC based software packages available in the market [1].

Name	Supplier	Application	Features
BOLT	G.S. SpringerStanford University	Design of pin-loaded holes in composites	• Prediction of failure strength and failure mode • Three types of bolted joints: Joints with a single hole, Joints with two identical holes in a row • Joints with two identical holes in tandem • Applicable to uniform tensile loads and symmetric laminates
BISEPSLOCO	AEA Technology,UK.	Closed form computer code for predicting stresses and strains in adhesively bonded single-lap joints	• Tensile/shear/bending moment loading • Adhesive peel and shear stress predictions • Allowance for plasticity in adhesive layer • Thermal stress analysis
BISEPSTUG	AEA Technology, UK	Closed form computer code for predicting stresses and strains in adhesively bonded coaxial joints	• Stepped and profiled joints • Orthotropic adherends • Torsional and axial loading • Allowance for plasticity in adhesive layer • Thermal stress analysis
CoDA	National Physical Laboratory, UK..	Preliminary design of composite beams and panels, and bolted joints	• Synthesis of composite material properties (lamina and laminates for a range of fibre formats • Parametric analyses • Panel and beam design • Bonded and bolted double shear joints • Bearing, shear-out, pin shear and by-pass tensile failure prediction
DLR	DLRMitteilung, Germany	Preliminary design of composite joints	• Adhesively bonded and bolted joints • Linear-elastic and linear-elastic/plastic behaviour • Tension and shear loading • Symmetric and asymmetric lap joints • Bearing, shear-out, pin shear and by-pass tensile failure prediction. (washers and bolt tightening)
FELOCO	AEA Technology, UK	Finite element module computer code for predicting stresses and strains in adhesively bonded lap shear joints	• Stepped and profiled joints • ensile/shear/bending moment/pressure loading • Linear and non-linear analysis • Peel, shear and longitudinal stress predictions in adhesive layer and adherends • Thermal stress analysis for adherend and adhesive
PAL	Permabond, UK	"Expert" system for adhesive selection	• Joined systems include: • Lap and butt joints, Sandwich structures, Bushes/gears/bearings/shafts/pipes/threaded fittings • Elastic analysis • Creep/fatigue effects on joint stiffness (graphical)
RETCALC	Loctite, UK	Interactive windows based software general purpose	• Joint strength • Correction factors (temperature and fatigue)

1.2 Programming software package choice

Several programming software packages were evaluated before starting to build the software. MAPLE, MAXIMA and MATLAB software packages were evaluated.

MAPLE is a Maplesoft software. Its current version is MAPLE 12 **[15]** released in 2008. Maplesoft is a Waterloo Maple Inc. division. MAPLE core intellectual property was developed as an advanced research project at the University of Waterloo, Canada, in the early 1980s. It is currently a privately held company, with headquarters in Waterloo, Ontario, Canada.

MAXIMA **[16]** is a software implemented in Lisp. Its current version is Maxima 5.16.3. MAXIMA is derived from the Macsyma system, developed at MIT in the years 1968 through 1982 as part of Project MAC. Nowadays MAXIMA (see Figure 2) is a SourgeForge Project, and being an open source software anyone can participate in its development team.

MATLAB **[17]** is a MathWorks software. Its current version is MATLAB 2008b released in 2008. MathWorks is a developer and supplier of software for technical computing and Model-Based Design, founded in 1984 has its headquartered in Natick, Massachusetts, USA.

The easiest software to learn is MAPLE because it has a good work interface and it was designed mostly for calculus and not for programming. The MAXIMA, although slightly different in the base kernel, does not differ much in use from MAPLE. MATLAB is a different case because it was built for programming, requiring programming knowledge and a more careful code implementation.

The general calculus capacity is different for all three software packages but for the intended use all three apparently have sufficient calculus capacity.

In terms of symbolic calculus, the most powerful is MAPLE. MATLAB uses the kernel of MAPLE but in an older version that the current MAPLE version. Being an open source software, MAXIMA presents some limitations in symbolic calculus, but in a general analysis the capacity of symbolic calculus was not a top priority in the evaluation.

Regarding the possibility of interface creation, MATLAB (see Figure 4) is the best of the three, because of its graphic user interface versatility, allowing the creation of user-friendly interfaces. The last versions of MAPLE (see Figure 3) also have the possibility to create user interfaces, but they are very limited, causing many difficulties in the creation of the interfaces and later in their use. MAXIMA does not have that possibility, working only in commands console or in a “pretty paper version” similar to MAPLE interface paper.

The last but not least important aspect was the licences that we had available. MAXIMA is a free software not requiring a licence payment but MAPLE and MATLAB require a licence payment. The faculty currently only has a MATLAB licence, having dropped the MAPLE licence in the last year.

Next is shown a representative figure of the three software packages analyzed.

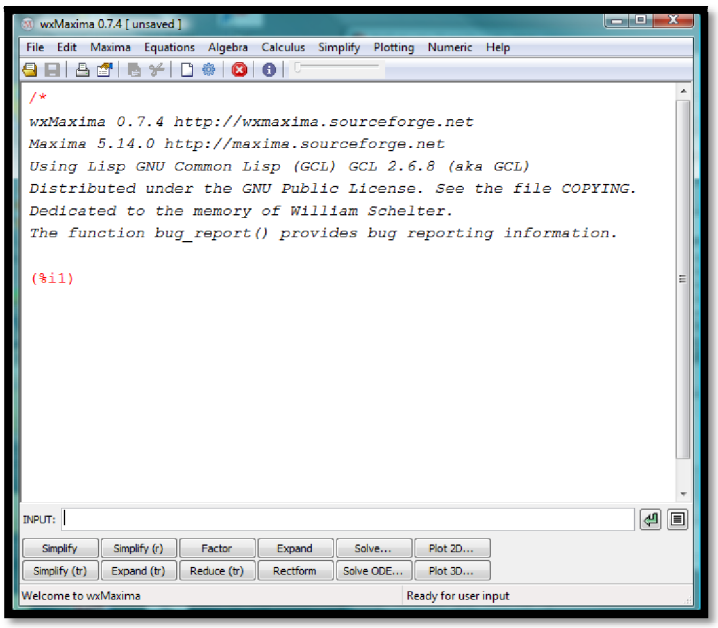

Figure 2 - MAXIMA 5.14 "pretty paper" interface.

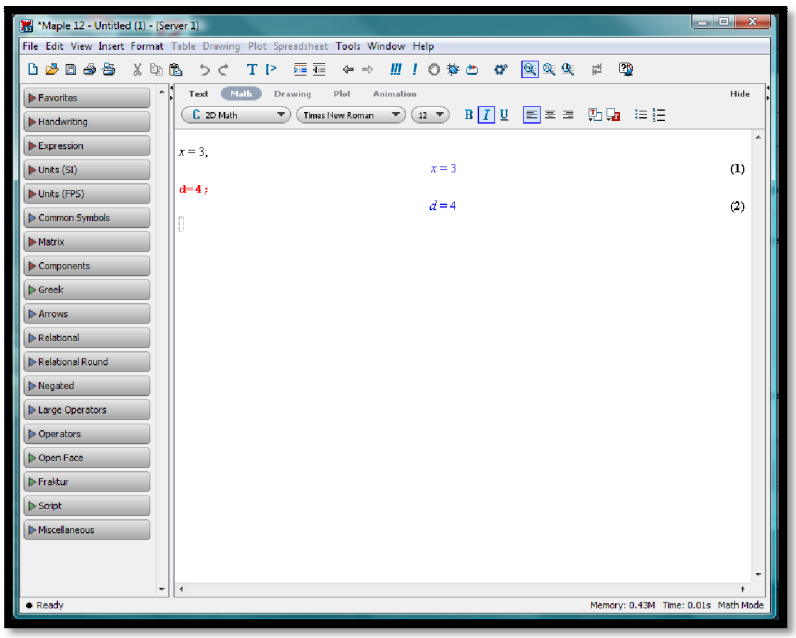

Figure 3 - MAPLE 12 work interface.

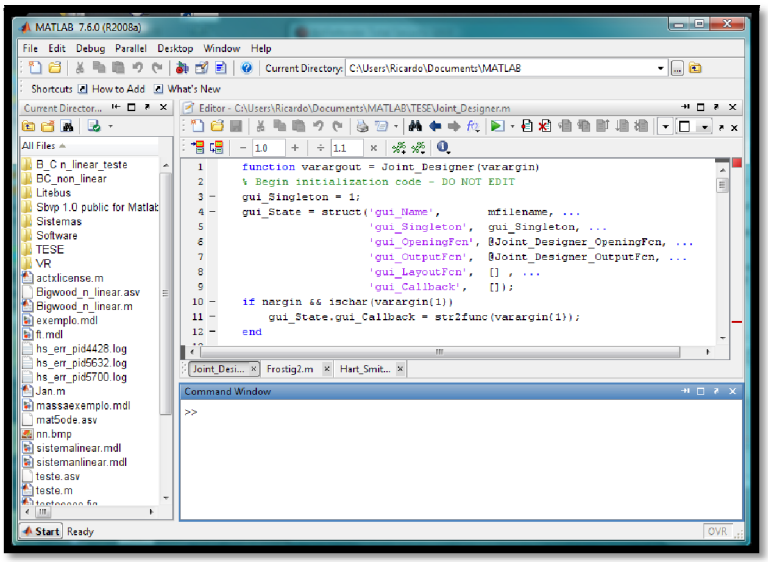

Figure 4 - MATLAB 7.6.0 work interface.

After the evaluation of the three software packages, MATLAB was chosen for the design of the new stress analysis software because of its GUI (Guide User Interface) versatility, its programming strength and for the fact that we already had a paid license from the Faculty.

1.3 Getting Started with MATLAB

After the software package was chosen, a learning process was undertaken along several weeks. To help the learning process several MATLAB introduction books **[18-22]** were consulted. At the same time, the first software interfaces started to be made.

In the beginning of this work the software creation aim was a single interface (see Figure 5) where the user could enter the data, choose the closed-form models and see the results. But as the software became more complex, the single interface construction had become a constraint in the development of the software.

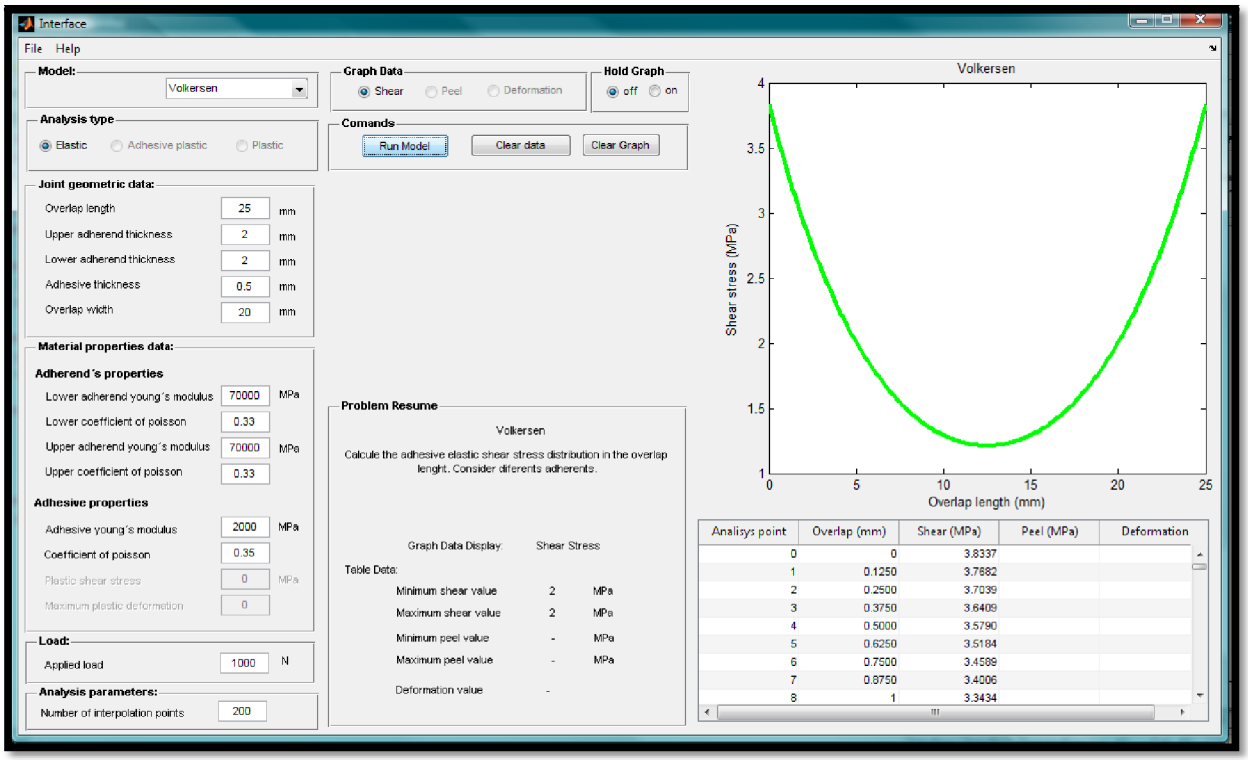

Figure 5 - Single interface software.

Therefore, it was decided to use several windows, and with the aid of several MATLAB GUI's books **[23-27]** a set of interfaces were created and connected in order to form an user-friendly software.

As the software grew and the models were implemented in the software, an iterative process of interfaces creation was used to adapt the interfaces to the models and their capacities.

The software developed is shown in the next chapter.

Chapter 2

Software Description

"Joint Designer" was the name selected for the software created in MATLAB. A search on the web on patents showed that there is not a similar name registered.

The software starts with an initial window shown below that has some information about the authors and institutions that have supported financially the project. This window only appears in the initial run of the software.

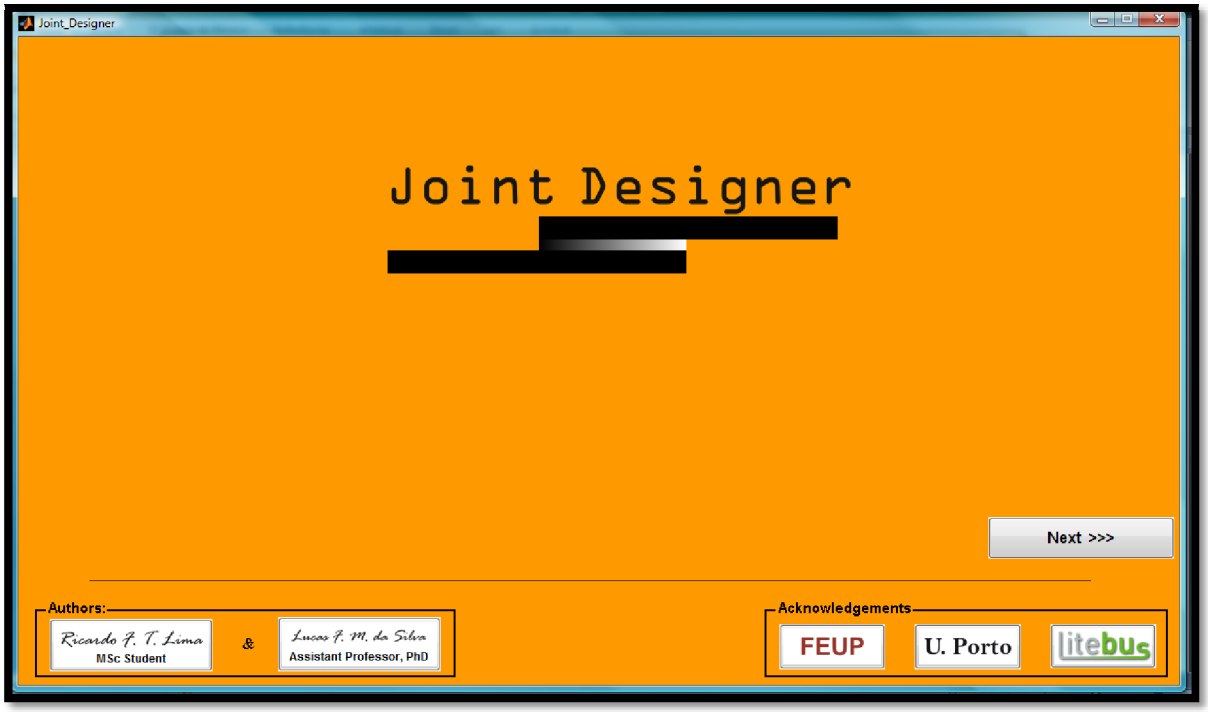

Figure 6 - Initial window of the "Joint Designer" software.

2.1 Selection of joint type

By pressing the button labelled **NEXT** in the initial window, another window emerges with different types of joints geometries; single and double lap joint (SLJ and DLJ), T-joint, sandwich, tubular and corner joint. Although there are six different types of adhesive joints, only three are available at the moment, SLJ, DLJ and sandwich joint.

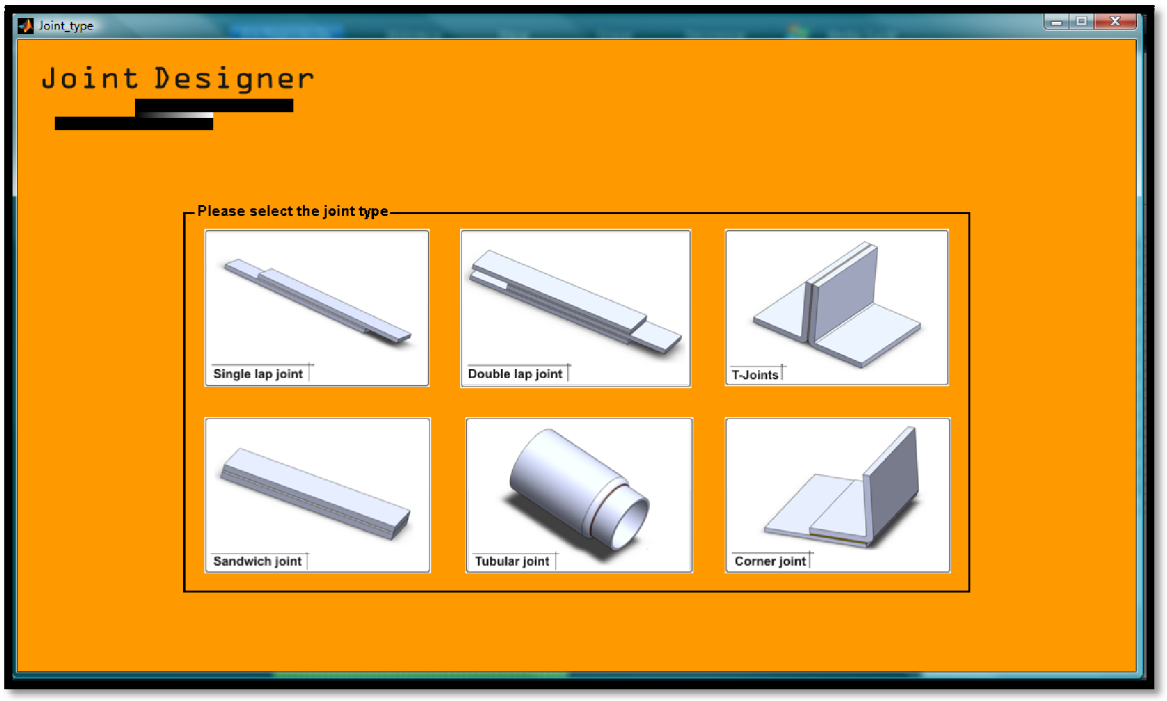

Figure 7 – Joint type selection window.

2.1.1 Single Lap Joint

Once the user selects the SLJ button, a new window appears for the user to select the type of load applied to the SLJ, in this case traction or compression load.

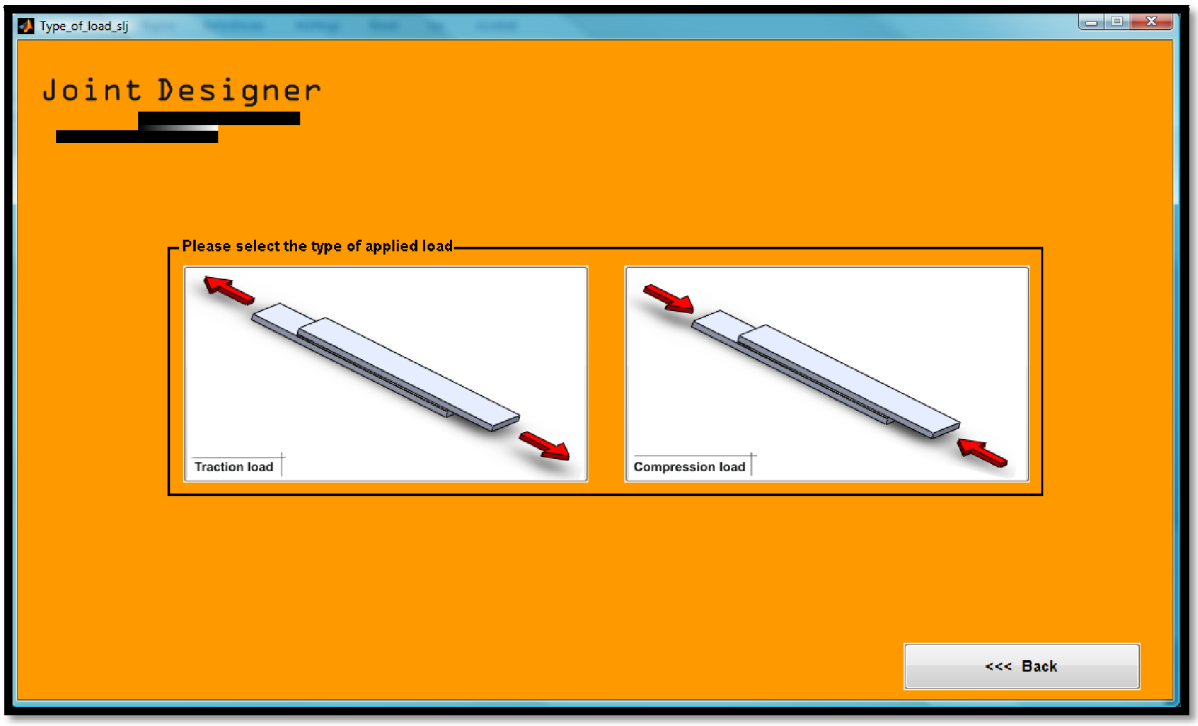

Figure 8 - Type of applied load in SLJ.

2.1.2 Double Lap Joint

The same happens when the DLJ button is selected; a new window appears for the user to select the type of applied load (traction or compression load).

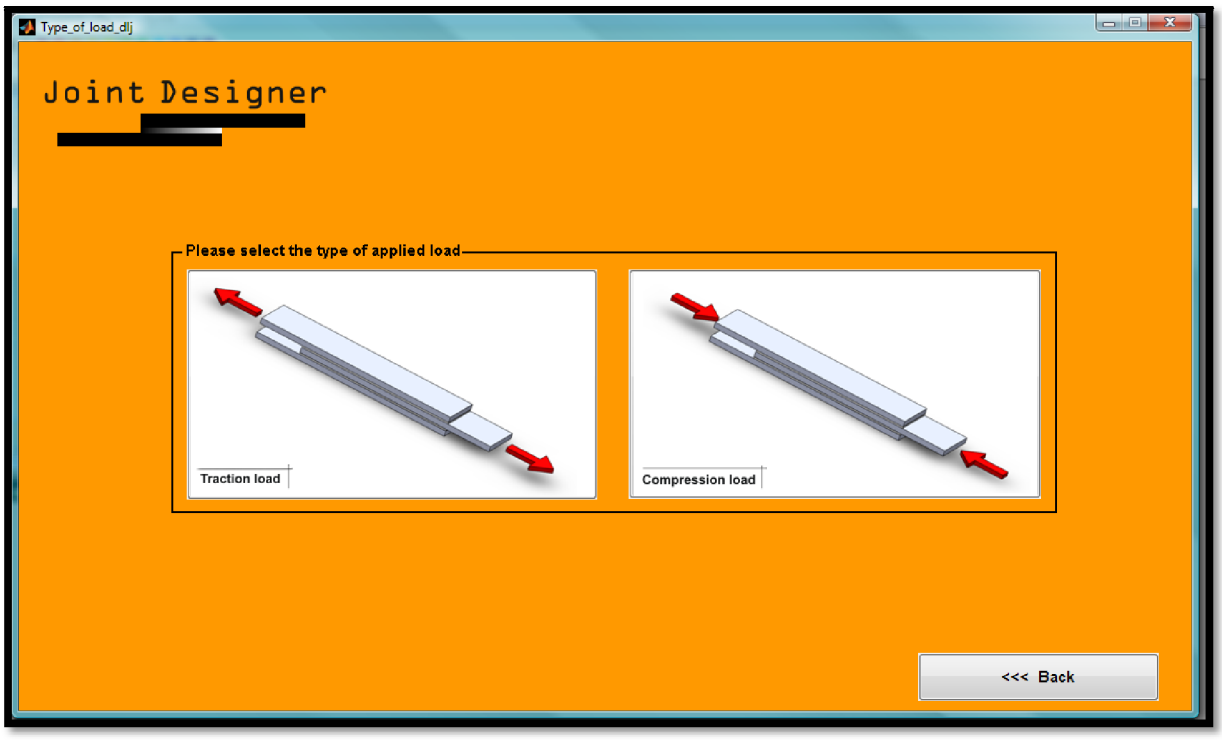

Figure 9 - Type of applied load in DLJ

2.1.3 Sandwich joint

When the user selects the sandwich geometry, where any type of load can be applied to the edge of the sandwich, a new window appears (see Figure 14) for the user to select the type of analysis; this window will be explained in the following section.

The software only allows the definition of the boundary loads in the sandwich joint, permitting the analysis of various configurations of adhesive joints under complex loading, consisting of tensile and shearing forces and a bending moment at the ends of the adherends. A simulation of almost any type of geometry can be done once the loads can be simplified to this form. An example is shown in Figure 10 for a corner joint.

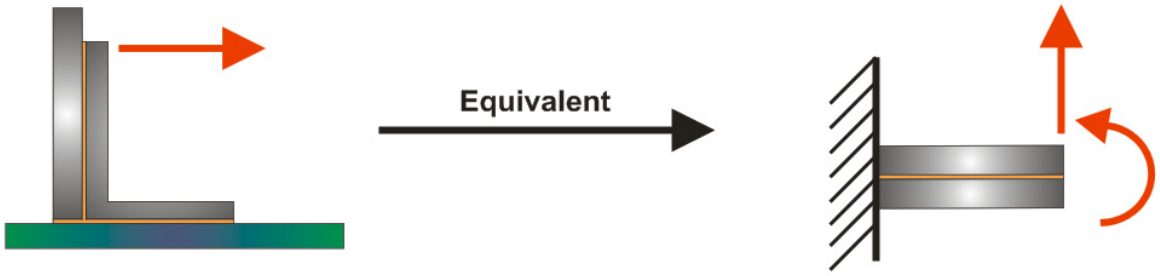

Figure 10 - Sandwich joint equivalent to the corner join.

In a total of twelve loads, the user can input two forces and one moment on each adherend edge. The loads can be entered in different units; forces can be entered in N, kN and MN and moments in N/m and N/mm.

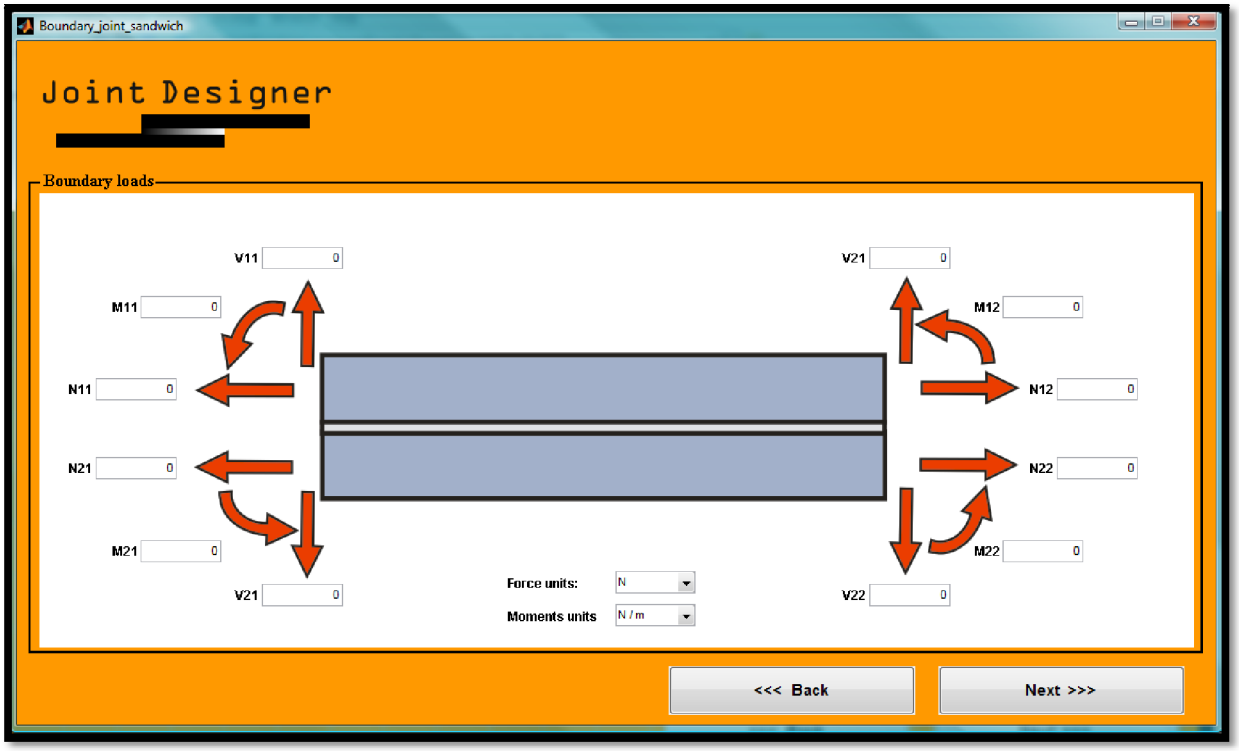

Figure 11 - Boundary loads window for sandwich joints.

2.2 Selection of material behaviour

Once the type of applied load is chosen, the user has to select the type of material behaviour.

The selection of analysis is equal for all geometries and the user has the possibility to select the behaviour of the adherends, adhesive and the material properties.

The behaviour can be elastic or plastic. If the user selects elastic, the software will only consider in the analysis the elastic behaviour of the material. However, if the user selects plastic, the software will consider the elastic and plastic behaviour of the material.

The adherend can be isotropic or anisotropic properties. Anisotropic properties only cover laminate layer composites.

Below are shown the window for the material behaviour selection in the case of SLJ, DLJ and sandwich.

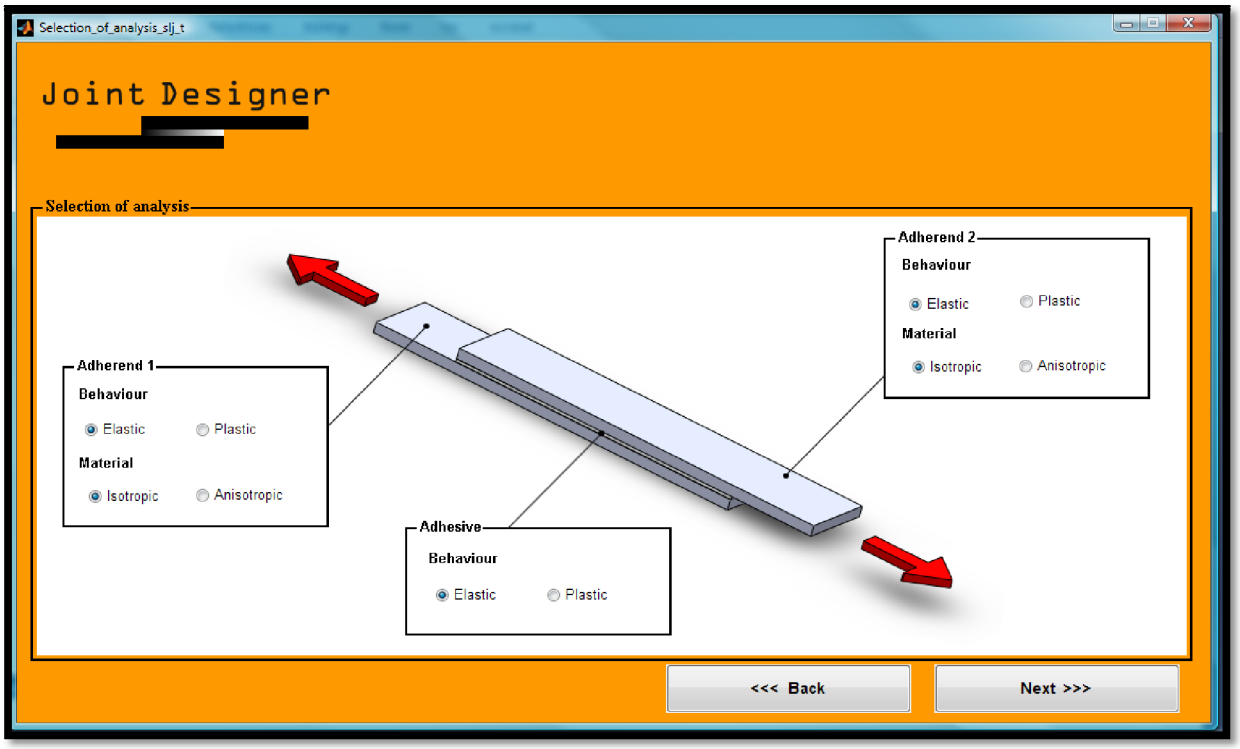

Figure 12 - Selection of material behavior for SLJ.

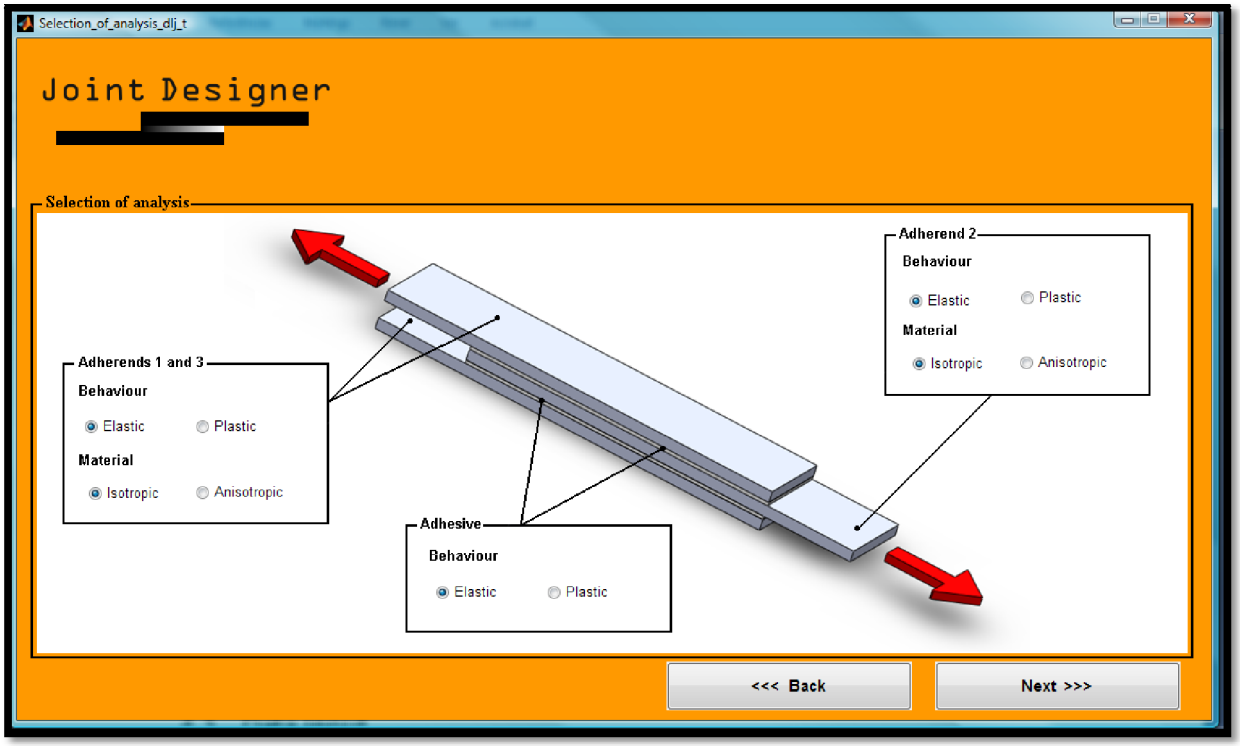

Figure 13 - Selection of material behaviour for DLJ.

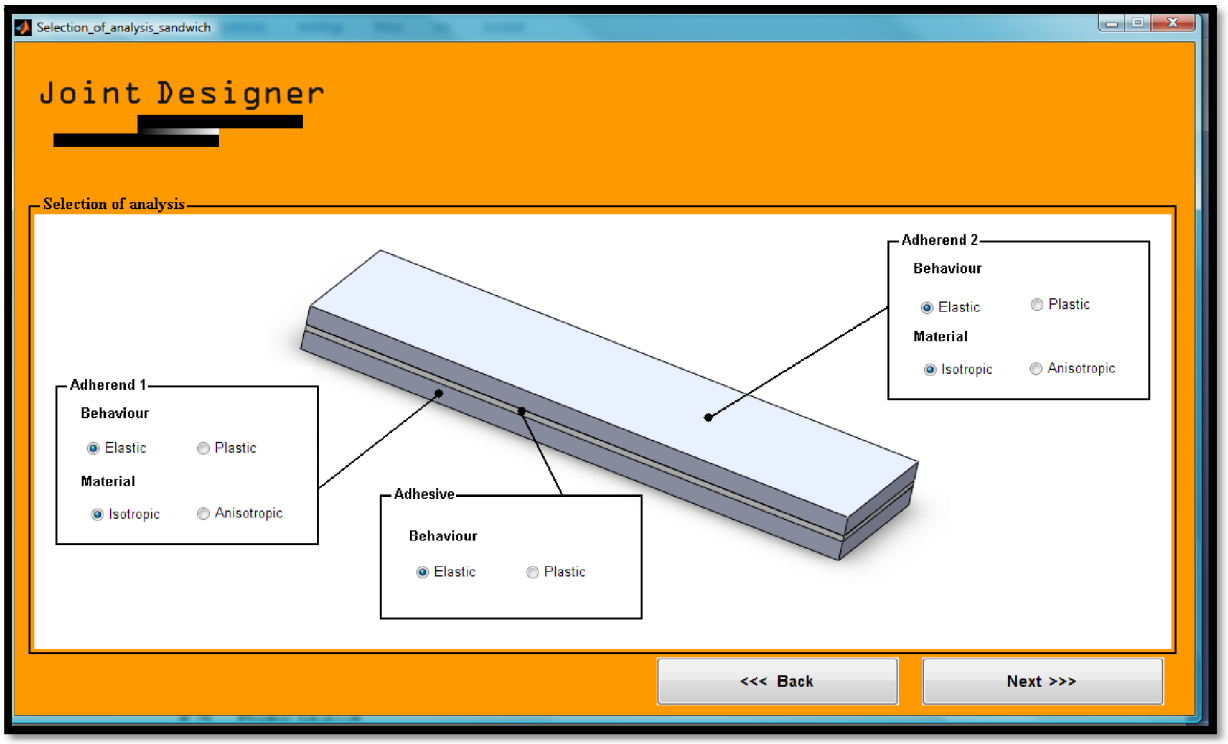

Figure 14 - Selection of material behaviour for sandwich geometry.

2.3 Isotropic adherends

2.3.1 Joint geometry

After selecting the material behaviour type, the user has to input the joint geometry data. The joint geometry data consists in the thickness of the adherends and adhesive layer, the overlap length and joint width. The magnitude of the load is also introduced here.

The software has the possibility to input the data in different units. For geometry data, the user can insert data in m, cm and mm. For the applied load, the data can be introduced in N, kN and MN.

The SLJ geometry window is shown next. In this case a tensile load is applied.

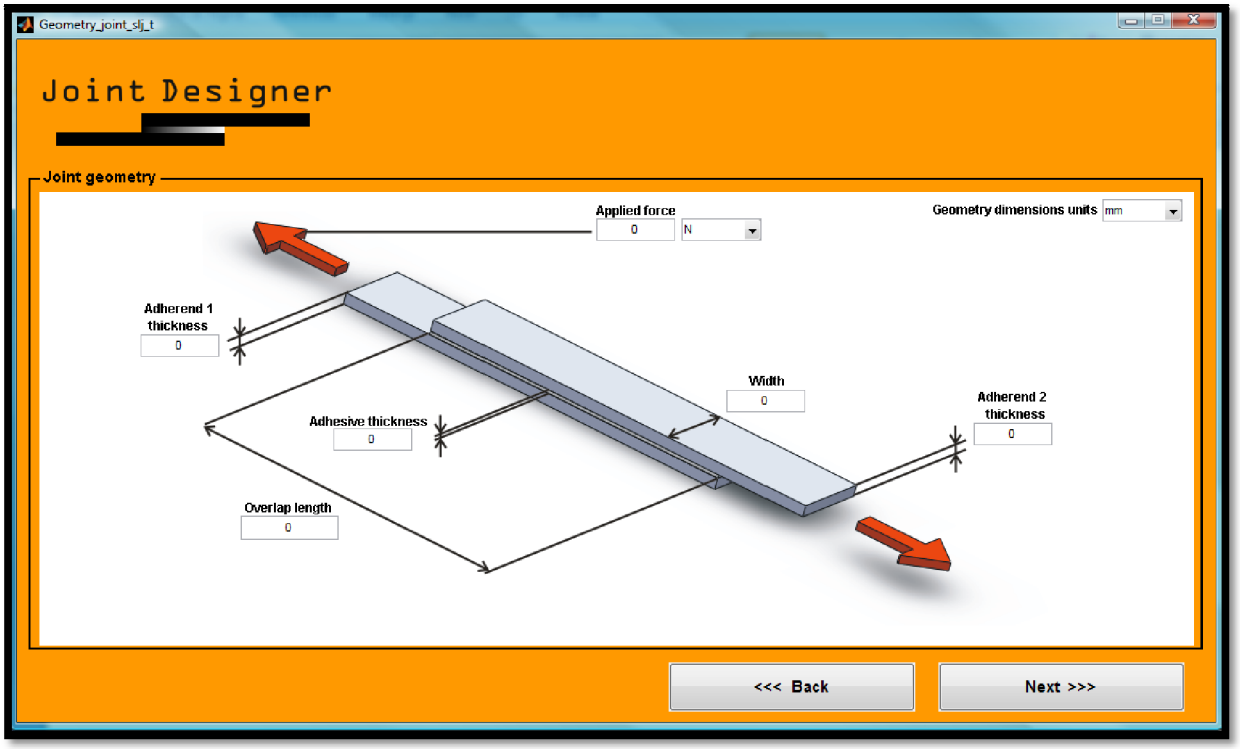

Figure 15 – Joint geometry input data window for SLJ.

At the moment the thermal effects are considered only for the DLJ. The temperature at which the adhesive was cured and the expected work temperature are introduced

The software gives the possibility to input the temperature data in different units; the user can insert the data in ºC,ºF and ºK.

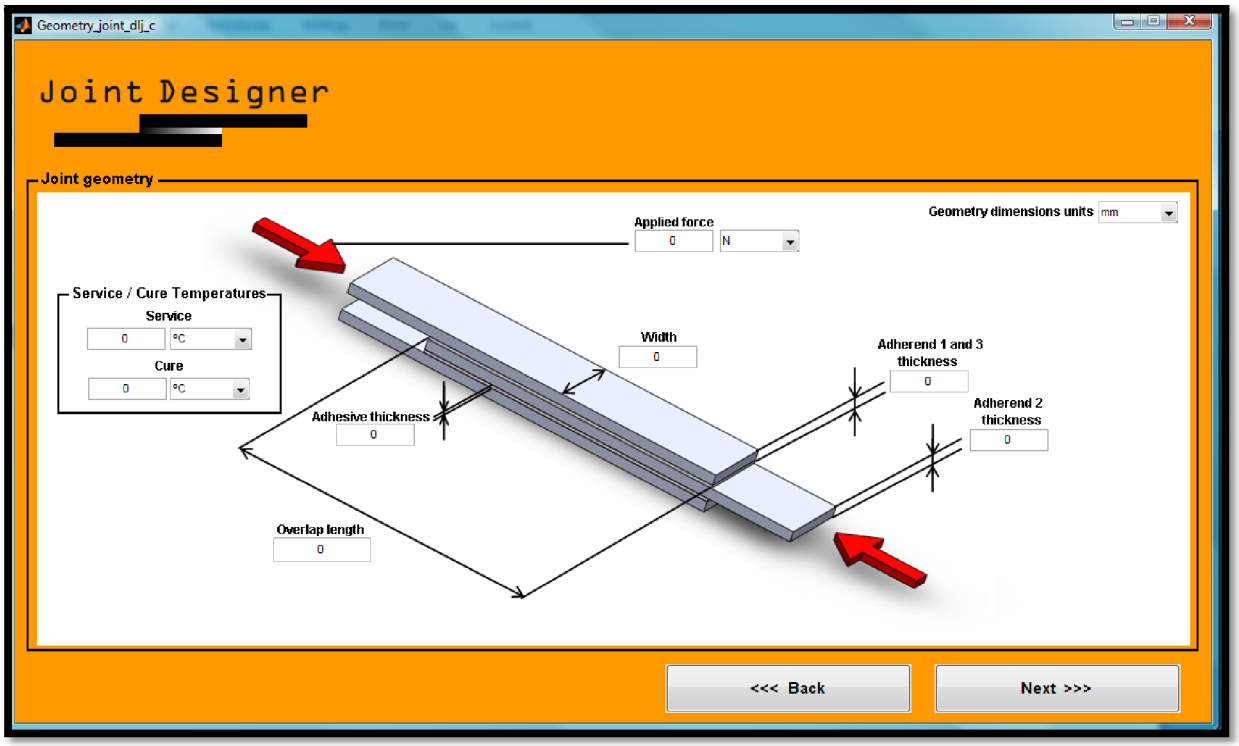

Figure 16 - Joint geometry input data window for DLJ.

For the sandwich joint geometry, the user just needs to input the geometry data since the loads will only be defined in a later window (see Figure 11).

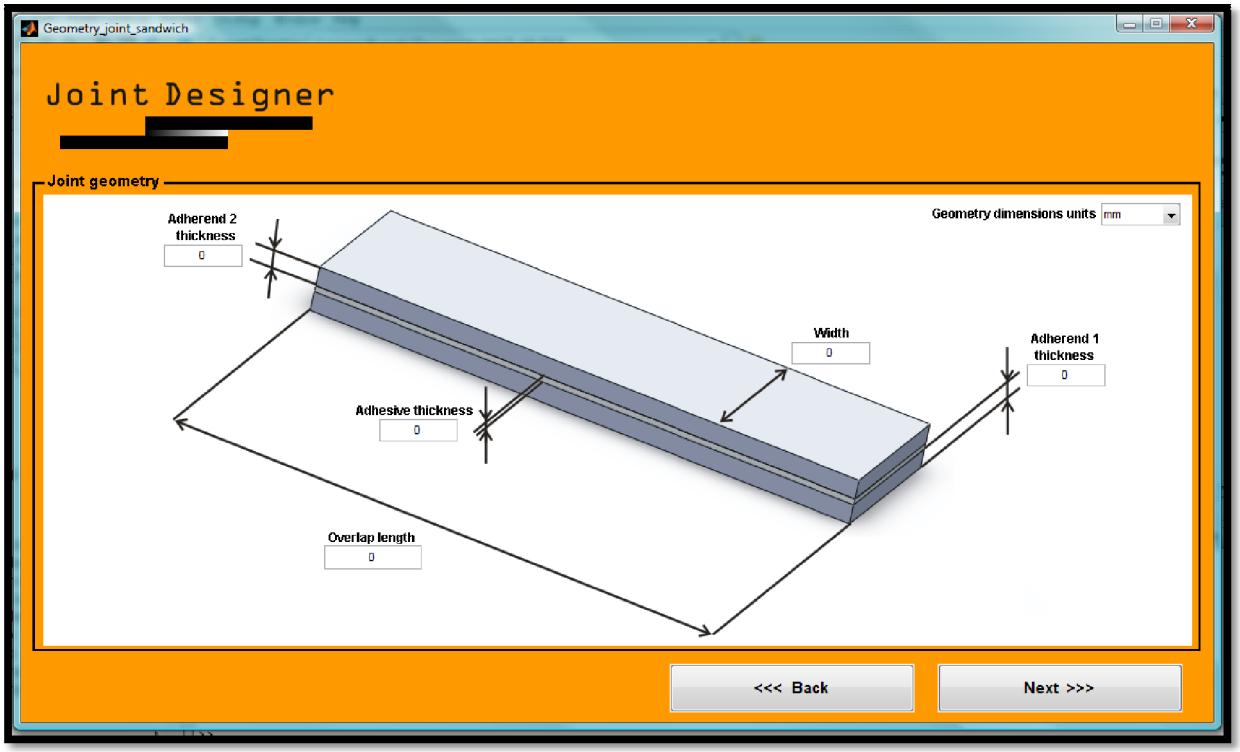

Figure 17 - Joint geometry input data window for sandwich joint.

2.3.2 Material properties

After the user defines all parameters in the geometry data window, the material properties window appears.

In the material properties window, the user has to introduce the Young's modulus and the Poisson's ratio of both adherends and adhesive. The software has the possibility to input the Young's modulus in different units; the data can be introduced in Pa, kPa, MPa e GPa.

The window for the input of material properties for the SLJ is shown next.

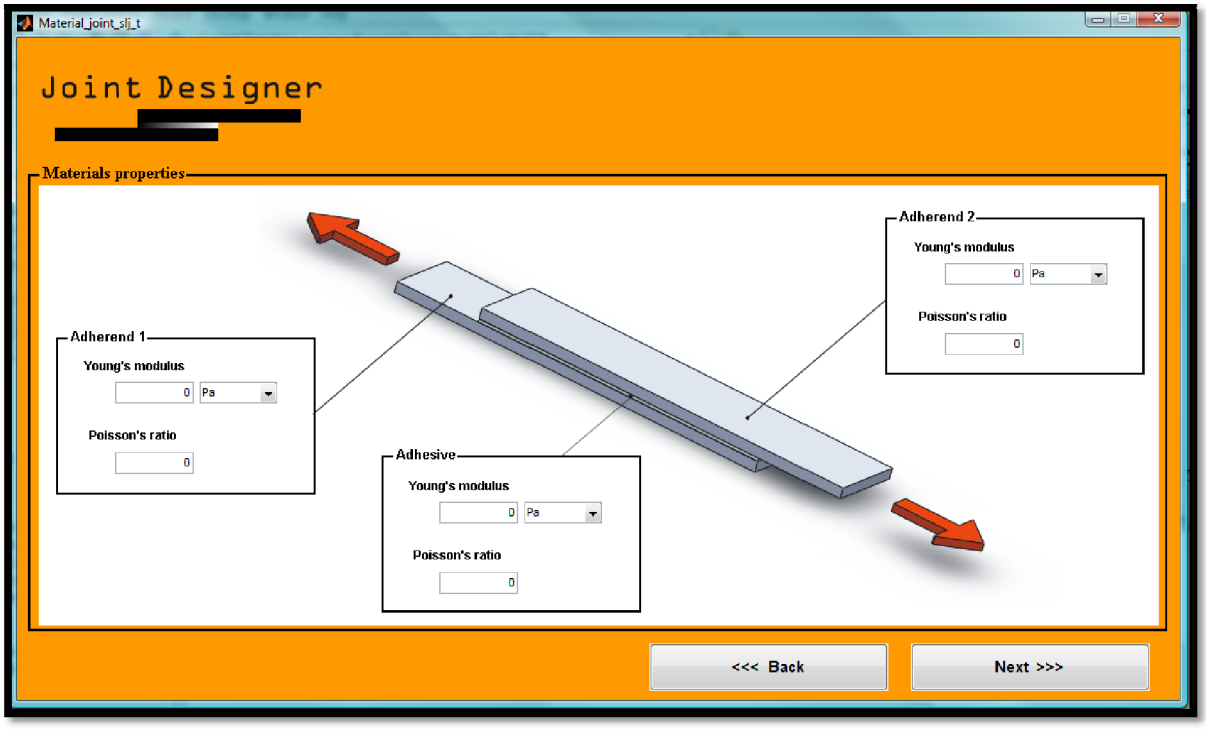

Figure 18 - Materials properties window for SLJ.

The DLJ has by definition three adherends which can be made from three different materials. In this case, the software considers only two different adherends. Top and bottom adherend are considered equal due to calculus modelling simplifications.

Due to the thermal effect consideration in DLJ, it is necessary to input the coefficient of thermal expansion of the adherends. Once again the user can insert the data in different units; data can be inputted in °C-1, °K-1 and °F-1.

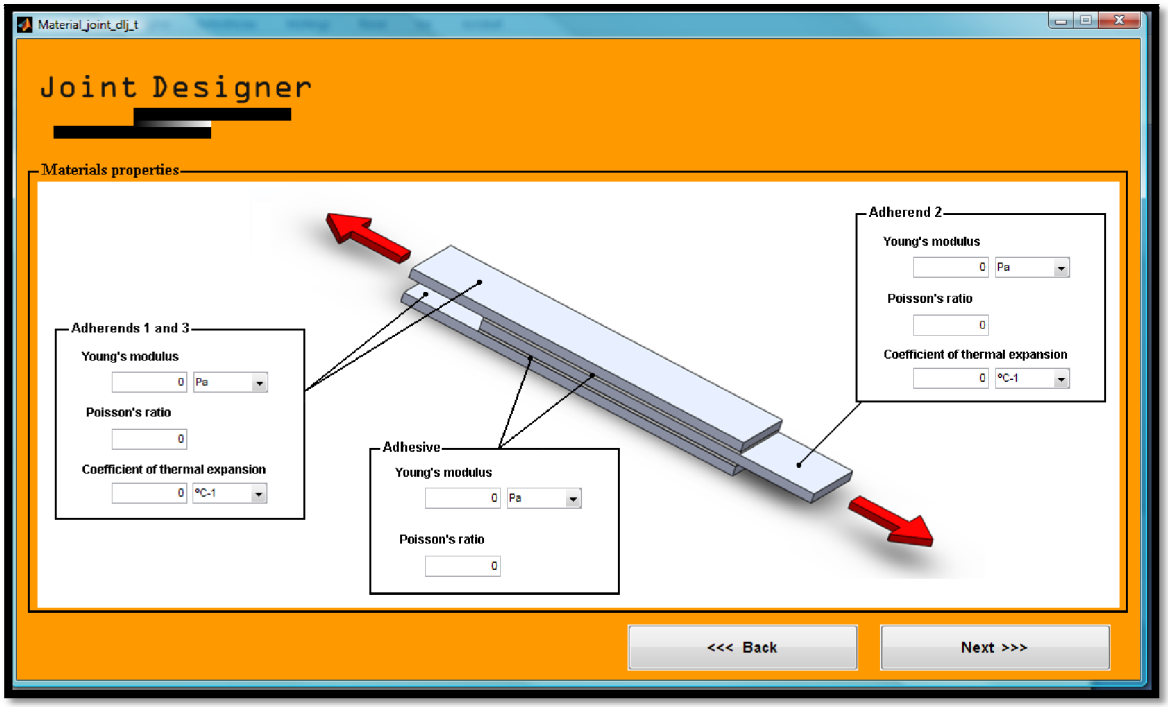

Figure 19 - Materials properties window for SLJ.

For sandwich joints, the window is similar to the SLJ window. The user has to input the Young's modulus and Poisson's ratio of adherends and adhesive materials.

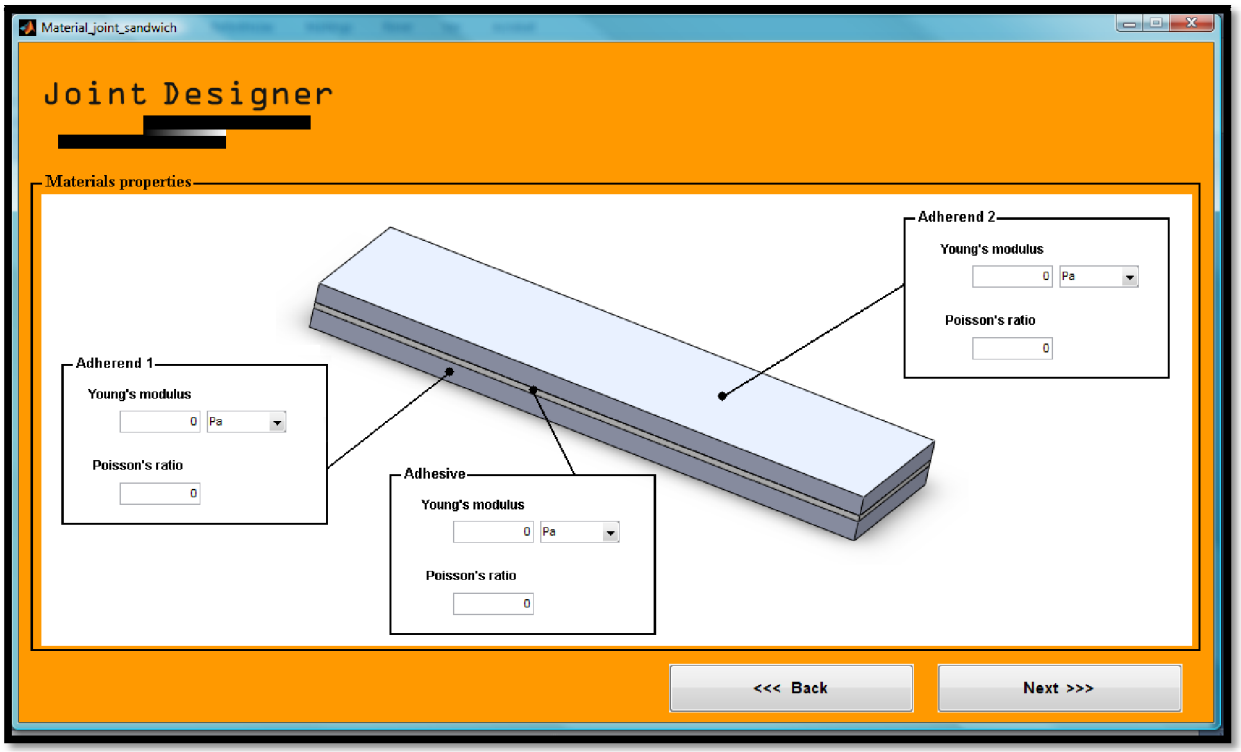

Figure 20 - Materials properties window for sandwich joint.

2.4 Anisotropic adherends

2.4.1 Joint geometry

The geometry input data is the same as for isotropic adherends (see Figure 23). The magnitude of the load is also introduced.

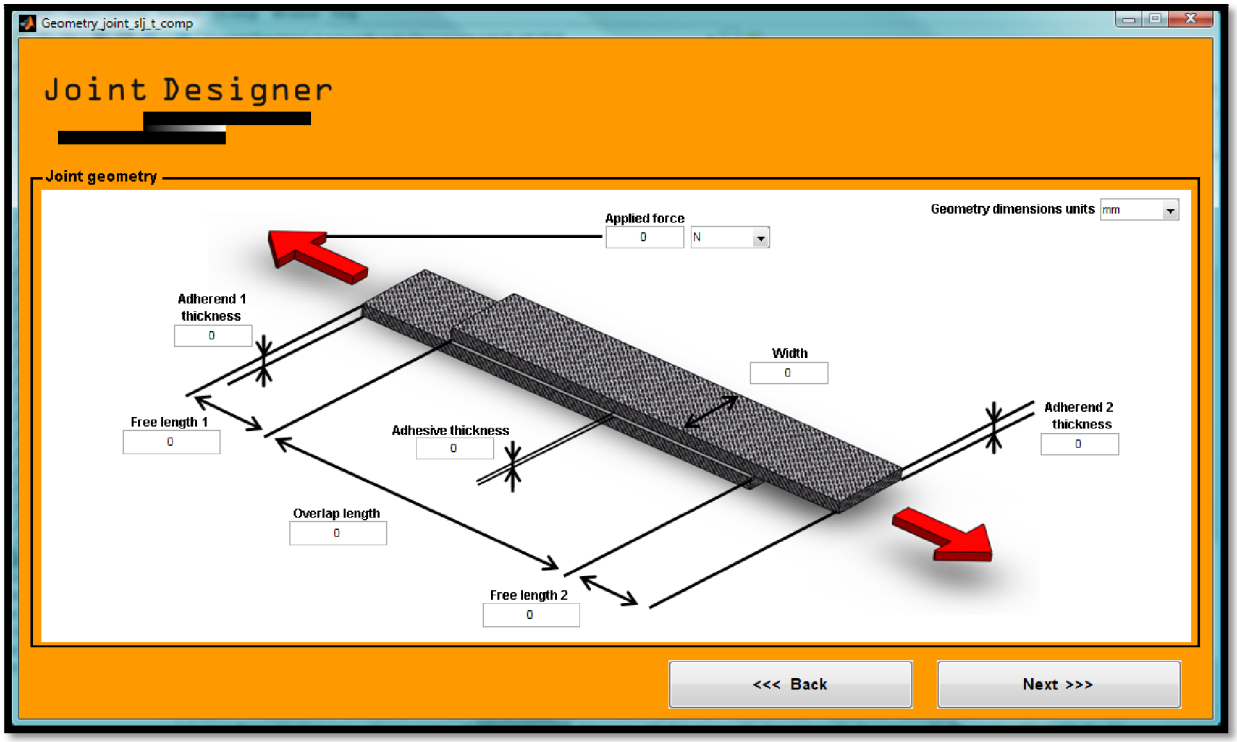

Figure 21 - Joint geometry input data window for anisotropic adherends SLJ.

2.4.2 Layer and adhesive properties

After the user defines all parameters in the geometry data window. The material properties window appears.

In the material properties window, the user has to introduce the Young's modulus and the Poisson's ratio of both adherends laminate layers in the x and y direction, and the Young's modulus and the Poisson's ratio of the adhesive.

The laminate layer **[28]** is orthotropic because it has three planes of symmetric mutually perpendicular, decreasing the number of elastics constants necessary for the characterization of the stress-strain behaviour of the laminate layer.

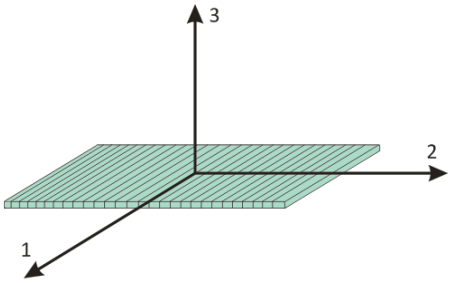

Figure 22 - Main axes of the laminate layer.

The main axes of the laminate layer were established so that the axis 1 is parallel to the fibers direction and the axis 3 is orthogonal to the layer plan. In a laminate layer it is known that the fibers are parallel to the plan <12> and randomly distributed in the transverse plan <23>. Therefore the laminate layer presents transversely isotropic properties, that is, its elastic constants are independent of the axes orientation in the plan.

The window for material properties input for SLJ is shown next.

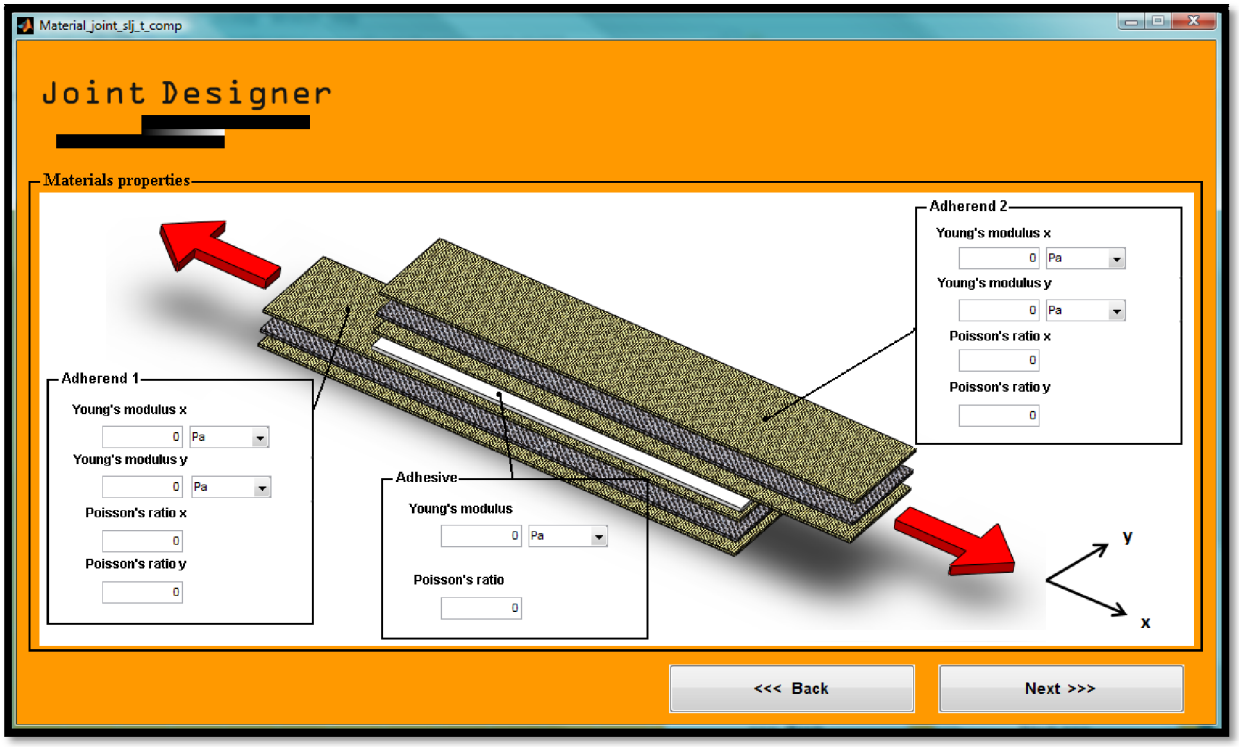

Figure 23 – Layer and adhesive properties window for anisotropic adherends SLJ.

2.4.3 Characterization of adherend layers

In the characterization of adherends window the user has to insert the number of laminate layers and the orientation of the fibers in each laminate layer in a vector format.

A laminate composite is composed by several layers that can be oriented in different directions (see Figure 25). To obtain the properties along the three main axes, we have to apply a transformation matrix that depends on the angle (θ) (see Figure 24).

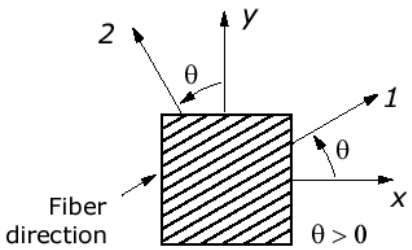

Figure 24 - Rotation of the principal axes according to the fiber angle of the laminate layer.

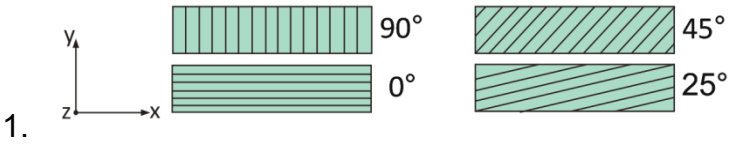

Figure 25 – Representation of some fiber angles orientation on laminate layers.

Figure 26 shows the anisotropic adherends characterization window where the user can insert the number of laminate layer that constitutes the adherends and the fiber orientation of each layer. The fiber orientation is inserted in a line vector format.

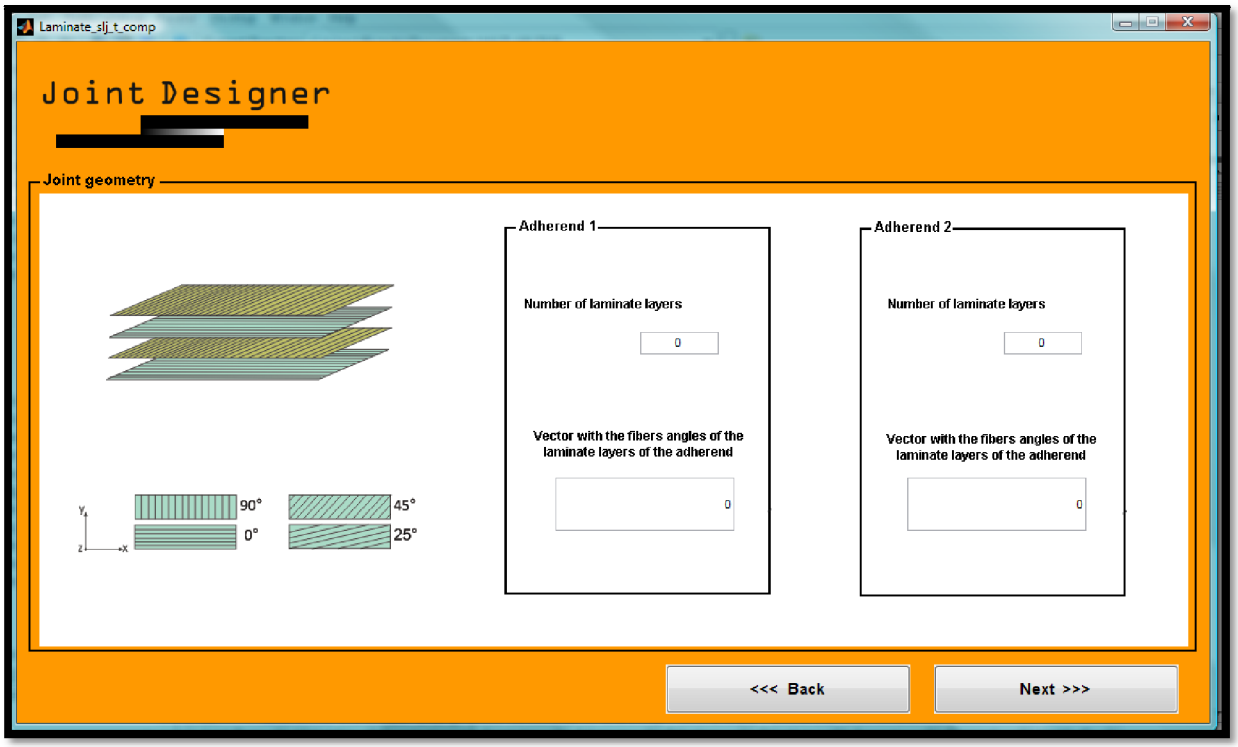

Figure 26 – Characterization of the adherend layers window.

2.5 Closed-form models

The user then chooses the available models to determine the stress distribution. The software only shows to the user the models that can be run for the selected material behaviour and geometry. For example, if the user previously selected to include the plasticity of the adherend, the only model available is that of Adams **[35]**.

Next, the model selection window with all models available is shown.

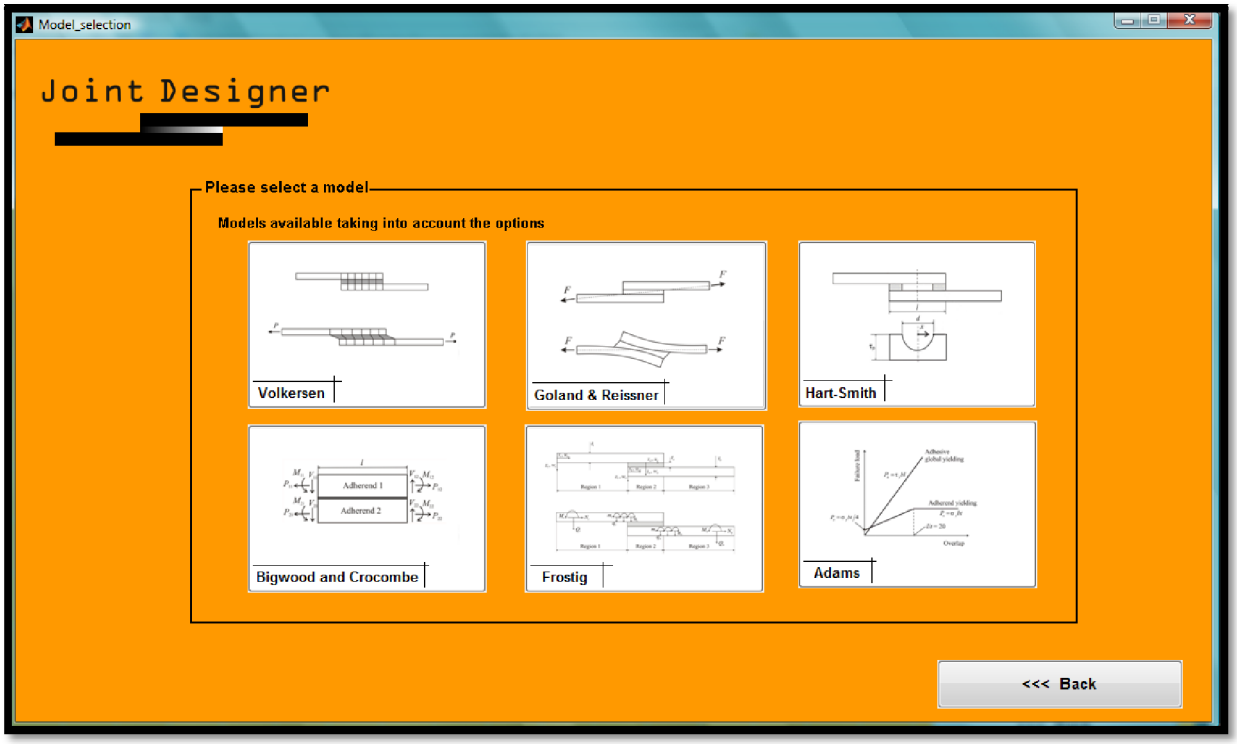

Figure 27 - Models selection window.

A description of the closed-form models implemented in the software is presented in Chapter 3.

2.6 Selection of failure criteria

After the selection of the closed-form model, the user can select a failure criterion. The software has a total of four criteria; the shear stress, the peel stress, the adherend yield stress and the von Mises stress limit. According to the model selected, the software makes available or unavailable the selection for the criteria.

The software has the possibility of introducing the failure criteria in different units, for the stresses the user can insert in Pa, kPa, MPa e GPa.

The selection of failure criteria window is shown next.

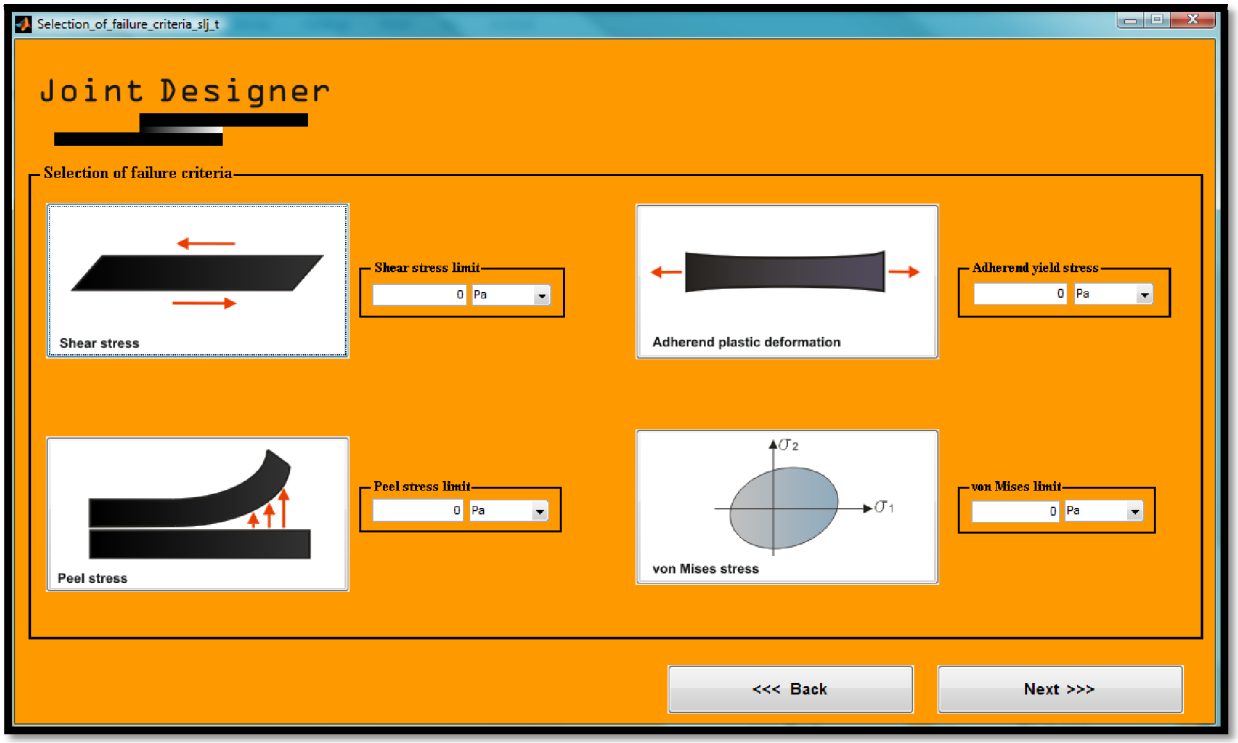

Figure 28 - Failure criteria selection window.

2.7 Selection of analysis refinement level

In this window (see Figure 28) the user can choose the level of analysis refinement, done by selecting the number of calculation points along the overlap length.

The software permits three levels of analysis. The rough analysis calculates fifty points equally distributed along the overlap, the normal analysis calculates two hundred points and the refined analysis calculates five hundred points.

The user also has the possibility to choose the number of calculation points by selecting the custom analysis button and entering the number of points.

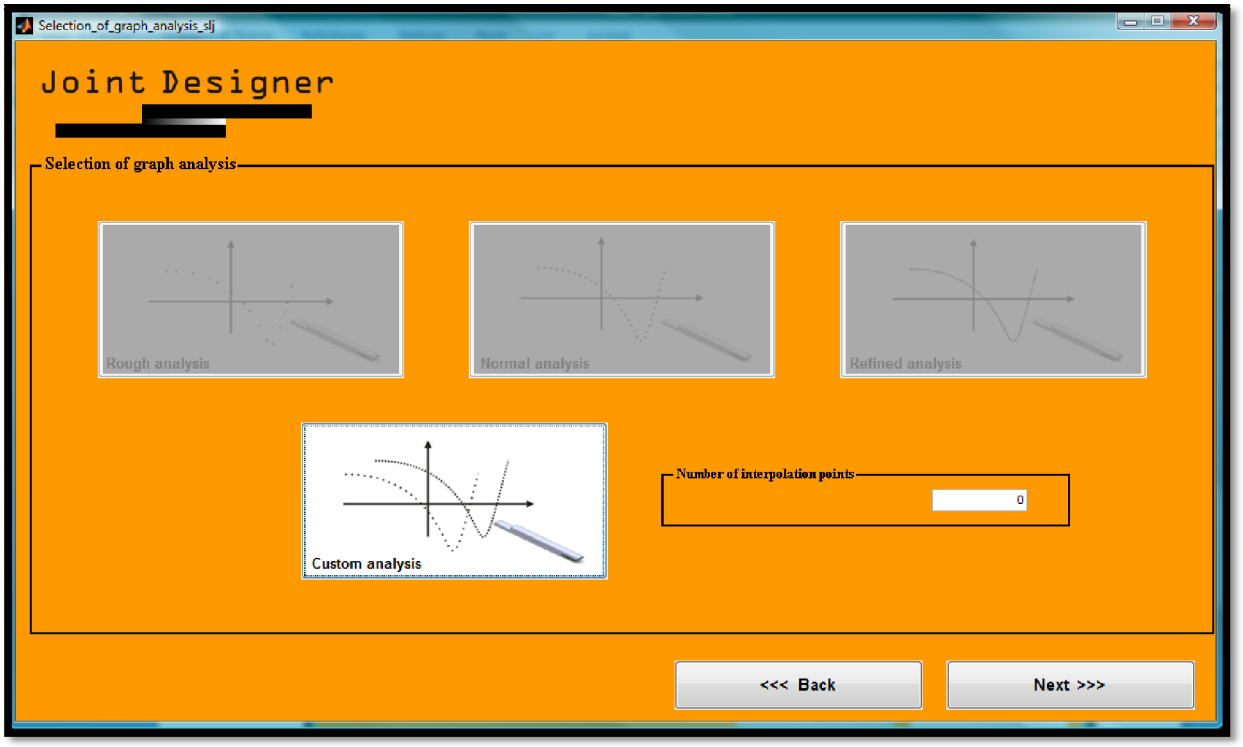

Figure 29 – Selection of the analysis refinement level.

2.8 Results

Finally the results are shown to the user. The result window shows the data in two ways. A list window allows the user to look at particular points along the overlap, while the plot form allows the user to have a global view of the stress distributions, as shown in Figure 30 for Goland and Reissner's analysis.

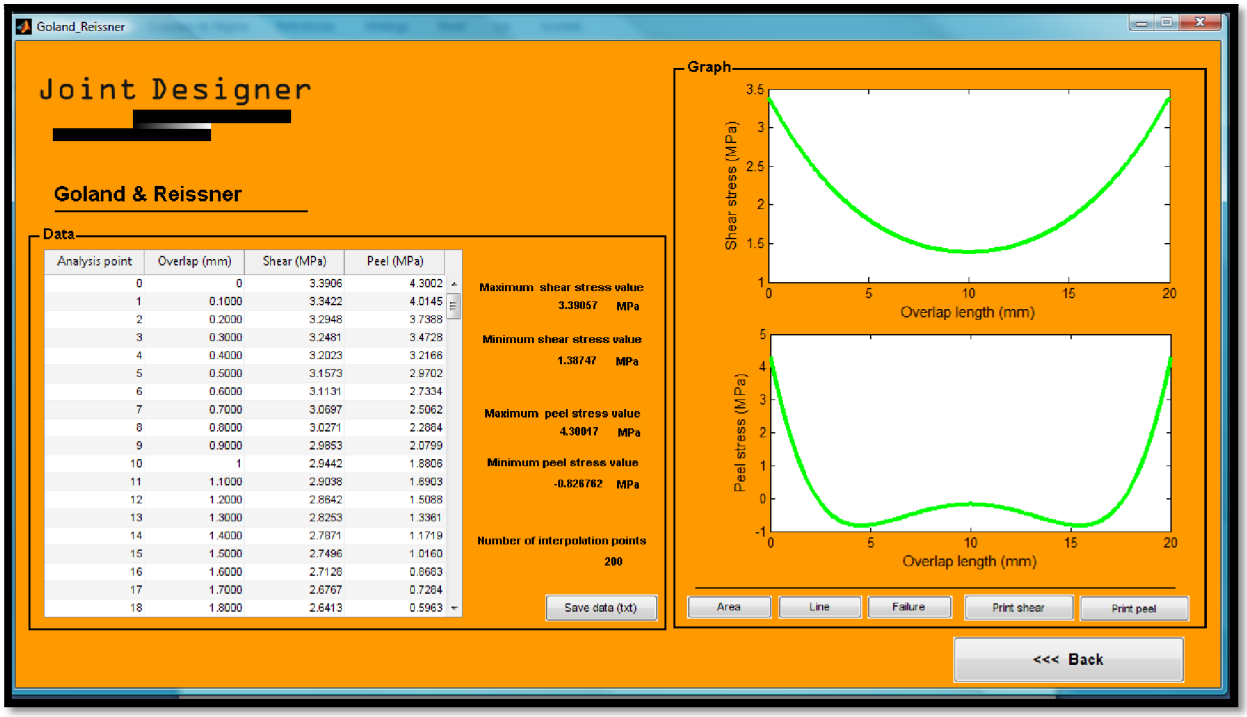

Figure 30 - Goland and Reissner's results window.

If the user selects the labelled **Save data (txt)** button a small window appears (see Figure 31). The user can then type the path and name of the text file.

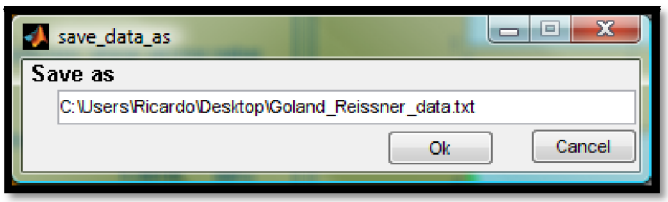

Figure 31 - Save data as window.

When the user presses the **Ok** labelled button a text file is created (see Figure 32). The result data in a list format is written in this text file. The file also contains the model designation and the date and time that the file was created, allowing for better file management.

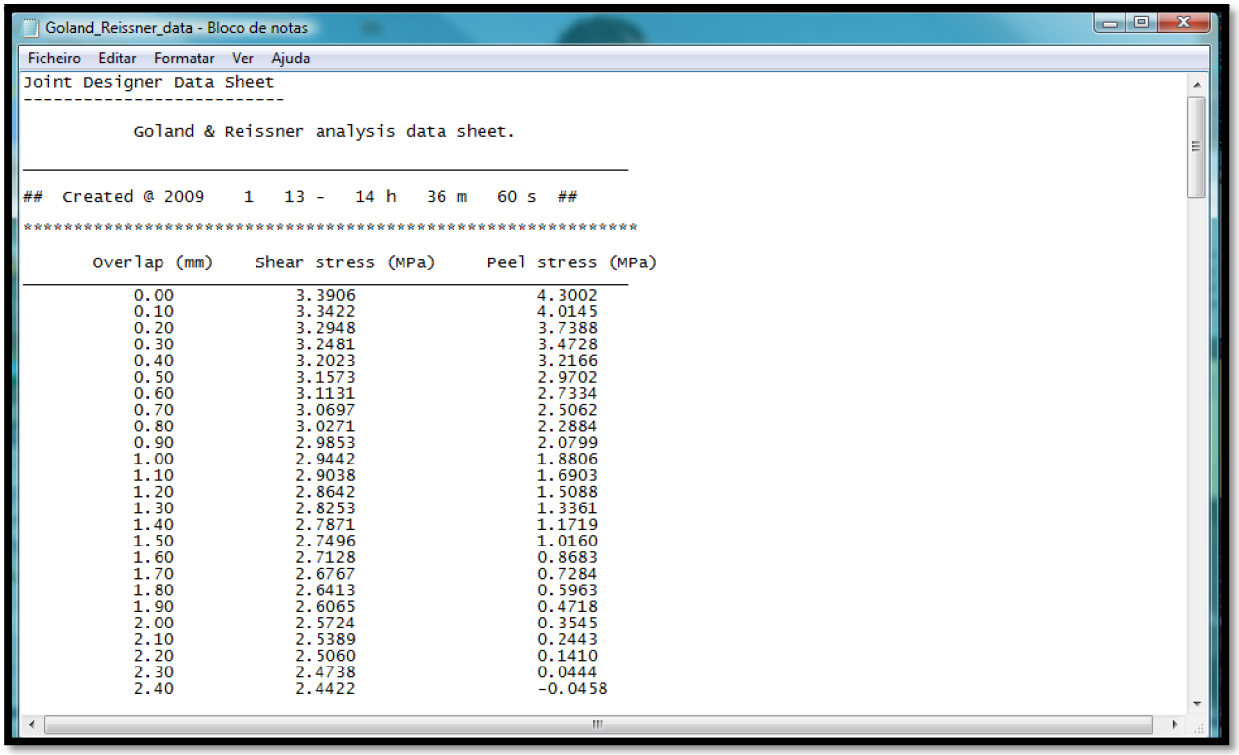

Goland_Reissner_data - Bloco de notas

Ficheiro Editar Formatar Ver Ajuda

Joint Designer Data Sheet

Goland & Reissner analysis data sheet.

Created @ 2009 1 13 - 14 h 36 m 60 s

Overlap (mm)	Shear stress (MPa)	Peel stress (MPa)
0.00	3.3906	4.3002
0.10	3.3422	4.0145
0.20	3.2948	3.7388
0.30	3.2481	3.4728
0.40	3.2023	3.2166
0.50	3.1573	2.9702
0.60	3.1131	2.7334
0.70	3.0697	2.5062
0.80	3.0271	2.2884
0.90	2.9853	2.0799
1.00	2.9442	1.8806
1.10	2.9038	1.6903
1.20	2.8642	1.5088
1.30	2.8253	1.3361
1.40	2.7871	1.1719
1.50	2.7496	1.0160
1.60	2.7128	0.8683
1.70	2.6767	0.7284
1.80	2.6413	0.5963
1.90	2.6065	0.4718
2.00	2.5724	0.3545
2.10	2.5389	0.2443
2.20	2.5060	0.1410
2.30	2.4738	0.0444
2.40	2.4422	-0.0458

Figure 32 - Goland and Reissner's analysis data sheet.

If the user selects the **Print shear** or **Print peel** labelled button, a PDF file is created in the computer, with the name that the user chooses in the small print window that appears just after the user selects the print buttons (see Figure 33).

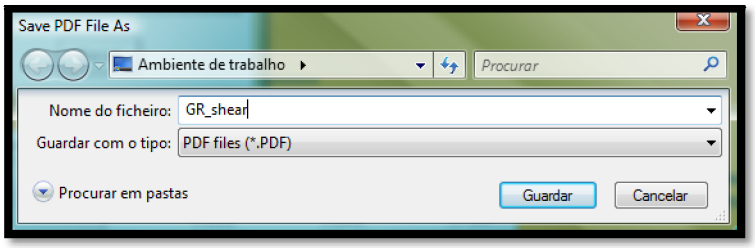

Figure 33 - Save PDF file as window.

The PDF file is shown next:

Figure 34 - PDF file created that shows the shear stress along the overlap joint.

The results form can also show the plot data in two different forms; in a line form (see Figure 30) and in an area form (see Figure 35). The plot that is shown in the results form is the same that is printed in PDF file.

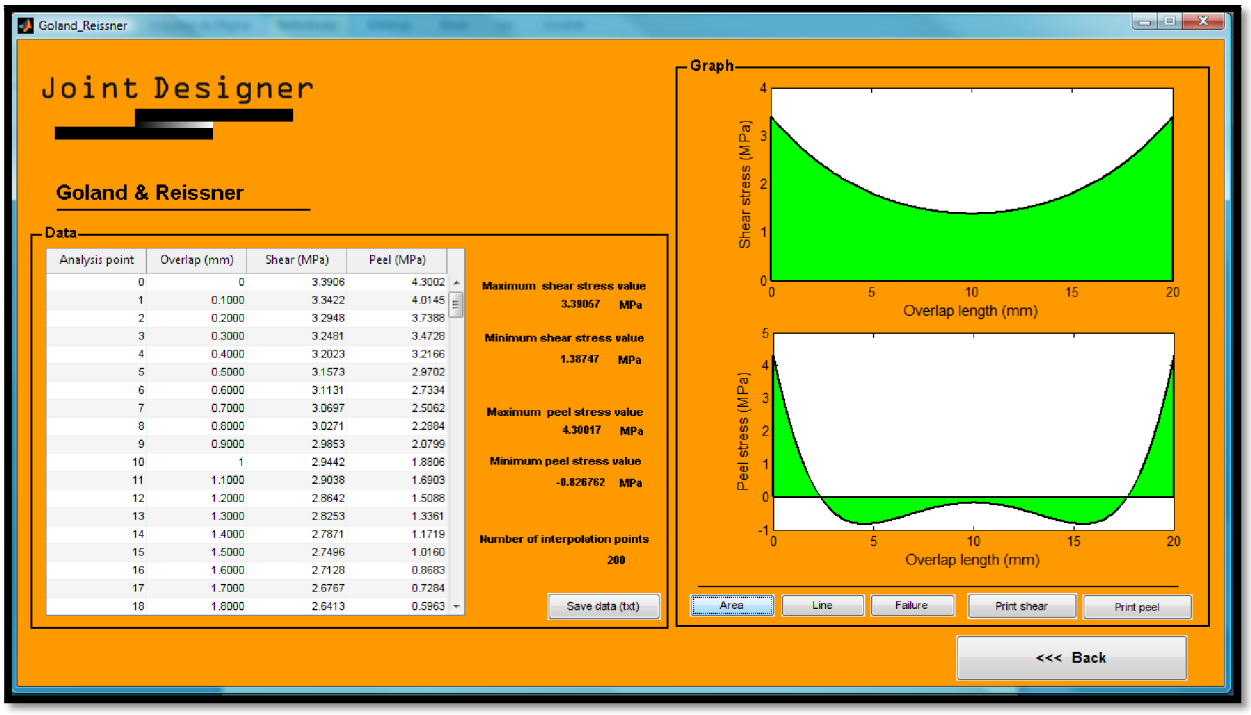

Figure 35 - Goland and Reissner's results window with area display.

If the user has selected previously a failure criterion and entered the maximum limit for the failure criteria, a red line appears in the plots indicating the limit of stress failure. If the stress distribution passes this value, the limit stress line appears in red (see Figure 36).

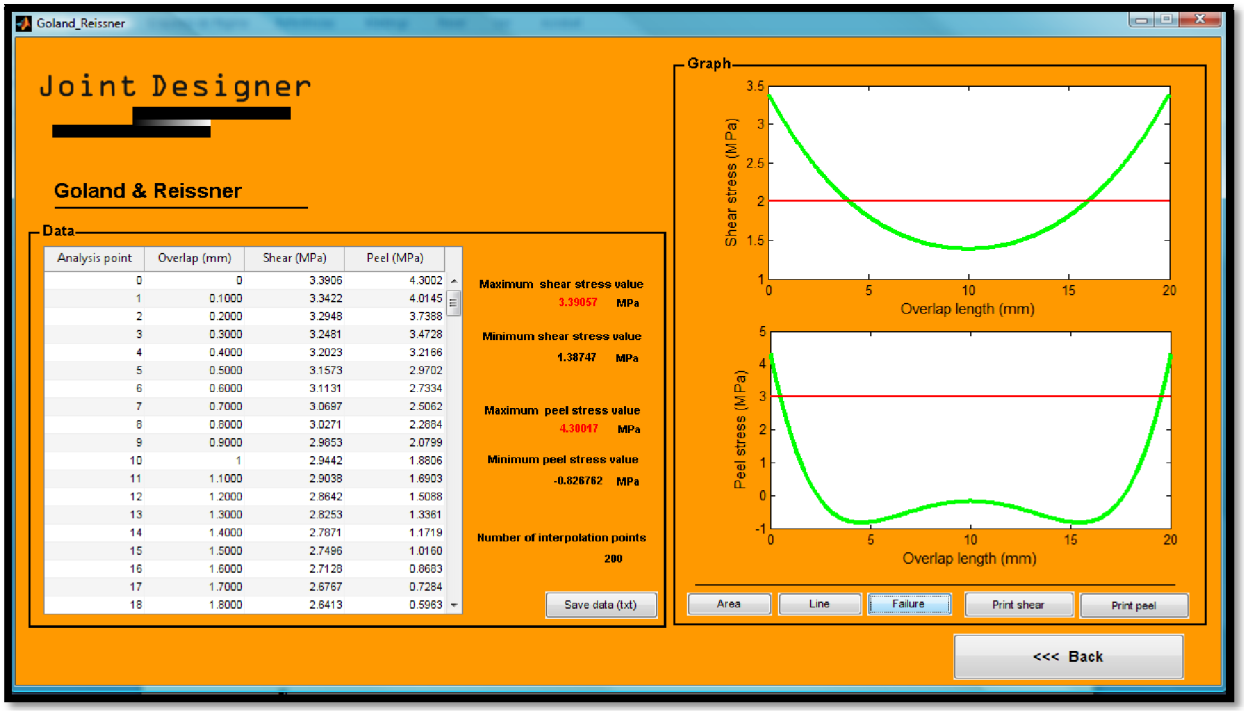

Figure 36 - Goland and Reissner's results window with failure criteria enabled.

Chapter 3

Analytical Models

3.1 Volkersen [6-7]

Volkersen **[2]** introduced the concept of differential shear, illustrated in Figure 37. It was assumed that the adhesive deforms only in shear but that the adherends can deform in tension, as can be seen in Figure 38, because they are considered elastic and not rigid (see Figure 39). The tensile stress in the upper adherend, is maximum at A (see Figure 37) and decreases to zero at B (free surface), so the strain must progressively reduce from A to B. The reduction of the strain in the adherends along the overlap and the continuity of the adhesive/adherend interface cause a non uniform shear strain (and stress) distribution in the adhesive layer. The shear stress is maximum at the ends of the overlap and is much lower at the middle, as shown in Figure 39. However, this analysis does not account for the bending effect caused by the eccentric load path of SLJs. The solution is more representative of DLJ than a SLJ since in a DLJ the overall bending of the adherends is not as significant as in the SLJ.

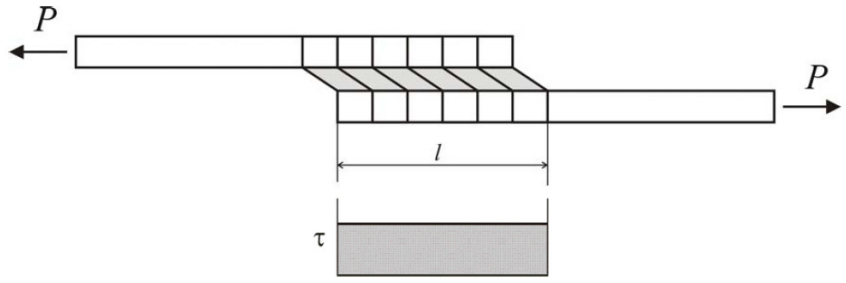

Figure 37 - Deformations in loaded single-lap joints with rigid adherends [29].

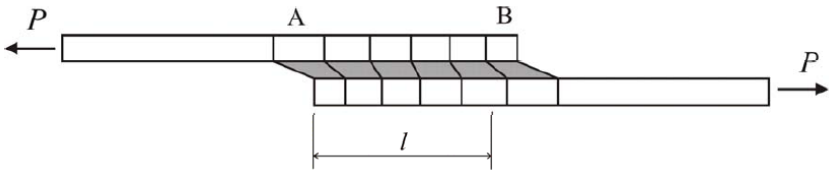

Figure 38 - Deformations in loaded single-lap joints with elastic adherends [29].

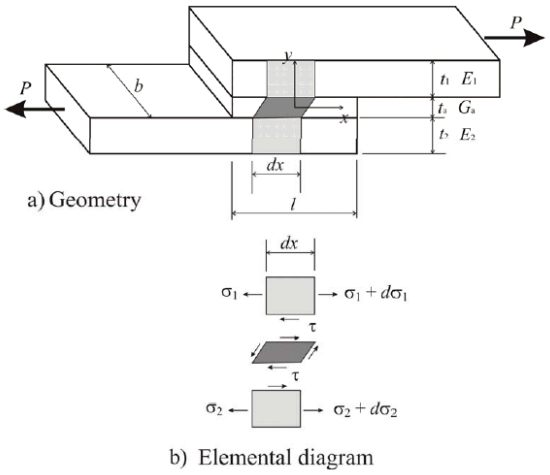

Figure 39 - Single-lap joint analyzed by Volkersen [29].

The adhesive shear stress distribution (τ) is given by:

$$\tau = \frac{P}{bl}\frac{w}{2}\frac{\cosh(wX)}{\sinh(w/2)} + \left(\frac{\psi-1}{\psi+1}\right)\frac{w}{2}\frac{\sinh(wX)}{\cosh(w/2)} \quad (1)$$

where P is the applied load, b the joint width, l the overlap, t_1 the adherend 1 thickness, t_2 the adherend 2 thickness, E the adherends modulus, G_a the adhesive shear modulus, t_a the adhesive thickness,

$$w^2 = (1+\psi)\,\phi \quad (2)$$

$$\psi = t_1/t_2 \quad (3)$$

$$\phi = \frac{G_a\, l^2}{E\, t_1 t_a} \quad (4)$$

$$X = {}^{x}/_{l} \qquad -\frac{1}{2} \le X \le \frac{1}{2} \quad (5)$$

The origin of the longitudinal co-ordinate x is the middle of the overlap.

3.2 Goland and Reissner [6-7]

The eccentric load path of a SLJ causes a bending moment (M), and a transverse force (V) to be applied to the joint ends in addition to the applied tensile load per unit width (P), as shown in Figure 40. Because of this bending moment, the joint will rotate, altering the direction of the load line with the tendency of the applied tensile forces to come into line. As the joint

rotates, the bending moment will decrease, giving rise to a nonlinear geometric problem where the effects of the large deflections of the adherends must be accounted for.

The first to consider these effects were Goland and Reissner **[30]**. They used a bending moment factor (k) and a transverse force factor (k') that relate the applied tensile load per unit width (P) to the bending moment (M) and the transverse force (V) at the overlap ends If the joint does not rotate, i.e. for very small applied loads, the factors k and k' will be approximately equal to 1. As the joint rotates with the increase of load, k and k' will decrease and, consequently, the bending moment and the transverse load will decrease too. Goland and Reissner took into account the effect of large deflections of the adherends, but assumed that the adherends were integral, with an infinitely thin adhesive layer.

Algebraic solutions for the elastic shear and peel adhesive stresses are available.

The expression for the adhesive shear stress is:

$$\tau = -\frac{1}{8}\frac{\bar{P}}{c}\left\{\frac{\beta c}{t}(1+3k)\frac{\cosh\left(\frac{\beta c x}{t\ c}\right)}{\sinh\left(\frac{\beta c}{t}\right)} + 3(1-k)\right\} \tag{6}$$

where $\bar{P}$ is the applied tensile load per unit width, c is half of the overlap length,

$$\beta^2 = 8\frac{G_a}{E}\frac{t}{t_a} \tag{7}$$

$$k = \frac{\cosh\,(u_2 c)}{\cosh\,(u_2 c) + 2\sqrt{2}\,\sinh(u_2 c)} \tag{8}$$

$$u_2 = \sqrt{\frac{3\,(1-\nu^2)}{2}}\frac{1}{t}\sqrt{\frac{\bar{P}}{tE}} \tag{9}$$

The expression for the adhesive peel stress is:

$$\sigma = \frac{1}{\Delta}\frac{\bar{P}t}{c^2}\left[\left(R_2\lambda^2\frac{k}{2} + \lambda k'\cosh(\lambda)\cos(\lambda)\right)\cosh\left(\frac{\lambda x}{c}\right)\cos\left(\frac{\lambda x}{c}\right) + \right.$$

$$\left. + \left(R_1\lambda^2\frac{k}{2} + \lambda k'\sinh(\lambda)\sin(\lambda)\right)\sinh\left(\frac{\lambda x}{c}\right)\sin\left(\frac{\lambda x}{c}\right)\right] \tag{10}$$

where

$$\lambda = \gamma\frac{c}{t} \tag{11}$$

$$\gamma^4 = 6\frac{E_a}{E}\frac{t}{t_a} \tag{12}$$

E_a is the adhesive Young's modulus

$$k' = \frac{kc}{t}\sqrt{3(1-\nu^2)\frac{\bar{P}}{tE}} \tag{13}$$

$$R_1 = \cosh(\lambda)\sin(\lambda) + \sinh(\lambda)\cos(\lambda) \tag{14}$$

$$R_2 = \cosh(\lambda)\sin(\lambda) + \sinh(\lambda)\cos(\lambda) \quad (15)$$

$$\Delta = \frac{1}{2}(\sin(2\lambda) + \sin h(2\lambda)) \quad (16)$$

The origin of the longitudinal co-ordinate *x* is the middle of the overlap.

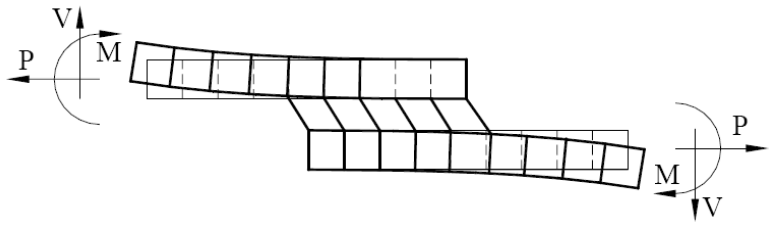

Figure 40 - Goland and Reissner's model [29].

3.3 Hart-Smith [6-7]

One of the most important works considering adhesive plasticity was done by Hart-Smith for SLJs **[11]** and DLJs **[10]**. Hart-Smith developed the analyses of Volkersen **[2]** and De Bruyne **[31]** for DLJs and the work done by Goland and Reissner **[30]** for SLJs **[11]**, for which he presented an alternative expression for the bending moment factor.

Hart-Smith's solutions accounted for adhesive plasticity, using an elastic-plastic shear stress model. He also included adherend stiffness imbalance and thermal mismatch. If we allow for adhesive plasticity, the joint strength prediction is higher than for an elastic analysis. The maximum lap-joint strength was calculated by using the maximum shear strain as the failure criterion. Any differences between the adherends result in a decrease of the joint strength.

To characterize the adhesive behaviour, Hart-Smith chose an elasto-plastic model (see Figure 41) such that the ultimate shear stress and strain in the model are equal to the ultimate shear stress and strain of the real stress-strain curve of the adhesive, the two curves having the same strain energy. He showed that any adhesive model defined by two straight lines that have the same failure stress and strain and the same strain energy predicts the same maximum joint strength developed between uniform adherends.

According to Hart-Smith, failure occurs when the adhesive reaches its limiting shear strain. For the case of a DLJ, this is illustrated in Figure 41 for balanced joints. Any thermal mismatch between adherends decreases the joint strength and this reduction is more significant with the increase of adherend thickness and stiffness. The equations require an iterative solution and describe the shear stress and strain distributions for the elastic and plastic regions in the overlap.

For SLJs, the effects of the peel stresses are more pronounced than in DLJs due to the eccentric load path, this being a particular problem for composites which have a low interlaminar tensile strength.

This problem gets more serious as the adherend thickness increases, since the total in-plane load carried can increase with thickness, but the transverse tensile stresses due to the load transfer mechanism are limited by the transversal tensile strength of the composite. Even for DLJs, the adhesive peel stress can induce composite failure. For sufficiently thin adherends, the peeling stresses are not important. Hart-Smith took that into consideration and combined elastic peel stress with plastic shear stresses. He obtained an equation for DLJs that gives the peak peel stress as a function of the peak shear stress. The adhesive peel stresses were confined to the elastic range because the interlaminar tensile strength of the laminate is generally smaller than the peel strength of typical adhesives.

A well-designed joint is one that fails outside the overlap i.e. the adhesive should never be the weak part of the joint. Therefore, for Hart-Smith, if there is a risk of high peel stresses occurring in the adhesive, this should be minimized by tapering the adherends or by locally thickening the adhesive layer. Several authors proposed analytical solutions for such cases.

Hart-Smith analysis gives a closed-form algebraic solution for the elastic shear and peel adhesive stresses

The origin of x is the middle of the overlap. The adhesive shear stress is given by

$$\tau = A_2 \cosh(2\lambda' x) + C_2 \tag{17}$$

where,

$$\lambda' = \sqrt{\left[\frac{1+3(1-\nu^2)}{4}\right]\frac{2G_a}{t_a E t}} \tag{18}$$

$$A_2 = \frac{G_a}{t_a E t}\left[\bar{P} + \frac{6(1-\nu^2)M}{t}\right]\frac{1}{2\lambda' \sinh(2\lambda' c)} \tag{19}$$

$$C_2 = \frac{1}{2c}\left[\bar{P} - 2\frac{A_2}{2\lambda'}\sinh(2\lambda' c)\right] \tag{20}$$

$$M = \bar{P}\left(\frac{t+t_a}{2}\right)\frac{1}{1+\xi c+\frac{\xi^2 c^2}{6}} \tag{21}$$

$$\xi^2 = \frac{\bar{P}}{D} \tag{22}$$

The adhesive peel stress is given by

$$\sigma = A\cosh(\chi x)\cos(\chi x) + B\sinh(\chi x)\sin(\chi x) \tag{23}$$

where

$$\chi^4 = \frac{E_a}{2Dt_a} \tag{24}$$

$$A = -\frac{E_a M[\sin(\chi c) - \cos(\chi c)]}{t_a D \chi^2 e^{(\chi c)}} \tag{25}$$

$$B = \frac{E_a M[\sin(\chi c) + \cos(\chi c)]}{t_a D \chi^2 e^{(\chi c)}} \tag{26}$$

Hart-Smith also considered adhesive shear stress plasticity, keeping the peel stress elastic. The shear stress is modelled using a bi-linear elastic-perfectly plastic approximation. The overlap is divided into three regions, a central elastic region of length *d* and two outer plastic regions. The overlap length is *l* and for a balanced lap-joint both non-linear regions have length (*l* – *d*)/2. Co-ordinates *x* and *x´* are defined in these regions

The shear stress in the plastic region is given by:

$$\tau = A_2 \cosh(2\lambda' x) + \tau_a(1 - K) \tag{27}$$

And the shear strain in the plastic region is given by:

$$\gamma = \gamma_e\{1 + 2K[(\lambda' x')^2 + \lambda' x' \tanh(\lambda' d)]\} \tag{28}$$

where

$$A_2 = \frac{K\tau_p}{\cosh(\lambda' d)} \tag{29}$$

K and *d* are solved by an iterative approach using the following equations (30-32),

$$\frac{\bar{P}}{l\tau_p}(\lambda' l) = 2\lambda'^{\left(\frac{l-d}{2}\right)} + (1 - K)(\lambda' d) + K\tanh(\lambda' d) \tag{30}$$

$$\left[1 + 3k(1 - \nu^2)\left(1 + \frac{t_a}{t}\right)\right]\frac{\bar{P}}{\tau_p}\lambda^2\left(\frac{l-d}{2}\right) = 2\left(\frac{\gamma_p}{\gamma_e}\right) + K\left[2\lambda'\left(\frac{l-d}{2}\right)\right]^2 \tag{31}$$

$$2\left(\frac{\gamma_p}{\gamma_e}\right) = K\left\{\left[2\lambda'\left(\frac{l-d}{2}\right) + \tanh(\lambda' d)\right]^2 - \tanh^2(\lambda' d)\right\} \tag{32}$$

An initial value of the bending moment factor *k* is given and the system solved for *P*, *K* and *d*. This process is repeated until there is convergence of *k*.

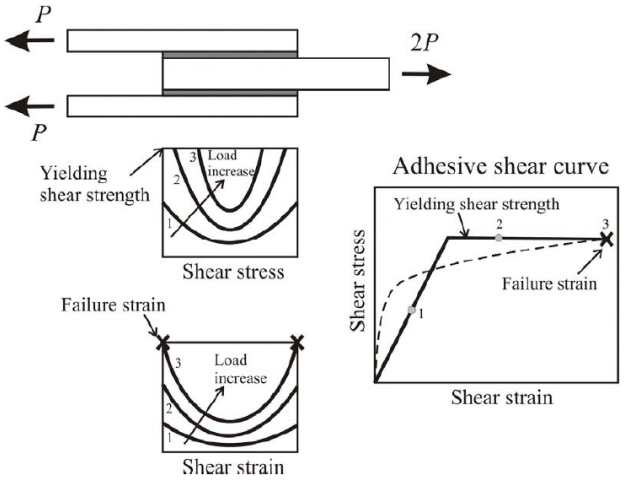

Figure 41 - Schematic explanation of shear plastic deformation of the adhesive according to Hart-Smith [6].

3.4 Bigwood and Crocombe [6-7]

Bigwood and Crocombe **[32]** initially proposed a closed-form elastic analysis of a sandwich specimen (see Figure 42) subjected to general loading. The origin of x is the left end of the overlap. A general elastic analysis and a simplified peel and shear analysis was done

Adhesive plasticity was introduced in a later paper **[33]**. The non-linear adhesive joint problem consists of a system of six, first order, non-linear differential equations. These six differential equations in conjunction with the adhesive yield model and a continuous mathematical model to represent the adhesive stress-strain curve are solved numerically using a finite difference technique.

The adherend plasticity was included in a later paper **[34]**. The problem is still governed by a system of six, first order, non-linear differential equations, but some functions appearing in that system are implicit and take different forms according to the type of loading which makes the problem more complex. The finite difference technique was also used to solve the problem.

The great advantage of the model of Bigwood and Crocombe is that it is a sandwich that can be used for any type of joint provided the boundary conditions are known. The present software includes the general elastic analysis and the adhesive plasticity. The adherend plasticity is not implemented because of the complexity of the mathematic resolution. For that case, the model of Adams is simpler to use.

The simplified adhesive peel stress is given by,

$$\sigma = A_1 \cos(K_5 x)\cosh(K_5 x) + A_2 \cos(K_5 x)\sinh(K_5 x) + \\ + A_3 \sin(K_5 x)\cosh(K_5 x) + A_4 \sin(K_5 x)\sinh(K_5 x) \quad (33)$$

And the simplified adhesive shear stress is given by,

$$\tau = C_1 \cosh(K_6 x) + C_2 \sinh(K_6 x) + C_3 \quad (34)$$

The constants $A_{1\text{-}4}$, $K_{5\text{-}6}$ and $C_{1\text{-}3}$ can be found in Bigwood and Crocombe's paper **[33]**

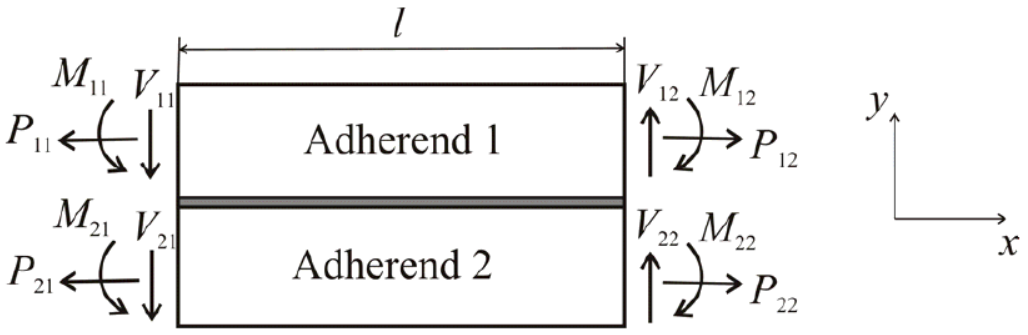

Figure 42 - Bigwood and Crocombe's diagram of adherend-adhesive sandwich under general loading [6].

Until now the Bigwood and Crocombe **[33]** (non-linear) is not fully implemented. The model was not possible due to a convergence problem in the BVP MATLAB solver, the bvp4c routine. To run the model it is necessary to solve two sets of six nonlinear (35-40), first-order differential equations. The first set has some approximations to enable the resolution of the system (see Figure 43), giving a start value to the second set of equations. In the second equations set the stresses distributions along the overlap length are given. But using the bvp4c MATLAB routine the values of the second equations set does not converge. To overcome this problem several searches were done in the web **[17-18]** and in BVP books **[38-43]**.

The system of six non-linear first order equations (35-40), where *K* is dummy parameter that has been introduced to express the second order equation in direct strain, in terms of two first order equations, is shown next.

$$\frac{dT_{1x}}{dx} = \frac{E_s * \gamma_{xy}}{2*(1+\upsilon_p)} \tag{35}$$

$$\frac{dV_{1x}}{dx} = \frac{E_s * \varepsilon_y}{(1-\upsilon_p^2)} \tag{36}$$

$$\frac{dM_{1x}}{dx} = V_{1x} - \frac{(t_1+t_a)*E_s*\gamma_{xy}}{4*(1+\upsilon_p)} \tag{37}$$

$$\frac{dK}{dx} = \frac{1}{t_a} * \left[\frac{M_{11}+M_{21}+(V_{11}+V_{21})*x-M_{1x}-(T_{1x}-T_{11})*h\prime}{D_2} - \frac{M_{1x}}{D_1}\right] \tag{38}$$

$$\frac{d\gamma_{xy}}{dx} = \frac{1}{E_2*t_2*t_a}\left\{T_{1x} * \left[1 + \frac{E_2*t_2}{E_1*t_1} + \frac{6*(1-\upsilon_2^2)*h}{t_2}\right] + 6 * M_{1x} * \left[\frac{(1-\upsilon_2^2)}{t_2} - \frac{E_2*t_2*(1-\upsilon_1^2)}{E_1*t_1^2}\right] - \right.$$
$$\left. - \frac{6*(1-\upsilon_2^2)*(V_{11}+V_{21})*x}{t_2} - (T_{11}+T_{21}) - \frac{6*(1-\upsilon_2^2)*(M_{11}+M_{21}+T_{11}*h\prime)}{t_2}\right\} \tag{39}$$

$$\frac{d\varepsilon_x}{dx} = K \tag{40}$$

Where,

$$h' = t_a + \frac{(t_1+t_2)}{2} \tag{41}$$

and ε_x , ε_y and γ_{xy} are the adhesive strains, E_s is the secant modulus and υ_p is the plastic Poisson's ratio.

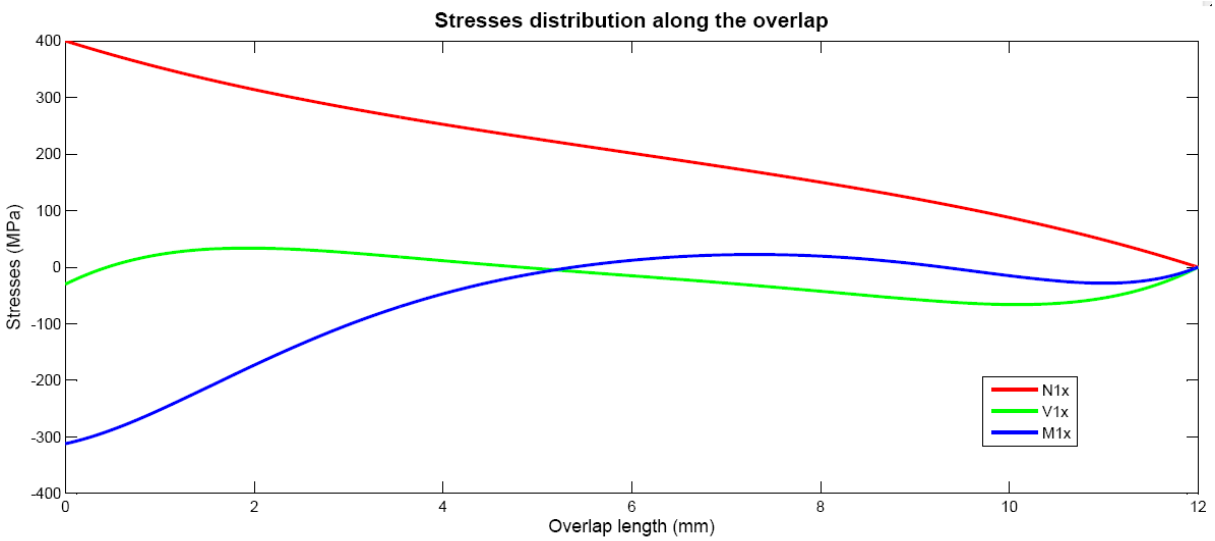

Figure 43 - Stresses distribution given by the first equations set.

3.5 Adams [6-7]

Adams **[35]** proposed a simple predictive model gives the adhesive global yielding and the adherend yielding. For substrates that yield, a plateau is reached for a certain value of overlap corresponding to the yielding of the adherend, the joint strength being easily predicted. For intermediate or brittle adhesives and non-yielding adherends, the analysis is less robust and the author suggests using the finite element method or a more complete analytical solution. The failure load of the adhesive joint (P_a), with elastic adherends, correspond the total plastic deformation of the adhesive (i.e. everywhere in yield), and the maximum load which can be carried which just creates adherend yield correspond to failure load of the adhesive join (P_s). The design methodology is represented graphically in Figure 44.

The failure load of the adhesive joint (P_a), corresponding to the total plastic deformation of the adhesive is given by,

$$P_a = \tau_y bl \tag{42}$$

where σ_y is the yield strength of the adherend.

$$\sigma_t = P/bt \tag{43}$$

$$\sigma_s = 6M/bt^2 \tag{44}$$

$$M = KPt/2 \tag{45}$$

The failure load of the adhesive joint (P_s), corresponding to the total plastic deformation of the adherends is given by,

$$P_s = \sigma_y bt/(1+3k) \tag{46}$$

The variable k is the bending moment factor which reduces (from unity) as the lap rotates under load. For low loads and short overlaps, k is approximately 1. Therefore, for such a case,

$$P_s = \sigma_y bt/4 \tag{47}$$

However, for joints which are long compared to the adherend thickness, such that $l/t \geq 20$, the value of k decreases and tends to zero. In this case, the whole of the cross-section yields in tension and:

$$P_s = \sigma_y bt \tag{48}$$

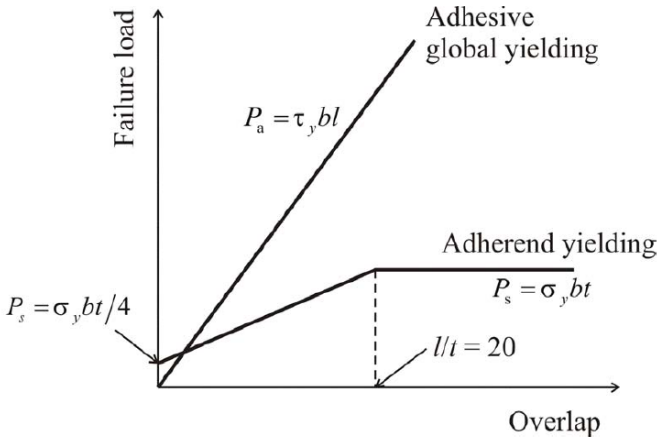

Figure 44 - Simple design methodology of single lap joints based on the adherend yielding according to Adams [7].

3.6 Frostig [6-7]

The two-dimensional linear elastic analysis of Frostig **[36]** is an extension of their previous work on the analysis of sandwich panels with a transversely flexible or stiff core, with a closed-form high-order (CFHO) theory **[37]**. The principle of virtual displacements, a variational principle, was used to derive the governing equations, the boundary conditions, and the continuity requirements. The CFHO also has the advantage of modelling the shear

stress free condition at the ends of the overlap. The adhesive shear stress was considered constant through the adhesive thickness and the peel stress was allowed to vary through the thickness. The adherends were modelled as linearly-elastic, thin beams or panels (wide beams) obeying the Euler-Bernoulli assumptions. The stress and deformation fields were uniform across the width. The adherends could be either metal or laminated composites. The shear and transverse normal (through thickness) deformations in the adherends were neglected.

Frostig's analysis was the only analytical model that considers the spew fillet. The spew fillet is a surplus of adhesive that results from the manufacturing process that is 'squeezed out' at the ends of the overlap. Real joints are always associated with this surplus material. The spew fillet was modelled by Frostig et al. using two approaches, having in mind that when there is a spew fillet the adhesive stress free condition is no longer valid or needed. In the first approach, the adhesive transverse displacement (through its thickness) was equated to the transverse displacements of both upper and lower adherends. In the second, the spew fillet was modelled as an inclined equivalent elastic bar with in-plane longitudinal stiffness only, as shown in Figure 45.

Frostig's analysis does not account for some points that are important when analysing adhesive joints, such as the shear deformation in the adherends, nonlinear geometric effects and adhesive plasticity.

This model considers composite materials in his analysis, and gives the elastic shear and peel stress in the adhesive.

The governing equations and boundary conditions, and the continuity requirements are derived for each region using the principle of virtual displacements:

$$\partial U + \partial V \equiv \partial W = 0 \tag{49}$$

where ∂U and ∂V are the internal and the external virtual work, and ∂W is the total virtual work.

The general expression that gives the natural boundary conditions at a point between regions i and $i + 1$ ($i = 1, 2$) is

$$\begin{aligned}\left(N_{jxxi} - N_{jxx(i+1)} - N_j\right)\delta u_{0j} + \left(-M_{jxxi} + M_{jxx(i+1)} - M_j\right)\phi_j + \left(Q_{jxxi} - Q_{jxx(i+1)} - \right.\\ \left. - Q_j\right)\delta w_j + b\int_0^{t_a} \tau_a \delta w_a|_{L_1}^{L_2} dz = 0\end{aligned} \tag{50}$$

where N_{xx} is the adherend longitudinal normal stress resultant, M_{xx} is the bending moment, Q_{xx} is the adherend transverse shear stress resultant, u_0 is the longitudinal displacement in the midplane of the adherends, w is the adherend transverse displacement, τ_a is the adhesive shear stress and w_a is the adhesive transverse displacement. The subscript j refers to the top and bottom adherends (j = t, b).

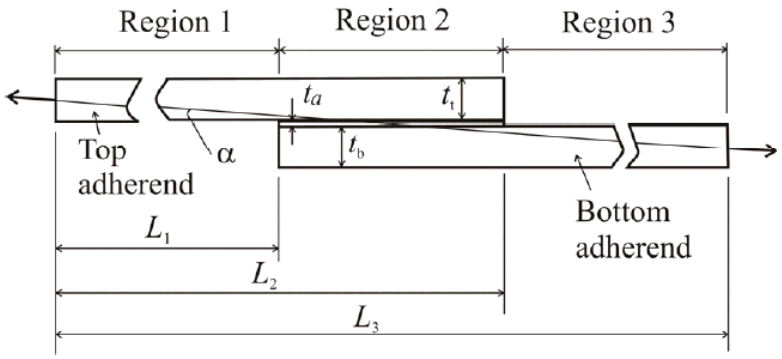

Figure 45 - Geometry and loading of typical adhesive-bonded single-lap joint with square-ends according to Frostig [7].

Due to its mathematical complexity, more than three hundred command lines in the MATLAB m file implementation, the Frostig model is mathematically implemented, but because of its complexity more time is needed to fully complete the Frostig model to a user level.

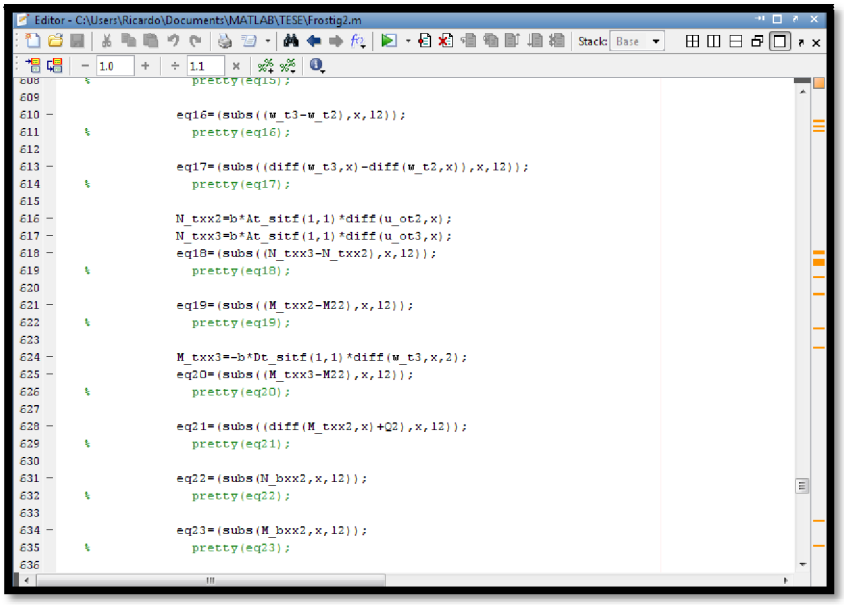

Figure 46 - Frostig MATLAB m-file.

3.7 Comparison between models

A summary of the implemented model is showed in Table 2 and Table 3.

Table 2 shows the different possibilities of analysis for each analytical model implemented in the software, showing the elasticity and/or plasticity of the materials, the geometries covered and the results given.

Table 2 - Comparison between the models implemented in the software.

Models	Adhesive Elastic	Adhesive Plastic	Adherend Elastic	Adherend Plastic	Isotropic Adherends	Anisotropic Adherends	Geometries covered	Results Given
Volkersen	Yes	No	Yes	No	Yes	No	SLJ	Shear stress
Goland and Reissner	Yes	No	Yes	No	Yes	No	SLJ	Shear/Peel Stress
Hart-Smith	Yes	Yes	Yes	No	Yes	No	SLJ and DLJ	Shear/Peel/ Deformation
Bigwood and Crocombe	Yes	Yes	Yes	No	Yes	No	Sandwich	Shear/Peel Stress
Adams	Yes	Yes	Yes	Yes	Yes	No	SLJ and DLJ	Failure load
Frostig	Yes	No	Yes	Yes	Yes	Yes	SLJ	Shear/Peel/ Displacements

In Table 3 the failure criterion is shown for each model (τ shear stress, τ_r shear strength, σ peel stress, σ_r tensile strength, γ shear strain, γ_p plastic shear failure strain, ε_e equivalent strain (von Mises), ε_r tensile failure strain, GY global yielding – all in the adhesive; AY adherend yielding). The models that have two criteria, the one that exceeded first is the valid criteria for a given case.

Table 3 - Failure criteria used for the models implemented

Models	Analysis	Failure criterion
Volkersen	Elastic	$\tau > \tau_r$
Goland and Reissner	Elastic	$\tau > \tau_r$ or $\sigma > \sigma_r$
Hart-Smith	Linear	$\tau > \tau_r$ or $\sigma > \sigma_r$
	Non-linear	$\gamma > \gamma_r$ or GY
Bigwood and Crocombe	Linear	$\tau > \tau_r$ or $\sigma > \sigma_r$
	Non-linear	$\varepsilon_e > \varepsilon_r$ or GY
Frostig	Linear	$\tau > \tau_r$ or $\sigma > \sigma_r$
Adams	Elastic/plastic adherend and ductile adhesives	GY or AY

Chapter 4

Experimental Details

Several specimens were manufactured to compare experimental results with the results obtained in the developed software. Two types of specimens were done, bulk and SLJ specimens.

The bulk specimens were used to characterize the mechanical behaviour of the adhesives. SLJ was the geometry chosen to validate the models, because it is the most common geometry in the software.

4.1 Bulk specimens

Figure 47 shows the geometry of the bulk specimens used in this work. The specimen geometry was adapted from the British Standards Institution BS 2782 standard method 320C. Two adhesives were used, one rigid (AV118) and another ductile (Araldite 420), from Huntsman Advanced Materials Americas Inc., Los Angeles, USA.

The manufacture data sheets of the adhesives are available in Annex B and C.

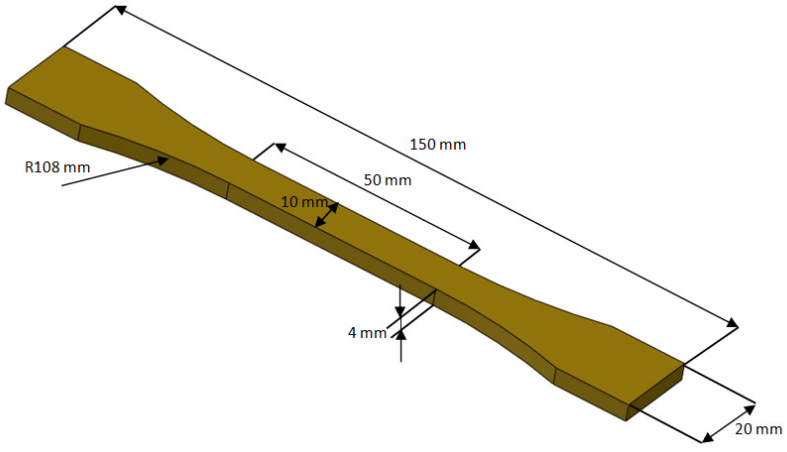

Figure 47 - Bulk specimen geometry (all dimensions in mm).

For the bulk specimen manufacture, a steel mould with a silicone frame was used (see Figure 48). The mould cavity was filled directly with the adhesive with the top mould base removed (see Figure 49). After the adhesive was subjected to the cure cycle, the adhesive plate was removed from the mould.

The mould surfaces were previously covered with mould release agent to simplify the removal of the plate (see Annex D). Each adhesive plate (see Figure 50) resulted in two bulk specimens after the machining process (see Figure 51).

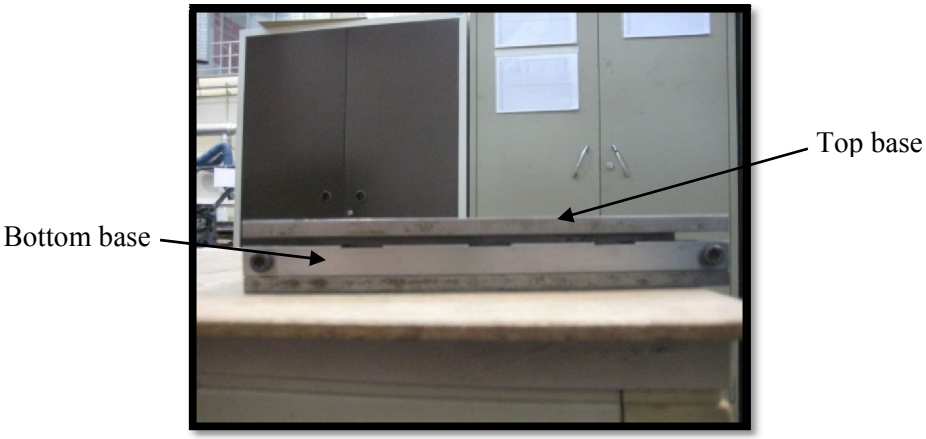

Figure 48 - Bulk steel mould.

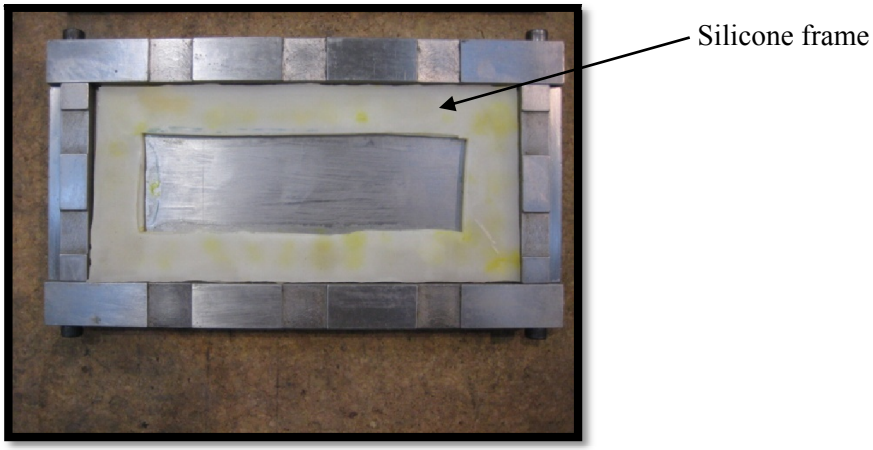

Figure 49 - Bulk specimen mould base.

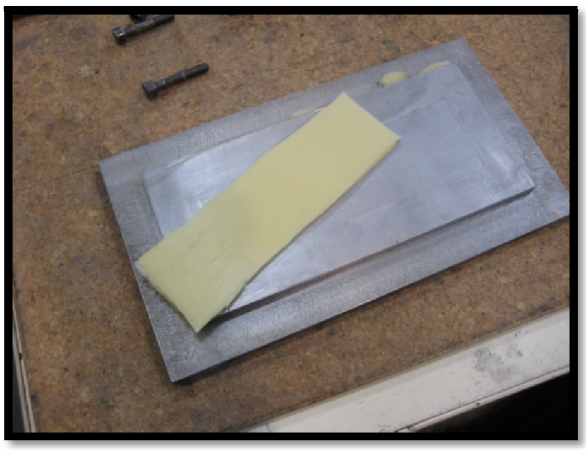

Figure 50 - Adhesive plate.

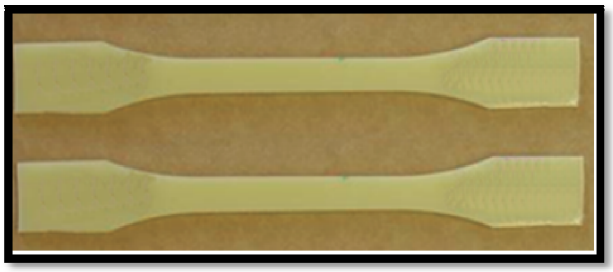

Figure 51 – Bulk specimens.

A detailed procedure of the bulk experimental process is described in Annex E.

Figure 52 shows the stress-strain curve of Araldite 420 and AV118. The ductility of Araldite 420 is clear, reaching almost nine percent of failure strain. AV 118 is more brittle presenting less plasticity at failure. The yield and failure stress are shown in Table 4.

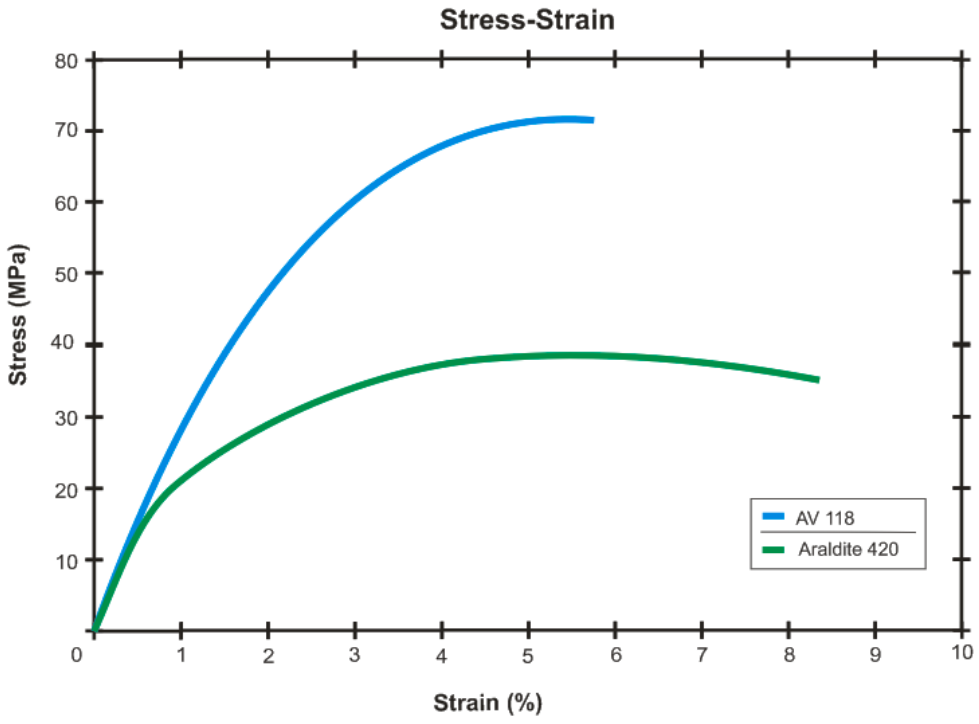

Figure 52 – Stress-Strain curve of Araldite 420 and AV 118 (1 mm/min displacement rate).

These tests were performed in IFREMER because the author had to travel there under a different project, and this way the IFREMER resources were used to the benefit of this work.

Figure 53 shows the machine where the specimens were tested (bulk and SLJ). The machine frame is a 200 kN Roell and Korthaus (Germany), retrofitted to be controlled by Bluehill software from Instron (UK). The machine was adapted by IFREMER to work with hydrostatic pressure.

a) 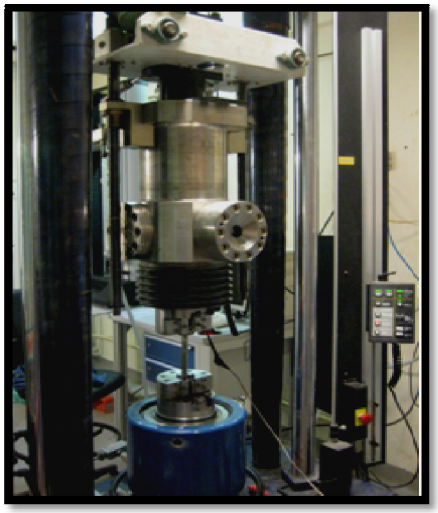 b) 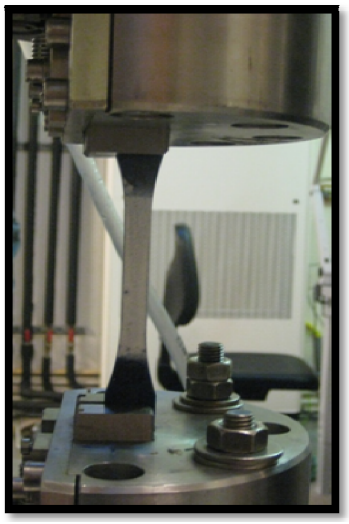

Figure 53 – Experimental testing; a) test machine b) bulk specimen in tensile machine.

The Table 4 gives the yield stress (σ_y) and the failure stress (σ_r) obtained for the two adhesives in the tensile tests.

Table 4 - Adhesive tensile yield and failure stresses.

Adhesive	Yield Stress (MPa)	Failure Stress (MPa)
AV 118	72 ± 4	73 ± 4
Araldite 420	33 ± 3	38 ± 3

With the experimental data (see Figure 52), it is possible to obtain the adhesives Young's modulus (see Table 5). The obtained Young's modulus compared well with literature results **[44-46]**.

Since it was not possible to obtain experimental adhesive Poisson's ratio values, those values were obtained from literature **[45-46]**.

Table 5 - Adhesives mechanical properties.

Material	Young's modulus (MPa)	Poisson's ratio
AV 108	2950	0.35
Araldite 420	1950	0.35

When the effect of the volumetric component of the stress is negligible, the shear strength can be predicted by the following equation **[47]**, which is derived from the von Mises criterion (see Equation 51).

$$\tau = \frac{\sigma}{\sqrt{3}} \quad (51)$$

Table 6 - Shear yield and failure stresses calculated by von Mises criterion.

Adhesive	Shear yield stress (MPa)	Shear failure stress (MPa)
AV 118	42	42
Araldite 420	19	22

However, unlike metals, polymer behaviour depends on both the hydrostatic and deviatoric stress components. The modelling of adhesives is a complex problem that is still under development **[48-49]**. There are three main pressure-dependent yield criteria described in the literature. These are the Drucker–Prager **[50]**, the Raghava **[51]** and the Dolev and Ishai **[52]** criteria. Using the Dolev and Ishai method, the strength in shear can be predicted according to Equations 52:

$$\tau = \frac{\sigma}{\sqrt{3}} \frac{2\lambda}{(\lambda+1)} \quad (52)$$

λ varies typically between 1.2 and 1.4 **[53]**. Taking a value of λ of 1.3, the shear stress given by Equation 52 are higher than the given by Equation 1 by 13%. The Dolev and Ishai criterion is more adequate for polymers than the von Mises criterion. Dolev and Ishai criterion was the used to predict the shear stress.

Table 7 - Shear yield and failure stresses calculated by Dolev and Ishai criterion.

Adhesive	Shear yield stress (MPa)	Shear failure stress (MPa)
AV 118	47	48
Araldite 420	22	25

4.2 SLJ specimens

SLJ specimens were also manufactured (see Figure 54) with the two types of adhesive previously mentioned. The adherend material chosen was an aluminium alloy from the 6000 series.

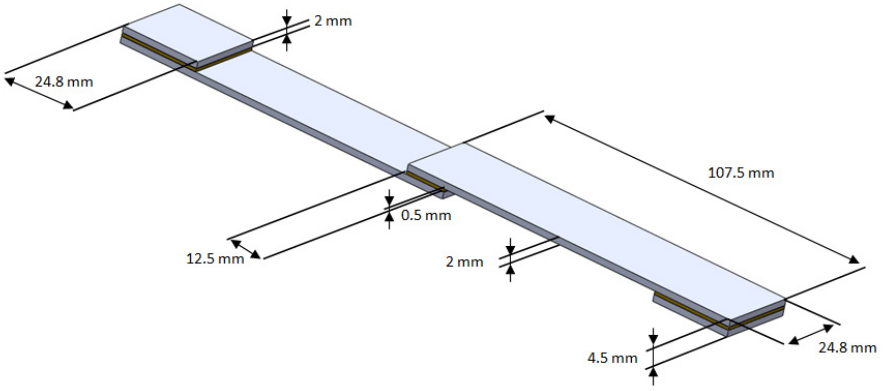

Figure 54 - SLJ specimen geometry (all dimensions in mm).

Table 8 shows the Young's modulus and Poisson's ratio of the aluminium alloy **[44]**

Table 8 - Mechanical properties of the adherend used.

Material	Young's modulus	Poisson's ratio	Yield Strength (σ_y)
Aluminium alloy	70 GPa	0.3	300 MPa

Tab ends were bonded to the edges to decrease the bending moment caused by the tensile test, although in a SLJ geometry it is impossible to have a pure shear stress. This is due to the rotation of the joint (see Figure 40).

To manufacture the SLJ specimens, a steel mould was designed to allow the production of six joints at one time (see Figure 56). The mould surfaces were previously covered with mould release agent to simplify the removal of the joints; this process is quite similar to that described in Annex D.

The adherends and tab ends were placed in the mould bottom base with the adhesive. Subsequent the mould was closed (see Figure 55) with the top plate and the cure cycle of the adhesive was applied. After the cure of the adhesive the joints were taken of the mould and separated. Finally the adhesive excess was removed of the specimens (see Figure 57).

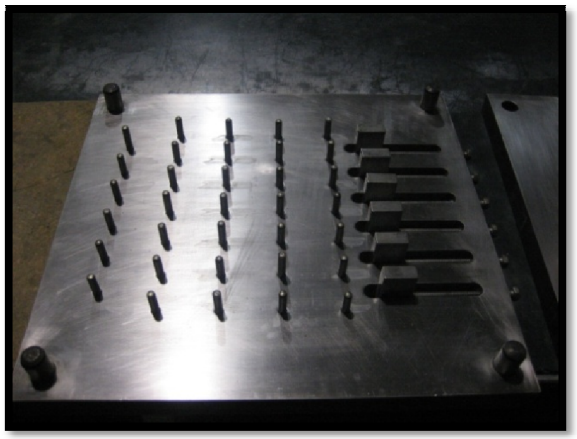

Figure 55 - SLJ specimen steel mould bottom base.

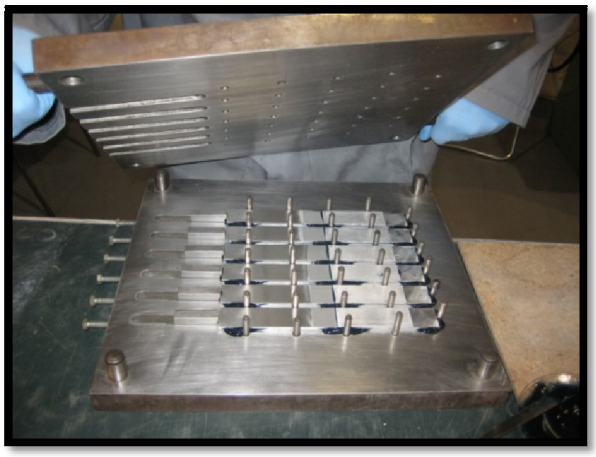

Figure 56 – Application of the top base of the SLJ mould.

Figure 57 - SLJ specimen.

A detailed procedure of the SLJ experimental manufacture is described in Annex F.

Figure 58 shows some SLJ being tested. The displacement rate for these tests was 1 mm/min.

a)

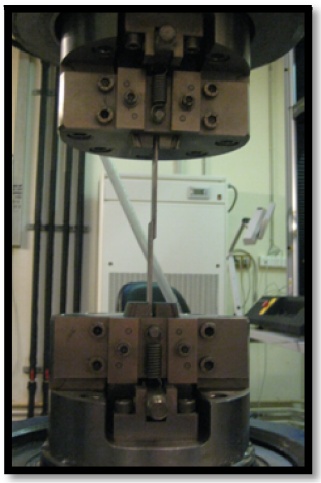

b)

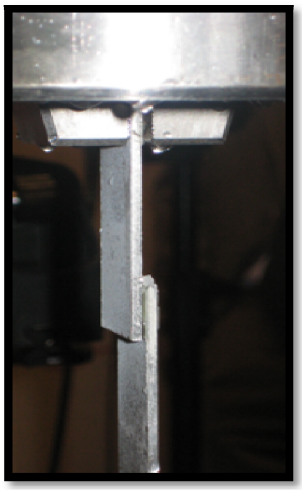

Figure 58 –SLJ specimens testing.

Chapter 5

Results

5.1 Experimental results

The Table 9 shows the failure load obtained for the two adhesives in the tensile tests.

Table 9 - Results obtained with the SLJ specimens.

Adhesive	Failure load (N)
AV 118	4900 ± 310
Araldite 420	7000 ± 455

Next are shown some images of the failure surfaces after the tests.

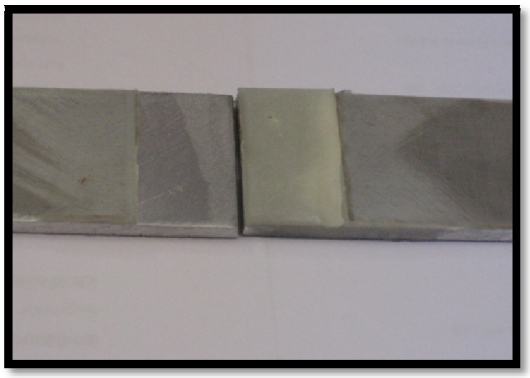

Figure 59 – AV118 SLJ failure surface.

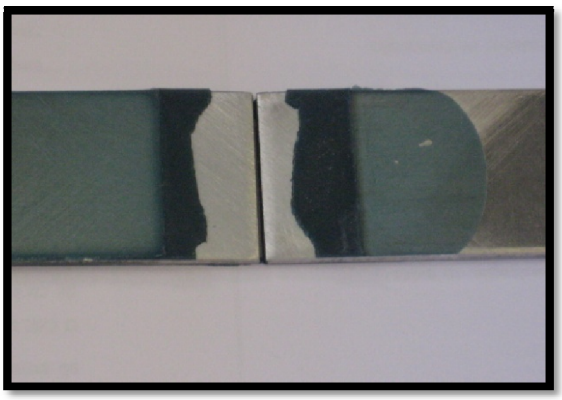

Figure 60 – Araldite 420 SLJ failure surface.

In adhesive joints, three types of failure can occur (see Figure 61); cohesive failure, adhesive failure and adherend failure. The first is when the crack failure appears in the adhesive layer, the second is when the crack appears in the interface between the adhesive and the adherend and the third occurs when the crack appears in the adherend.

Figure 61 - Different types of adhesive joint failure; a) cohesive failure b) adhesive failure c) adherend failure.

Though the expected failure was a cohesive failure, it was not apparent macroscopically. To confirm the failure type, the surfaces were analyzed in an electronic microscope, located in CEMUP (Materials Centre of the University of Porto). This analysis was only possible for Araldite 420 specimens.

The microscope used in CEMUP was the EDAX PEGASUS X4M / FEI QUANTA 400 FEG ESEM (see Figure 62) that allows the visualization of the surfaces without any type of coating or preparation.

Figure 62 - ESEM equipment in CEMUP.

After the ESEM (Environment Scanning Electron Microscope) analysis, the failure mode was not clear confirmed (see Figure 63 and Figure 64). Adhesive was almost exclusively found in the grooves formed during the surface preparation (see Figure 64).

Figure 63 shows the fracture surface of a SLJ specimen, where a piece of adhesive layer can be seen, as well as small points of adhesive in the adherend and the grooves caused by the sandpaper treatment of the adherends.

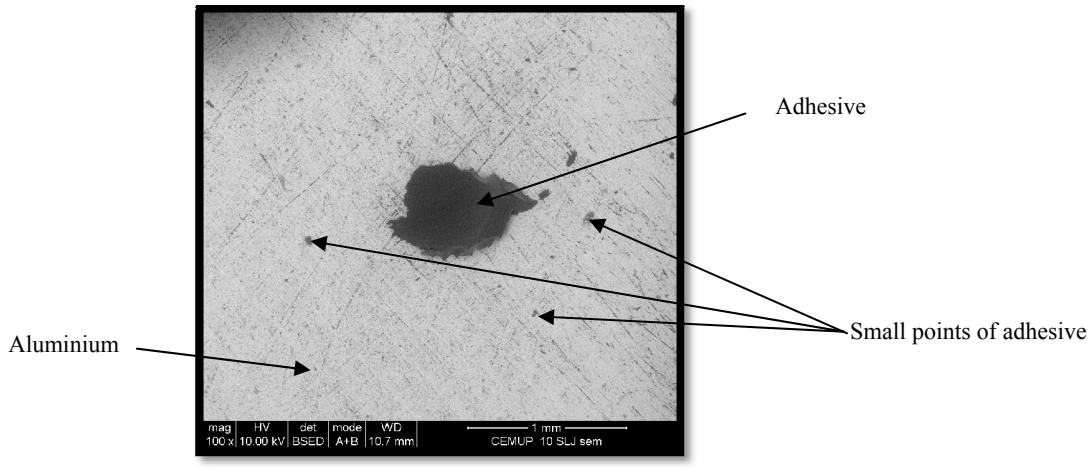

Figure 63 – Fracture surface amplified 100x.

In a more amplified image (see Figure 64), it can be seen the adherend grooves were completely filled with adhesive, being a possible indication of a very small adhesive layer in the fracture surface.

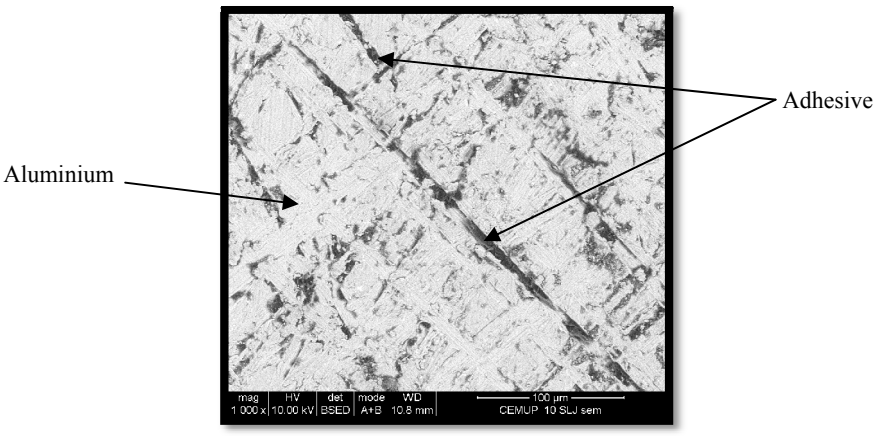

Figure 64 – Fracture surface amplified 1000x.

Without clear confirmation of the failure mode, an XPS analysis (X-ray Photoelectron Spectroscopy) was made. To obtain initial reference values, an XPS analysis was done to the adhesive (see Figure 65) and the adherend (see Figure 66). Those values were then compared with the values obtained in the SLJ failure surface (see Figure 67).

Figure 65 shows the most relevant elements present in the Araldite 420 bulk specimen. The analysis shows that C (carbon), O (Oxygen) and Si (silicon) are the major constitutive elements.

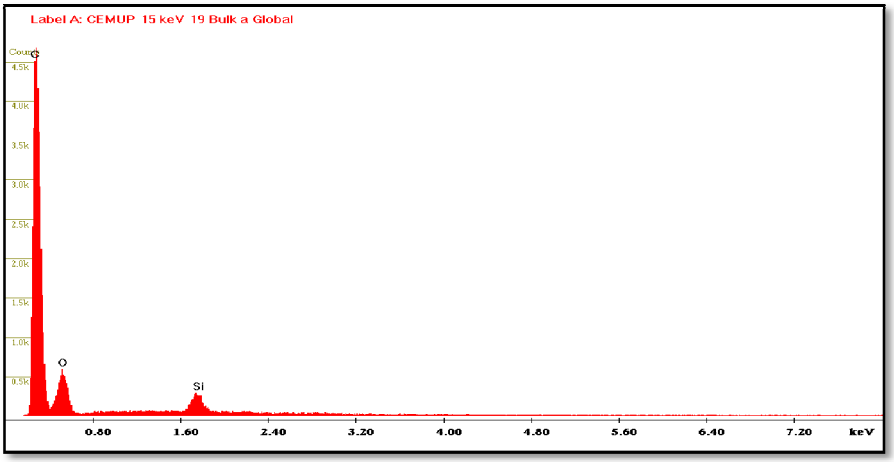

Figure 65 - XPS bulk analysis.

Figure 66 shows the major constitutive elements of the aluminium adherends. As expected, the analysis detected a large presence of Al (Aluminium). Others elements, like C and O were detected but in a very small quantity when compared with Al.

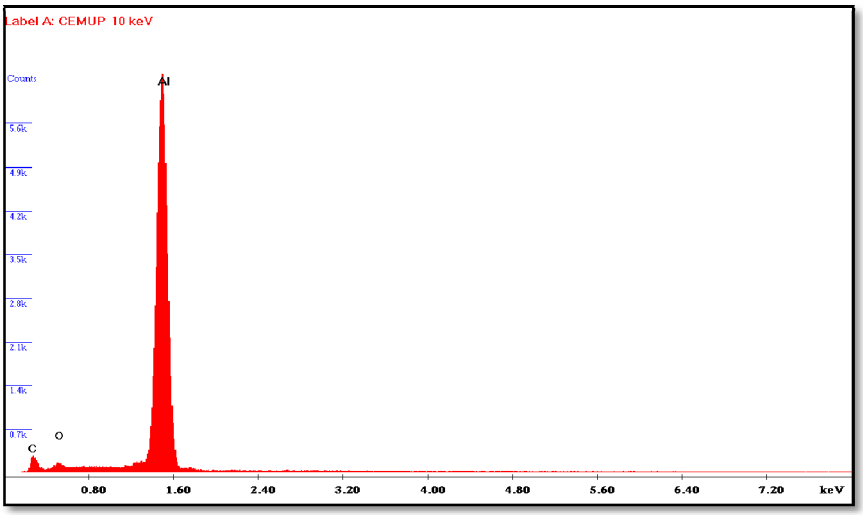

Figure 66 - Adherend XPS analysis.

Finally, an XPS analysis was made to the SLJ failure surface. In The elements present in the surface are shown in Figure 67.

The elements in greater quantity are C, O, Al and Si. This confirms the present of a very thin adhesive layer in the failure surface. The presence of Al elements is probably due the reduced thickness of the adhesive layer. The XPS analysis detects elements within 4-5 nm of the surface specimen, the thickness of the adhesive layer must be less than to 5 nm.

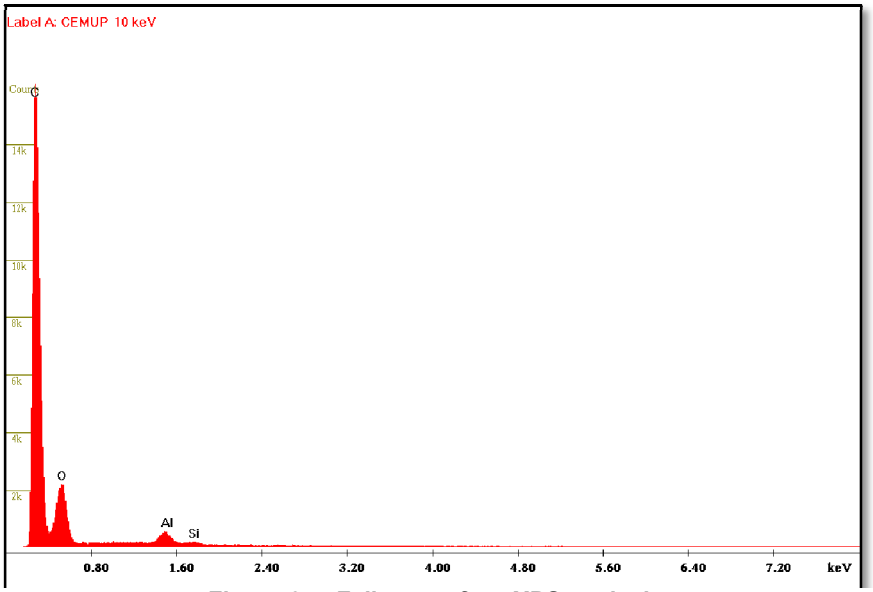

Figure 67 - Failure surface XPS analysis.

After the ESEM and XPS analysis it can be concluded that the failure was cohesive due to the presence of a small adhesive layer in the failure surface.

Another method of preparing the surfaces was attempted for increasing the adhesive layer present in the failure surface. The alternative method chosen was chromic acid etching (see Annex G). With this method the failure mode was the same (see Figure 68). The difference in this case was the increase of adhesive amount in the adherends surface detected in ESEM (see Figure 69). The failure load of the etched specimens increased slightly when compared with the sanded specimens.

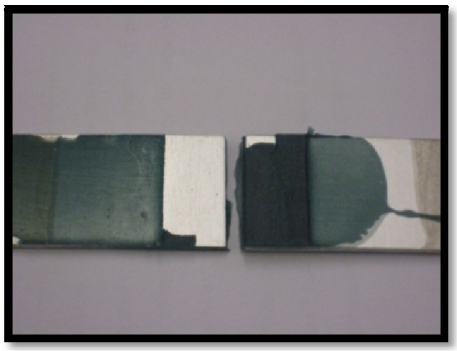

Figure 68 – Failure surface of the etched specimen.

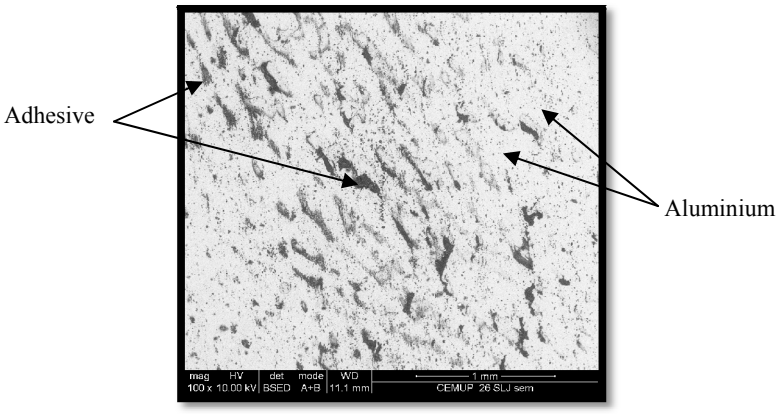

Figure 69 – Failure surface of the etched overlap amplified 100x.

For the AV 118 specimens this analysis was not done due to financial issues, but in a macroscopic view the failure looked identical to the Araldite 420 specimens. The failure strengths were very similar to those encountered by others researchers **[45]**. This fact allows us to extrapolate that the AV118 specimens failure mode was also cohesive. To confirm the failure, mode an ESEM/ XPS analysis should be done.

5.2 Joint strength prediction

The experimental results presented here and others taken from the literature [**7]** were used to assess the closed-form models implemented in the software.

The following conditions were used:

Table 10 - Summary of the aspect consider by the software.

Materials	Adherend behaviour	Adhesive behaviour	Adherend properties	Geometry consider	Applied force
AV118	Elastic	Elastic/Plastic	Isotropic	SLJ	Traction
Araldite 420	Elastic	Elastic/Plastic	Isotropic	SLJ	Traction

The adhesive behaviour type is the only difference between the experimental specimens. For the AV 118 specimens the chosen behaviour was elastic because AV 118 is an adhesive with reduced ductility. For Araldite 420 specimens the chosen adhesive behaviour was plastic because Araldite 420 is a ductile adhesive.

The models selected were the Volkersen, Goland and Reissner, Hart-Smith and Adams. A comparison between these models was made to discuss the ones that better predict the failure load in the two experimental cases.

Table 11 shows the software input data for the joint geometry used in the experimental tests.

Table 11 – Geometry and adherend properties input data.

Variable	Value	
	Geometry window	
Adherend 1 thickness (mm)	2	
Adherend 2 thickness (mm)	2	
Adhesive thickness (mm)	0.5	
Overlap length (mm)	12.5	
Width (mm)	24.8	
	Material window	
	Adherend 1	**Adherend 2**
Young's modulus (GPa)	70	70
Poisson's ratio	0.33	0.33
Yield stress (MPa)	300	300

Table 12 shows the software input data for the adhesive properties (Araldite 420 specimens and AV 118 specimens)

Table 12 – Adhesive properties input data

Variable	Value	
	Material window	
	AV 118 adhesive	**Araldite 420 adhesive**
Young's modulus (GPa)	2950	1950
Poisson's Ratio	0.35	0.35
Yield stress (MPa)	47	22
Failure stress (MPa)	48	25

Figure 70 shows the experimental results and the model predictions in terms of failure load for the AV 118 specimens.

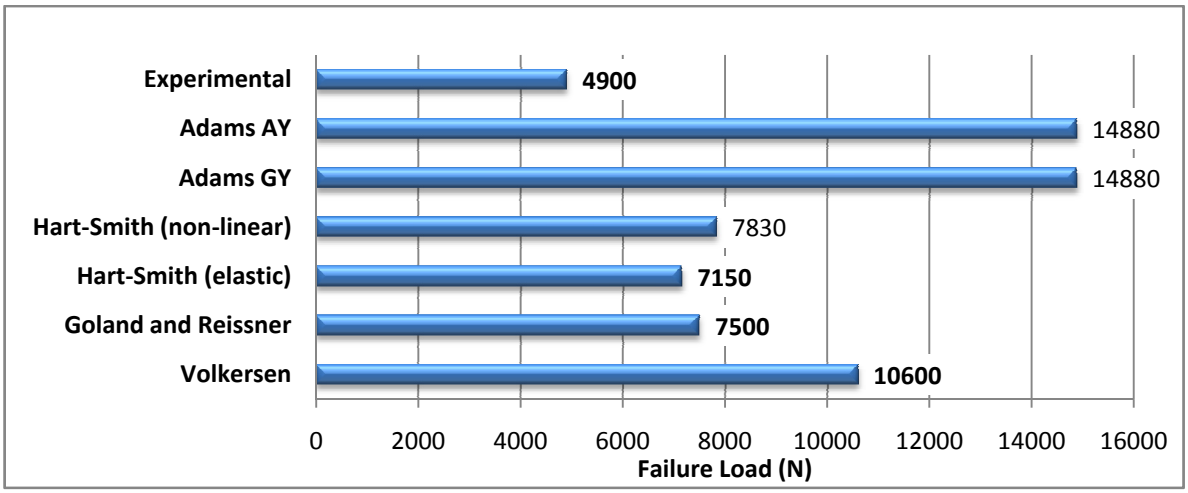

Figure 70 - Comparison between the experimental data and the model predictions for AV118 specimens.

The models that predict a failure load near the obtained experimental values were those that consider the adhesive elastic behaviour in their analysis, except for the Volkersen's model.

The Volkersen's model does not take into account the rotation of the SLJ, which increases the predicted failure load compared with the other elastic models.

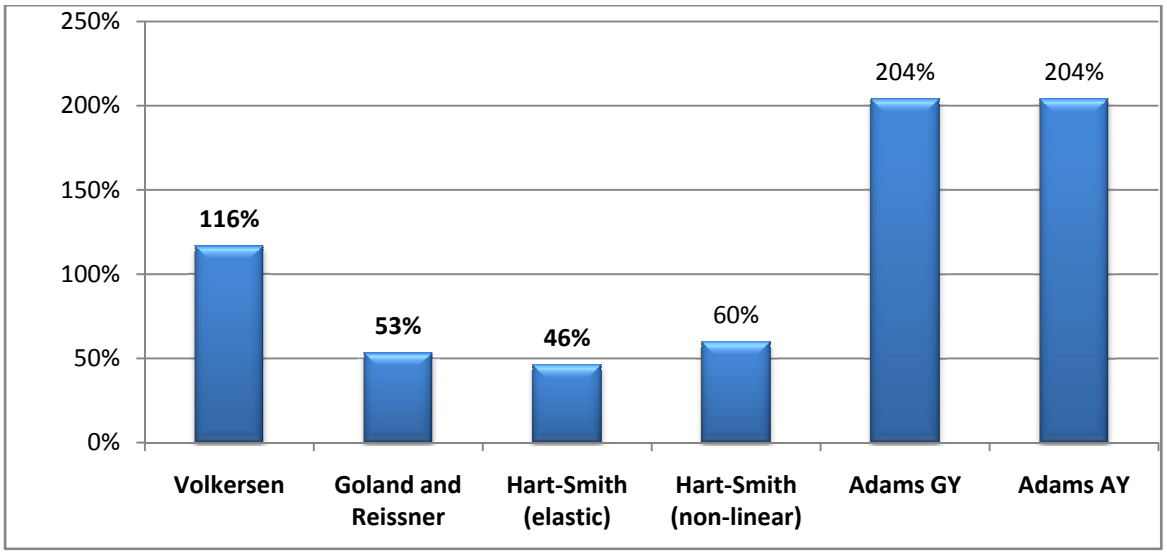

Figure 71 – Error comparison between the models predictions and the experimental results of AV 118 specimens.

The error between the predictions and the experimental values are relatively large, mainly due to the fact that the elastic models consider that the SLJ specimens failure load increases with the adhesive thickness, which in practice is not true.

The elastic models predict the failure load with more accuracy for joints that have a thin adhesive layer, approximately 0.1-0.3 mm. These values are the most used in practice because they allow for greater joint strength. It can be concluded that with brittle adhesives, SLJ specimen's failure load can be predicted using the models that consider the adhesive elasticity, being this prediction more accurate for joints that have a thin adhesive layer.

Figure 72 shows the comparison between the failure load prediction of the elastic models and the experimental values obtained in literature **[7]**. It can be seen that the increase of the adhesive thickness leads to an increase of the predicted failure loads. However, in practice this does not happen. The predicted failure load deviates from the experimental results as the adhesive thickness increases.

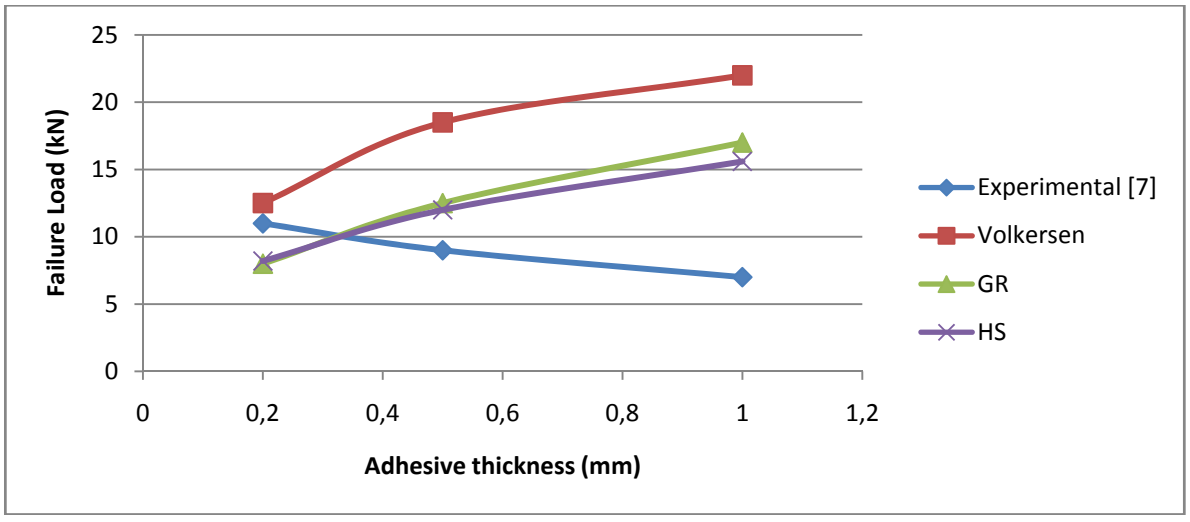

Figure 72 – Influence of the adhesive thickness in the failure load prediction of the elastic models.

Next is shown the input data used to obtain the results shown in Figure 72.

Table 13 shows the geometry and the adherends properties (high-strength steel) input data.

Table 13 - Geometry and adherends properties input data.

Variable	Value	
	Geometry window	
Adherend 1 thickness (mm)	2	
Adherend 2 thickness (mm)	2	
Overlap length (mm)	25	
Width (mm)	25	
	Material window	
	Adherend 1	**Adherend 2**
Young's modulus (GPa)	210	210
Poisson's ratio	0.33	0.33

Table 14 shows the software input data for the adhesive properties.

Table 14 – Adhesive properties input data

Variable	Value
	Material window
	Hysol 9321 adhesive
Young's modulus (GPa)	3870
Poisson's Ratio	0.35
Shear Yield stress (MPa)	25
Shear Failure stress (MPa)	33

Figure 73 shows the experimental results and the model predictions in terms of failure load for Araldite 420 specimens.

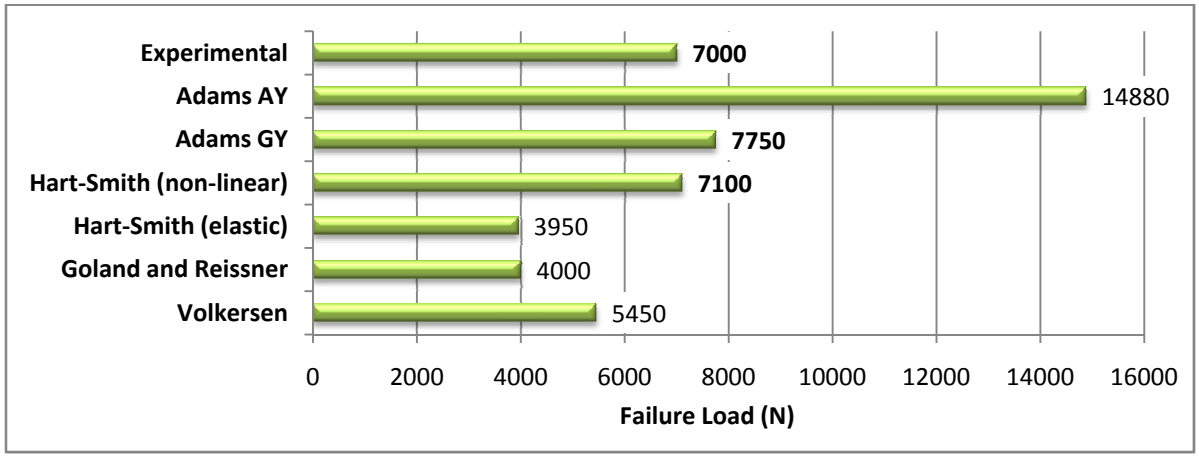

Figure 73 - Comparison between the experimental data and the model predictions for AV118 specimens.

In the Araldite 420 case, only the models that consider adhesive plasticity compare well with the experimental values. Due to the large ductility of Araldite 420, it has a different behaviour than an elastic adhesive. The plasticity of the adhesive causes a stress redistribution along the overlap using the less stressed parts of the overlap. The joint strength thus increases in relation to an adhesive with no ductility, where only the ends of the overlap work.

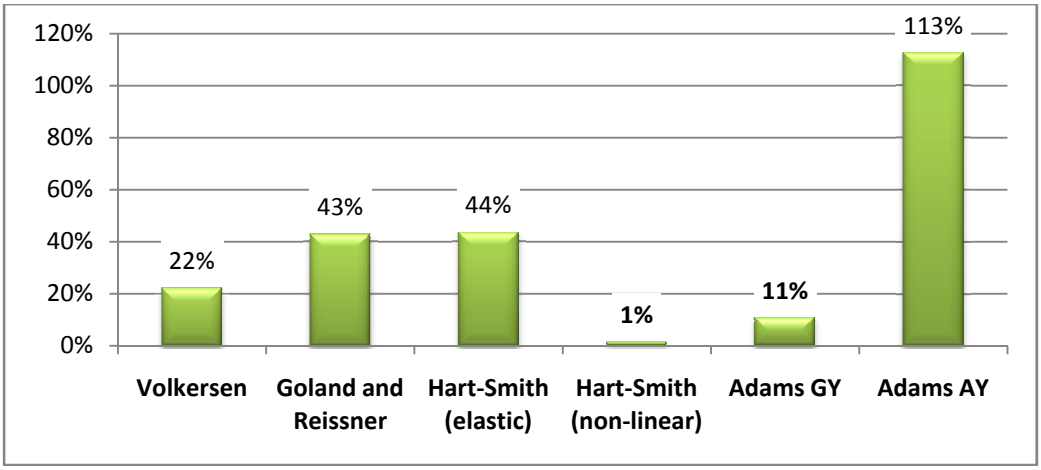

Figure 74 - Error comparison between the model predictions and the experimental results of Araldite 420 specimens.

It can be concluded that with ductile adhesives, SLJ specimen's failure load can be predicted using the models that consider adhesive plasticity.

When the adherends yield, the only implemented model capable to predict the failure load is the Adams' model. Comparison with experimental values **[7]** shows that the Adams' model for adherend plasticity predicts well the failure loads (see Figure 75).

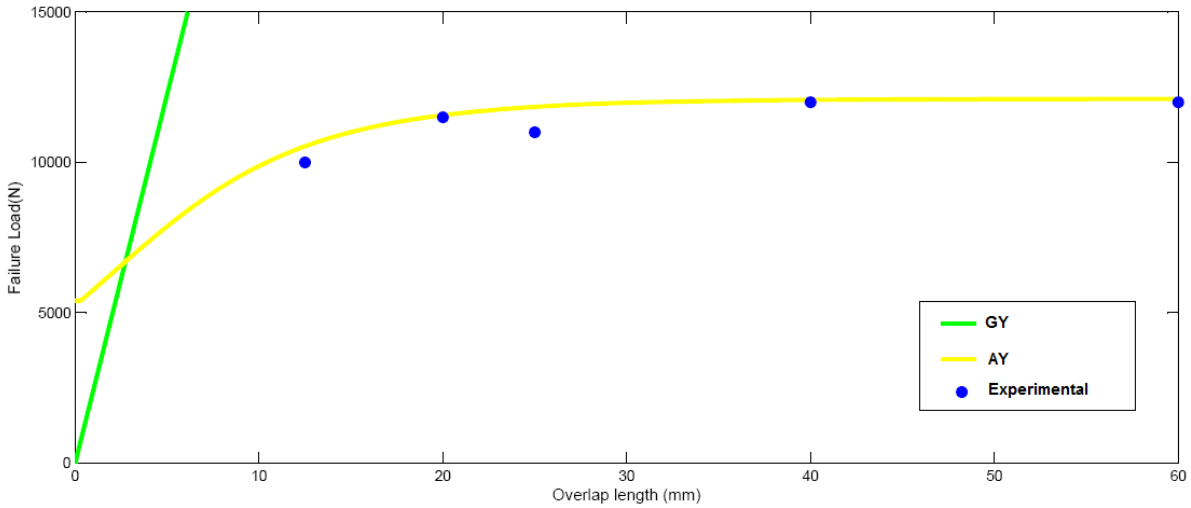

Figure 75 – Comparison between the literature experimental values [7] and the Adams' model prediction.

Next is shown the input data used to obtain the results show in Figure 75

Table 15 shows the geometry and the adherends properties (mild steel) input data-

Table 15 - Geometry and adherends properties input data.

Variable	Value	
	Geometry window	
Adherend 1 thickness (mm)	1.6	
Adherend 2 thickness (mm)	1.6	
Adhesive thickness (mm)	0.2	
Width (mm)	50	
	Material window	
	Adherend 1	**Adherend 2**
Young's modulus (GPa)	210	210
Poisson's ratio	0.33	0.33
Tensile Yield Stress (MPa)	270	270

Table 16 shows the software input data for the adhesive properties.

Table 16 – Adhesive properties input data.

Variable	Value
	Material window
	AV 119 adhesive
Young's modulus (GPa)	3050
Poisson's Ratio	0.35
Shear Yield stress (MPa)	49
Shear Failure stress (MPa)	49

Chapter 6

Conclusions and Future Work

6.1 Conclusions

After performing this work it is possible to conclude that there are several closed-form models in the literature but they are scattered and not ready to use.

Most of the models are applicable to single and double lap joints. However, the model of Bigwood and Crocombe can be used for any type of joint that contains a sandwich joint. Elastic and plastic analyses, whether in the adhesive or in the adherend, can be carried out. Isotropic and composite materials can also be studied.

The implementation of a closed-form model can take some minutes to several hours, depending on the complexity of the model.

The development software solve this problem due this user-friendly interfaces, which allows almost anyone to work with the software, requiring a minimal knowledge about the subject.

Once the software is fully completed the software will be able to predict the joint strength in practically all situations, covering isotropic and anisotropic materials, elasticity and plasticity of the adherends and adhesive and several different type of joints analysis, such as SLJ, DLJ, sandwich joint,T-joint, corner joint and tubular joints.

The closed-form models consider cohesive failure. The experimental failures were cohesive, as was confirmed in the ESEM / XPS analysis, which allowed to do a comparison between the experimental and the software results.

It can be concluded that with brittle adhesives, joint failure load can be predicted using the models that consider the adhesive elastic, but only for thin adhesive layer thickness. For thick layers this is not valid because the predicted loads diverge significantly from the experimental values.

For ductile adhesives, it was found that the models that consider adhesive plasticity are better suited to predict the failure load of the adhesive joint.

Adams' model can predict well the failure loads of joints where the adherends yield.

6.2 Future work

The creation of a software of this kind is a very long and meticulous process. To fully develop this software it would take several years.

As future work, a bug kill process of the development software can be performed, increasing its robustness and efficiency. The models under implementation (Frostig and Bigwood and Crocombe non-linear) should also be fully completed.

Other improvement possibilities are the implementation of more closed-form models, covering a wider scope of application analysis (more geometries and situations), and compiling the software in order to be a stand-alone executable program, not requiring the pre installation of MATLAB.

Modifications can also be done to some of the already implemented models, to include in the analysis the effect of temperature on the properties of the adhesive.

References and Bibliography

[1] National Physical Laboratory, "Design and Testing of Bounded and Bolted Joints", Queen's Printer, Scotland, 2007.

[2] Volkersen, O., "Die Niektraftvertleiling in Zugheanspruchten mit Konstanten Laschenquerschritten", *Luftfartfoeshing*, Volume 15, 1938, pp. 41–47.

[3] Chalkley, P. and Rose, F., "Stress Analysis of Double-Strap Bonded Joints Using a Variational Method", *International Journal of Adhesion and Adhesives*, Volume 21, Number 3, 2001, pp.241-247.

[4] Adams, R.D., "Strength Predictions for Lap Joints, Especially with Composite Adherents - A Review", *Journal of Adhesion*, Volume 30, 1989, pp.219-242.

[5] Carpenter, W.C., "A Comparison of Numerous Lap Joint Theories for Adhesively Bonded Joints", *Journal of Adhesion*, Volume 35, Number 1, 1991, pp.55-73.

[6] da Silva, L.F.M., das Neves P.J.C., Adams, R.D., Spelt, J.K., "Analytical models of adhesively bonded joints – Part I: Literature survey", *International Journal of Adhesion and Adhesives,* Volume 29, , 2009, pp.319-330.

[7] da Silva, L.F.M., das Neves, P.J.C., Adams, R.D., Wang, A., Spelt, J.K., "Analytical models of adhesively bonded joints – Part II: Comparative study", *International Journal of Adhesion and Adhesives*, Volume 29, 2009, pp.331-341.

[8] Hart-Smith, L.J., "Analysis and Design of Advanced Composite Bonded Joints", NASA Report CR 2218, 1974.

[9] Hart-Smith, L.J., NASA Report TR-11234, 1973.

[10] Hart-Smith, L.J., NASA Report CR-112235, 1973.

[11] Hart-Smith, L.J., "Adhesive-Bonded Single-Lap Joints", NASA Report CR-112236, 1973

[12] Hart-Smith, L.J., "Adhesive-Bonded Scarf and Stepped-Lap Joints", NASA Report CR-112237, 1973.

[13] Hart-Smith, L.J., "Adhesive-Bonded Double-Lap Joints", NASA Report CR-112238, 1973.

[14] Oakeshott, J.L., Soininen, R. and Matthews, F.L., "Review of Composites – Related Software. Final Report. Part I: Non-FE Software", Technical Report TR96/01, Centre for Composite Materials, Imperial College, London, 1996.

[15] Maplesoft, Canada, www.maplesoft.com.

[16] SourgeForge Project, USA, maxima.sourceforge.net.

[17] MathWorks, USA, www.mathworks.com.

[18] MathWorks, "MATLAB V7 Introductory and Programming- MathWorks Documentation", Massachusetts: The MathWorks, Inc., 2007.

[19] Hunt, B. R., Lipsman, R. L., Rosenberg, J. M., "A Guide to MATLAB for Beginners and Experienced Users", New York: Cambridge University Press, 2001.

[20] Register, A. H., "A Guide to MATLAB Object-Oriented Programming", Georgia: SciTech Publishing Inc., 2007.

[21] Knight, A., "Basics of MATLAB and Beyond", Florida: CRC Press LLC, 2000.

[22] Mirza, S.M., "Introduction to MATLAB", Pakistan: Pakistan Institute of Engineering and Applied Sciences, 2002.

[23] Otto, S.R., Denier, J.P., "An Introduction to Programming and Numerical Methods in MATLAB", Australia: Springer, 2005.

[24] Marchand, P., Holland, O.T., "Graphics and GUIs with MATLAB", Florida: Chapman & Hall/CRC, 2003.

[25] Davis, T.A., Sigmon, K., "MATLAB Primer", 7th Ed, Florida: Chapman & Hall/CRC, 2005.

[26] MathWorks, "Engineering Matlab Programming", Massachusetts: The MathWorks, Inc., 2004.

[27] Bielajew, A.F., "Introduction to Computers and Programming", Michigan: The University of Michigan, 2002.

[28] de Moura, M. F.S.F., de Morais, A.B., de Magalhães, A.G., "Materiais Compósitos - Materiais, Fabrico e Comportamento Mecânico", Porto: Publindústria, 2005.

[29] da Silva, L.F.M., de Magalhães, A.G. and de Moura, M.F.S.M., "Juntas Adesivas Estruturais", Porto: Publindústria, 2007.

[30] Goland, M., Reissner, E., "The stresses in cemented joints", *Journal of Applied Mechanics*, Volume 66, 1944, pp.A17-27.

[31] de Bruyne, N.A., "The Strength of Glued Joints", *Aircraft Engineering and Aerospace Technology*, Volume 16, 1944, pp.115-118.

[32] Bigwood, D.A., Crocombe, A.D., "Elastic analysis and engineering design formulae for bonded joints", *International Journal of Adhesion and Adhesives*, Volume 9, pp.229-242.

[33] Bigwood, D.A., Crocombe A.D., "Non-linear adhesive bonded joint design analysis", *International Journal of Adhesion and Adhesives*, Volume 10, 1990; pp.31-41.

[34] Crocombe A.D., Bigwood, D.A., **"**Development of a full elasto-plastic adhesive joint design analysis", *Journal of Strain Analysis for Engineering Design*, Volume 27, 1992, pp. 211-218.

[35] Adams, R.D., Comyn, J., Wake, W.C., "Structural adhesive joints in engineering", 2nd Ed, London: Chapman & Hall, 1997.

[36] Frostig, Y., Thomsen, O.T., Mortensen F., "Analysis of Adhesive-Bonded Joints, Square-End, and Spew-Fillet—High-Order Theory Approach", *Journal of Engineering Mechanics*, Volume 125, 1999, pp. 1298-1307.

[37] Frostig, Y., Baruch, M., Vilnai, O., Sheinman, I., "High-order theory for sandwich-beam bending with transversely flexible core", *Journal of Engineering Mechanics*, Volume 118, 1992, pp.1026-1043.

[38] Kiusalaas, J., "Numerical Methods in Engineering with MATLAB", New York: Cambridge University Press, 2005.

[39] Mathews, J.H., Fink, K.D., "Numerical Methods using MATLAB", USA: Prentice Hall, 1999.

[40] Lee, H.J., Schiesser, W.E., "Ordinary and Partial Differential Equation Routines in C, C++, Fortran, Java, Maple, and MATLAB", Florida: Chapman & Hall/CRC, 2004.

[41] Shampine, L.F., Gladwell, I., Thompson, S., "Solving ODEs with MATLAB", New York: Cambridge University Press, 2003.

[42] Shampine, L.F., Gladwell, I., "Solving ODEs with Matlab: Instructor's Manual", 2002.

[43] Zeitz, M., "Boundary Value Problem Solver in Matlab", Germany: University of Stuttgart/ISR, 2005.

[44] Automation Creations, Inc, Virginia, www.matweb.com.

[45] Banea, M.D., da Silva, Lucas F.M., "Mechanical Characterization of Adhesives for Automotive Industry Applications", Proceedings of CLME'2008, FEUP, 2008.

[46] Fawzia, S., Al-Mahaidi, R., Zhao, Xiao-Ling, "Experimental and finite element analysis of a double strap joint between steel plates and normal modulus CFRP", *Composite Structures*, 2006, pp.156-162.

[47] Jeandrau, J.P., "Analysis and Design Data for Adhesively-bonded Joints", *International Journal of Adhesion and Adhesives*, Volume 11, 1991, pp.71-79.

[48] Duncan, B., Dean, G., "Measurements and models for design with modern adhesives", *International Journal of Adhesion and Adhesives*, Volume 23, 2003, pp.141-149.

[49] Yu, X.X., Crocombe, A.D., Richardson, G., "Material modeling for rate-dependent adhesives", *International Journal of Adhesion and Adhesives*, Volume 21, 2001, pp.197–210.

[50] Drucker, D.C., Prager, W., "Soil mechanics and plastic analysis or limit Design", *Quarterly of Applied Mathematics*, Volume 10, 1952, pp.157-165.

[51] Raghava, R.S., Cadell, R.M., Yeh, G.S., "Macroscopic yield behaviour of polymers", *Journal of Material Science*, Volume 8, 1973, pp.225-232.

[52] Dolev, G., Ishai, O., "Mechanical Characterization of Adhesive Layer "In Situ" and as Bulk Material", *Journal of Adhesion*, Volume 12, 1981, pp.283-294.

[53] Adams, R.D., Comyn, J., Wake, W. C., "Structural Adhesive Joints in Engineering", 2nd Ed., London: Chapman & Hall, 1997.

Annexes

Annex A – Finite Elements Packages

Name	Supplier	Application	Features
ABAQUS	SIMULIA, Dassault Systèmes	• General purpose FE program • Linear, non-linear and coupled analysis • Large materials model library	• Anisotropic material models in all elements • 2-D and 3-D plate/shell and solid elements • Temperature and strain-rate dependence of properties • Fracture mechanic/ crack propagation analysis • Maximum stress and strain, Tsai-Hill, Tsai-Wu, Azzi-Tsai-Hill and user defined failure criteria
ANSYS	Swanson Analysis System Inc.	• General purpose FE program • Non-linear analysis (non-composite applicable) • Pre- and post-processing	• Isotropic and orthotropic material properties • 2-D and 3-D plate/shell and solid elements • Laminated shell elements • Crack-tip solid and thick-shell elements • Maximum stress and strain, Tsai-Wu and user defined failure criteria
LUSAS	FEA Ltd.	• General purpose FE program • Linear and non-linear analysis • Static, creep, fatigue and dynamic analysis	• Plate/shell and solid elements • 2-D and 3-D interface elements • Laminate analysis/Hashin damage model • Delamination elements for fracture mechanics • Fatigue analysis of structural components • Tsai-Hill, Hoffmann, Hashin, Tsai-Wu failure criteria
COSMOS	Structural Research& Analysis Corp.	• General purpose FE program • Linear and non-linear analysis • Static and dynamic analysis • 2-D and 3-D structural and thermal models	• Plate/shell and solid elements • Delamination elements for fracture mechanics • Fatigue analysis of structural components • Tsai-Hill and Tsai-Wu failure criteria
NASTRAN	MacNeal-SchwendlerCorp.	• General purpose FE program • Static and dynamic analysis • Linear and non-linear analysis • Pre- and post-processing by PATRAN	• Plate/shell elements - allowance for orthotropic temperature dependent properties • Ply stresses • Tsai-Hill, Hoffmann and Tsai-Wu failure criteria
NISA	Engineering Mechanics Research Corp.	• General purpose FE program • Linear, non-linear and coupled analysis	• Solid and thick-shell elements • Laminated shell elements • In-plane and interlaminar stresses • Maximum stress and strain, von Mises, Tsai-Wu, delamination failure criteria

Annex B – Araldite 420 Manufacture Data Sheet

Huntsman Advanced Materials Americas Inc.
5121 San Fernando Road West
Los Angeles, CA 90039
818.247.6210

Customer Service Hotline: 800.367.8793
Customer Service Faxline: 517.351.6255
Technical Inquiries: 800.817.8260

website: www.araldite.com
e-mail: adhesives_group@huntsman.com

HUNTSMAN

Product Data

ARALDITE® AV 118
EPOXY ADHESIVE PASTE

DESCRIPTION: Araldite AV 118 epoxy adhesive is a one-component, multi-purpose paste that is designed for heat curing at temperatures from 248°F to 356°F (120°C to 180°C). The tough, high-strength adhesive is well suited for metal bonding and joining materials including ceramics, glass, rubber and temperature-resistant plastics.

APPLICATIONS: Metal- to-metal bonding.

TYPICAL PROPERTIES:

Property	Test Method	Test Values[1] One Component Epoxy
Color/appearance	Visual	Beige paste
Specific Gravity	ASTM D-792	1.10 - 1.20
Viscosity at 77°F (25°C), cP		90,000

PROCESSING

Pretreatment

The strength and durability of a bonded joint are dependant on proper treatment of the surfaces to be bonded. At a minimum, joint surfaces should be cleaned with a good degreasing agent such as acetone or other proprietary degreasing agents in order to remove all traces of oil, grease and dirt.
Low grade alcohol, gasoline or paint thinners should never be used.
The strongest and most durable joints are obtained by either mechanically abrading or chemically etching ("pickling") the degreased surfaces. Abrading should be followed by a second degreasing treatment

Adhesive Application

The resin/hardener mix is applied with a spatula, to the pretreated and dry joint surfaces.
A layer of adhesive 0.002 to 0.004 in. (0.05 to 0.10mm thick) will normally impart the greatest lap shear strength to the joint.
The joint components should be assembled and clamped as soon as the adhesive has been applied. An even contact pressure throughout the joint area will ensure optimum cure.

Mechanical processing

Specialist firms have developed metering, mixing and spreading equipment that enables the bulk processing of adhesive.
Huntsman Advanced Materials will be pleased to advise customers on the choice of equipment for their particular needs.

Equipment maintenance

All tools should be cleaned with hot water and soap before adhesives residues have had time to cure. The removal of cured residues is a difficult and time-consuming operation.
If solvents such as acetone are used for cleaning, operators should take the appropriate safety precautions and, in addition, avoid skin and eye contact.

Curing times

Temperature	° F (°C)	248 (120)	284 (140)	320 (160)	356 (180)
Cure time	minutes	60	45	20	10
Lap shear strength at 74°F (23 °C)	psi (N/mm^2)	2900 – 3,480 (20-24)	3,625 – 4,060 (25-28)	4,205 – 4,640 (29-32)	4,060 – 4,640 (28-32)

Note: Temperatures below 248°F (120 °C) will not give adequate cure even when cure time is prolonged.
Cure temperatures above 302°F (150 °C) should be avoided when joining materials with different coefficients of linear thermal expansion because stresses will be set up in the bond line upon cooling. This effect is particularly marked where the bond surfaces are large.

Typical cured properties

Unless otherwise stated, the figures given below were determined by testing standard specimens made by lap-jointing 6.6 x 1.0 x 0.06 in.(170 x 25 x 1.5mm) strips of aluminum alloy. The joint area was 0.5 x 1.0 in. (12.5 x 25mm) in each case.
The figures were determined with typical production batches using standard testing methods. They are provided solely as technical information and do not constitute a product specification.

Average lap shear strengths of typical metal-to-metal joints (ISO 4587)

Cured for 45 mins at 302°F (150 °C) and tested at 74°F (23°C)
Pretreatment - Sand blasting

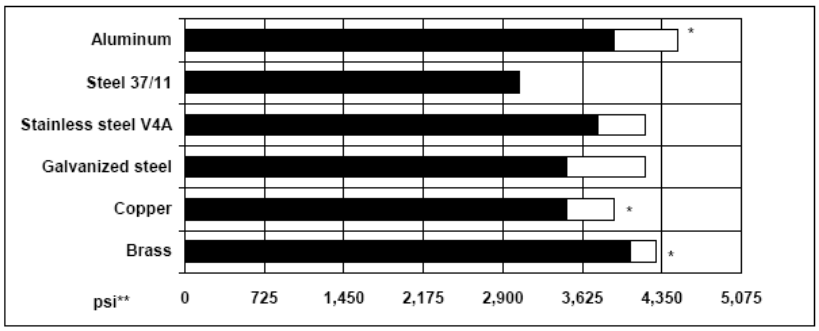

* Failure stress close to elastic limit yield stress of the metal.
** 725 psi = 5 N/mm^2; 1450 psi = 10 N/mm^2; 2,175 psi = 15 N/mm^2; 2,900 psi = 20 N/mm^2; 3,625 psi = 25 $/mm^2$; 4,350 psi = 30 N/mm^2; 5,075 psi = 35 N/mm^2.

Lap shear strength versus temperature (ISO 4587) (typical average values)
Cure: 45 mins at 302°F (150°C)

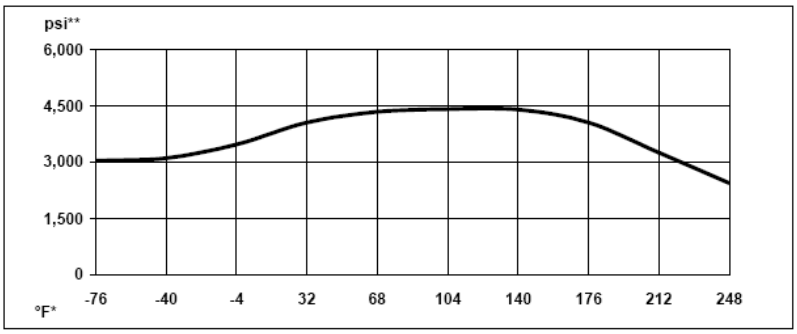

*-76°F = -60°C; -40°F = -40°C; -4°F = -20°C; 32°F = 0°C; 68°F = 20°C; 104°F = 40°C; 140°F = 60°C; 176°F = 80°C; 212°F = 100°C; 248°F = 100°C
** 1,500 psi = 10 N/mm^2; 3,000 psi = 20 N/mm^2; 4,500 psi = 30 N/mm^2; 6,000 psi = 40 N/mm^2

Roller peel test (ISO 4578)
Cured 30 mins at 302°F (150°C), pli (N/mm) 57.1 (10)

Coefficient of thermal expansion (VDE 304),
at 68°F-140°F (20°C-60°C) in./in./°C $57x10^{-6}$
at 68°F-212°F (20°C-100°C) in./in./°C $68x10^{-8}$

Electrolytic corrosion (DIN 53489) Grade A 1

Lap shear strength after 90 days immersion in various media
at 74°F (23°C), Typical average values.

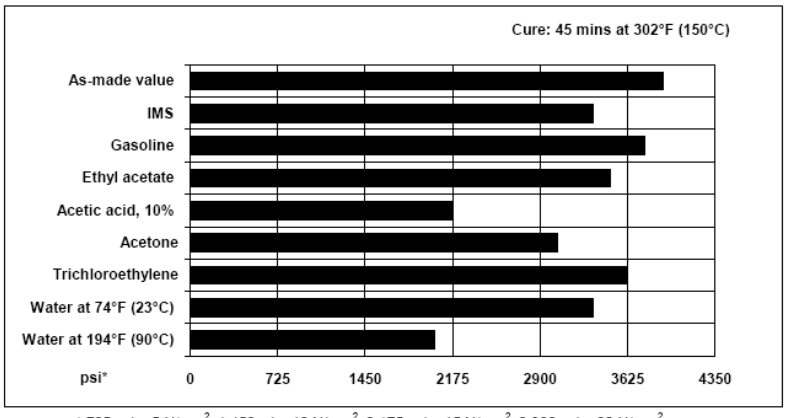

* 725 psi = 5 N/mm^2; 1,450psi = 10 N/mm^2; 2,175 psi = 15 N/mm^2; 2,900 psi = 20 N/mm^2; 3,625 psi = 25 N/mm^2; 4,350 psi = 30 N/mm^2;

Lap shear strength versus tropical weathering (40/92, DIN 50015; typical average values)

Cured: 30 min at 302°F (150°C); Tested at 74°F (23°C)

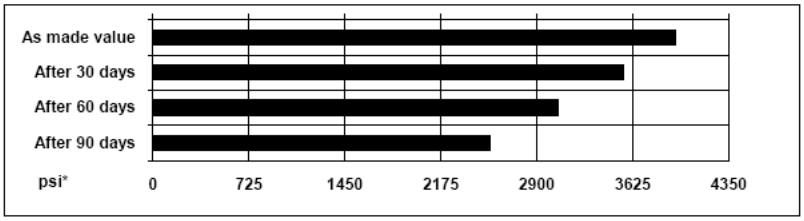

* 725 psi = 5 N/mm^2; 1,450psi = 10 N/mm^2; 2,175 psi = 15 N/mm^2; 2,900 psi = 20 N/mm^2; 3,625 psi = 25 N/mm^2; 4,350 psi = 30 N/mm^2;

Shear modulus (DIN 53445)

Cure:45 min/302°F (150°C), Ksi (GPa)	
77°F (25°C)	174 (1.2)
122°F (50°C)	160 (1.1)
167°F (75°C)	145 (1.0)
212°F (100°C)	102 (0.7)
257°F (125°C)	43.5 (0.3)
302°F (150°C)	1,305 psi (9 MPa)

Electrical Properties

Thermal Conductivity, W/mK	0.21
Surface Resistivity, ohms	4.8 E+13
Dielectric Strength, volt/mil	600
Volume Resistivity, ohms-cm	6.0 E+16
Dielectric Constant, at 50Hz/1KHz/10KHz	4.1/4.2/4.0
Loss Tangent, % at 50Hz/1KHz/10KHz	0.9/0.9/0.9

CAUTION:

Huntsman Advanced Materials Americas Inc. maintains up–to-date Material Safety Data Sheets (MSDS) on all of its products. These sheets contain pertinent information that you may need to protect your employees and customers against any known health or safety hazards associated with our products. Users should review the latest MSDS to determine possible health hazards and appropriate precautions to implement prior to using this material. Copies of the latest MSDS may be requested by calling our customer service group at 800-367-8793 or emailing your request to adhesives_group@huntsman.com.

FIRST AID!

Eyes and skin: Flush eyes with water for 15 minutes. Contact a physician if irritation persists. Wash skin thoroughly with soap and water. Remove and wash contaminated clothing before reuse.
Inhalation: Remove subject to fresh air.
Swallowing: Dilute by giving water to drink and contact a physician promptly. Never give anything to drink to an unconscious person.

KEEP OUT OF REACH OF CHILDREN

FOR PROFESSIONAL AND INDUSTRIAL USE ONLY

IMPORTANT LEGAL NOTICE:

Sales of a referenced product ("Product") are subject to the general terms and conditions of sale of Huntsman Advanced Materials Americas Inc. ("Huntsman").

WARRANTY: Huntsman warrants to the Buyer that the Product will conform to the published specifications for that Product at the time of manufacture, and that the Product will be free from defects in material and workmanship in normal use.

DISCLAIMER AND LIMITATION OF LIABILITY: EXCEPT AS SET FORTH ABOVE, SELLER MAKES NO WARRANTY OR REPRESENTATION, EXPRESS OR IMPLIED, INCLUDING WARRANTIES OF MERCHANTABILITY AND FITNESS FOR A PARTICULAR PURPOSE. Huntsman cannot control Buyer's application and use of the Product and accepts no responsibility therefore. No statement or recommendation contained in any Product literature may be construed as a representation about the suitability of a Product for the particular application of Buyer or user or as an inducement to infringe any relevant patent. Buyer is responsible to ensure that its intended use of the Product does not infringe any third-party's intellectual property rights. Seller neither assumes, nor authorizes any representative or other person to assume for it, any obligation or liability other than as is expressly set forth herein. UNDER NO CIRCUMSTANCES SHALL HUNTSMAN BE LIABLE FOR INCIDENTAL, CONSEQUENTIAL, SPECIAL OR OTHER INDIRECT DAMAGES AS A RESULT OF A BREACH OF ANY WARRANTY OR THE FAILURE OF A PRODUCT OR ANY CLAIM THAT IS ESSENTIALLY BASED UPON SUCH BREACH OR FAILURE. Any claim by Buyer, whether arising in contract, tort, negligence, breach of warranty, strict liability, or otherwise, related to a Product shall be limited to, and the sole liability of Seller and the sole remedy of Buyer for any claims shall be for, the purchase price of the Product in respect of which such claim is made. The foregoing DISCLAIMER and LIMITATION OF LIABILITY supercedes Buyer's documents.

WARNING: Technical data and results are based upon tests under controlled laboratory conditions and must be confirmed by Buyer by testing for its intended conditions of use. The Product has not been tested for, and therefore is not recommended or suitable for, uses for which prolonged contact with mucous membranes, abraded skin, or blood is intended or likely, or for uses for which implantation within the human body is intended, and Huntsman assumes no liability for any such uses.

Annex C – AV 118 Manufacture Data Sheet

HUNTSMAN

Structural Adhesives

Aerospace Adhesives
Araldite® 420 A/B
Two component epoxy adhesive

Key properties

- **Very high shear and peel strength**
- **Extremely tough and resilient**
- **Good moisture resistance**
- **Bonds a wide variety of materials including metal, wood, rubber, glass fibre reinforced composites and many plastics**

Description

Araldite 420 A/B is a two-component, room temperature curing paste adhesive of high strength and toughness.
It is suitable for a wide variety of metal, honeycomb and fibre reinforced composite bonding applications. It has very high shear strength even at temperatures up to 70°C and good peel strength.
Typical uses include:
- Bonding inserts, ferrules, aluminium and composite edge members, joining strips, etc, in both metallic and non-metallic honeycomb sandwich structures.
- Fabrication of composite components using the cut and fold technique.

Typical product data

Property	Araldite 420 A	Araldite 420 B	Mixed adhesive	Test Method
Colour (visual)	yellow	blue	dark green	visual
Specific gravity	ca.1.2	ca.1.0	1.1 - 1.2	ASTM-D-792
Viscosity at 25ºC (Pas)	100 - 300	0.6 - 1.4	35 - 45	ASTM-D-2196
Gel time (100 gm at 25°C) mins	-	-	60	ASTM-D-2471

Processing

Pretreatment
The strength and durability of a bonded joint are dependant on proper treatment of the surfaces to be bonded.
At the very least, joint surfaces should be cleaned with a good degreasing agent such as acetone or other proprietary degreasing agents in order to remove all traces of oil, grease and dirt. Alcohol, gasoline (petrol) or paint thinners should never be used.
The strongest and most durable joints are obtained by either mechanically abrading or chemically etching ("pickling") the degreased surfaces. Abrading should be followed by a second degreasing treatment.

Mix ratio	Parts by weight	Parts by volume
Araldite 420 A	100	100
Araldite 420 B	40	50

Stir the two components thoroughly together until the two colours are completely blended, without any visible streaks. Automatic mixing / dispensing may be used.

Araldite 420 A/B is also supplied in cartridges incorporating mixers and can be applied as ready to use adhesive with the aid of the tool recommended by Huntsman Advanced Materials.

Usable life
Due to exothermic reaction between the two components the usable life depends to some extent on the quantity mixed and the shape of the container. Use of a shallow container will extend the usable life and as a rough guide:
For a 50gm mix, usable life at 25°C is 2 hours
For a 100gm mix, usable life at 25°C is 1 hour

Application of adhesive
The resin/hardener mix is applied directly or with a spatula to the pretreated and dry joint surfaces.
A layer of adhesive 0.05 to 0.10 mm thick will normally impart the greatest lap shear strength to the joint.
The joint components should be assembled and clamped as soon as the adhesive has been applied. An even contact pressure throughout the joint area will ensure optimum cure.

Curing
Once applied, Araldite 420 A/B will gel in 3 - 4 hours at 25°C and will be sufficiently cured after 5 hours to allow the bonded component to be handled. After 4 - 5 days the adhesive will obtain 90% of its full strength and achieve full strength after 1 to 2 weeks at room temperature.

Cure can be accelerated by heating. 4 hours at 50°C or 1 hour at 120°C will be sufficient to achieve full strength.

Shear properties can be improved, particularly at elevated temperatures, by post-curing for up to 24 hours at 70°C.

Lap shear strength after various cure times at 23°C
5 hours: 1 N/mm²
6 hours: 8 N/mm²
7 hours: 9 N/mm²

Typical cured properties

These figures are for guidance and do not constitute a specification.

Bell peel 150 N/25mm (60°C peel using 2024-T3 clad aluminium adherents at 25°C).

Honeycomb bonding results (in accordance with MIL-A-25463)
Beam shear at 22°C: 12kN (core failure); Flatwise tensile at 22°C: 8.5 N/mm^2
Metal: 2024 - T3; Core: 7.9 - ¼ - 40 5052

Variation of lap shear strength as a function of temperature

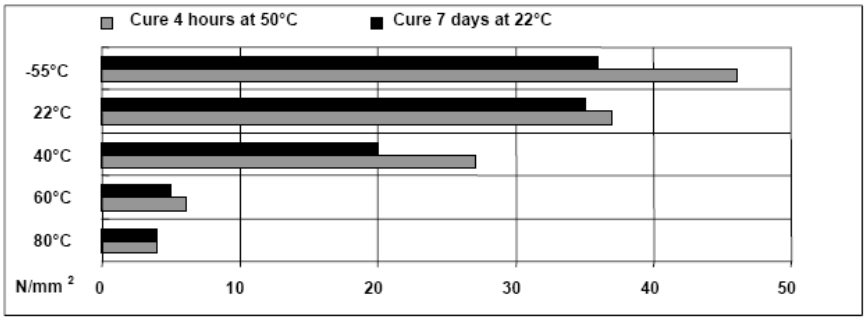

Lap shear strength: variation after exposure to 95% RH at 60°C
(cured 7 days at 23°C)
C = 30 days exposure
A = 90 days + drying for 16 hours at 60°
B = 90 days exposure

Variation of lap shear strength as a function of temperature

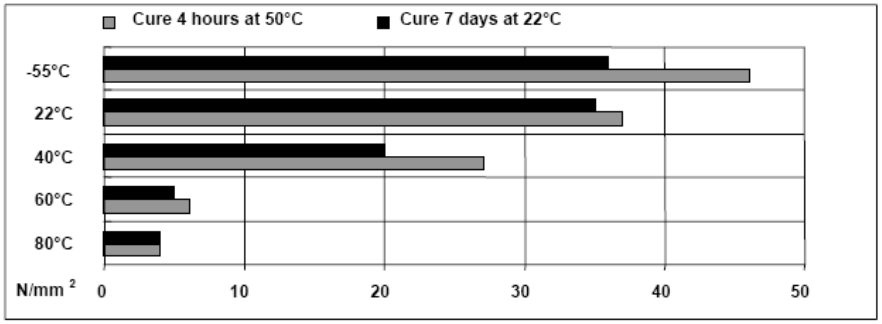

Lap shear strength: variation after exposure to 95% RH at 60°C
(cured 7 days at 23°C)
C = 30 days exposure
A = 90 days + drying for 16 hours at 60°
B = 90 days exposure

Effects of alternative cure schedules on lap shear strength performance (LSS)

Test	**Results**		**Test methods**
Cure cycle	**Test temp (°C)**	**LSS (MPa)**	
70°C for 1 hour	22	37	A.E.C.M.A. EN2243-1
	70	4	
2 hours	70	6	
6 hours	70	11	
16 hours	70	10	
24 hours	70	8	
120°C for 1 hour	22	43	A.E.C.M.A. EN2243-1
	50	29	
	70	10	

Storage

Araldite 420 A/B may be stored for up to 36 months at 2-40°C, provided that the components are stored in their original sealed containers. The expiry date is indicated on the label.

Handling precautions	**Caution** Our products are generally quite harmless to handle provided that certain precautions normally taken when handling chemicals are observed. The uncured materials must not, for instance, be allowed to come into contact with foodstuffs or food utensils, and measures should be taken to prevent the uncured materials from coming in contact with the skin, since people with particularly sensitive skin may be affected. The wearing of impervious rubber or plastic gloves will normally be necessary; likewise the use of eye protection. The skin should be thoroughly cleansed at the end of each working period by washing with soap and warm water. The use of solvents is to be avoided. Disposable paper - not cloth towels - should be used to dry the skin. Adequate ventilation of the working area is recommended. These precautions are described in greater detail in the Material Safety Data sheets for the individual products and should be referred to for fuller information.

Huntsman Advanced Materials

Duxford, Cambridge
England CB2 4QA

Tel: +44 (0) 1223 832121
Fax: +44 (0) 1223 493322
www.araldite.com

Annex D - Procedure for the Preparation of the Adhesive Bulk Mould

1) Dismantle the mould with the help of a hexagonal key.

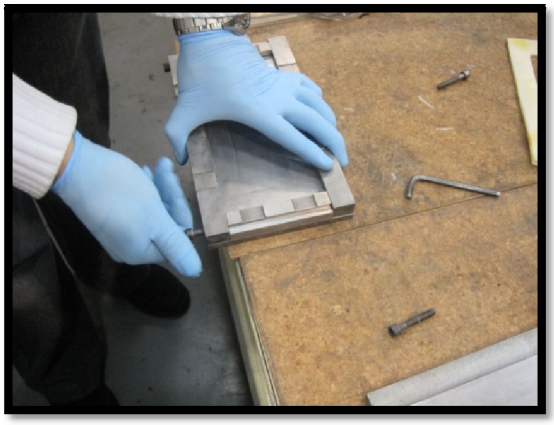

Figure D 1 – Mould dismantle.

2) Remove all adhesive remnants with the aid of an aluminum scraper or sandpaper.

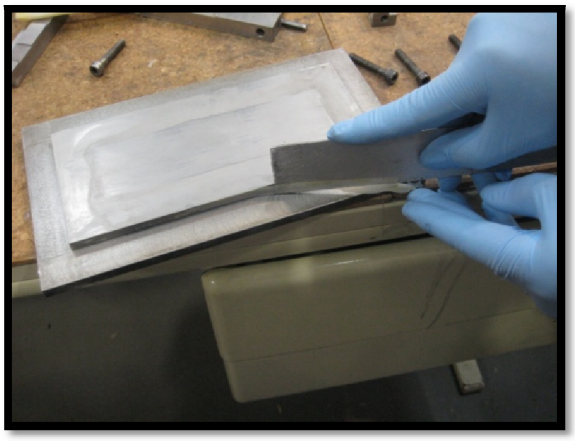

Figure D 2 – Adhesive removal.

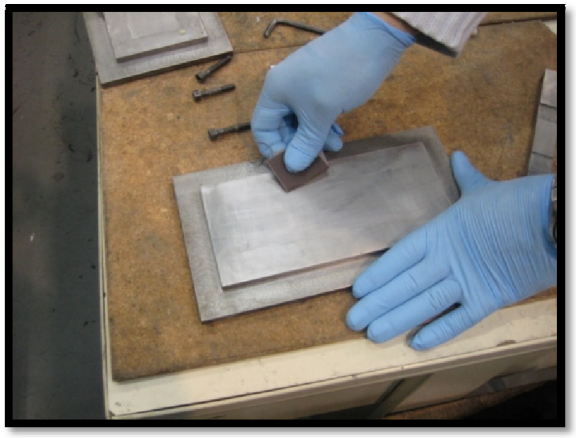

Figure D 3 – Adhesive removal with sandpaper.

3) Sand and clean with acetone all parts of the mould that are in contact with the adhesive, cleaning the mould release agent in the mould.

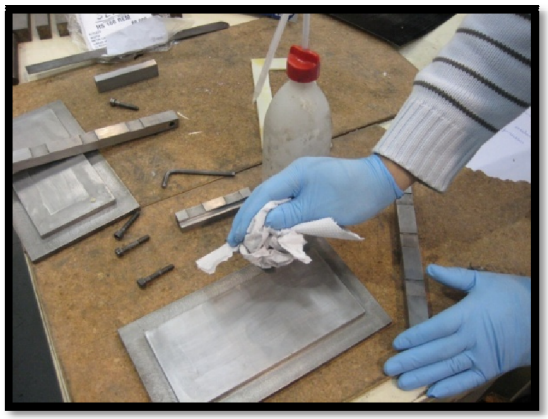

Figure D 4 – Acetone mould cleaning.

4) Heat the mould parts at 50°C for approximately 10 minutes.

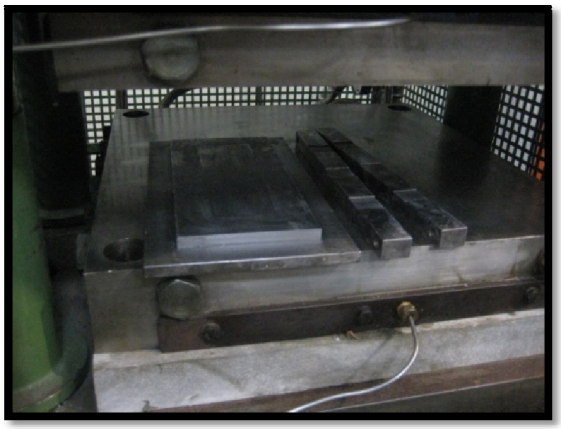

Figure D 5 – Mould parts heating.

5) Apply the mould release agent on the surfaces in contact with the adhesive. The toxicity of the mould release agent should be remembered and any application with the mould release agent should be done with the air suction on and with the suction devices always below the user head level.

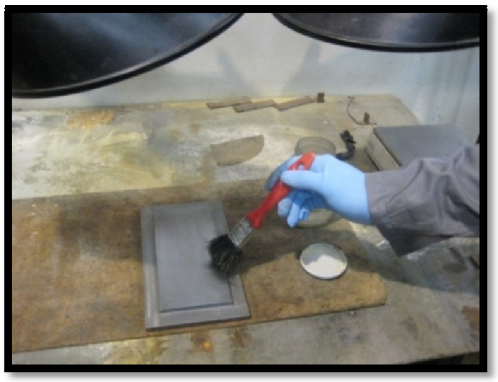

Figure D 6 – Mould release agent application.

6) Repeat steps four and five at least one time.

7) Assemble the mould with the help of a hexagonal key.

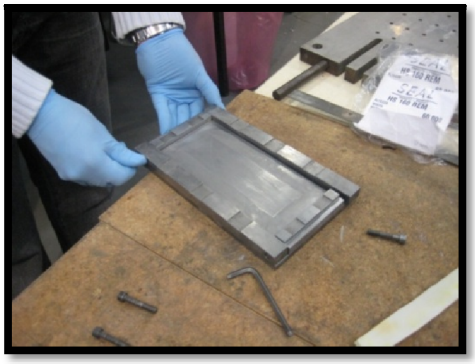

Figure D 7 – Mould assembly.

8) Place the silicone frame into the mould, taking care that the frame is perfectly seated in the mould base.

Figure D 8 –Silicone frame placement.

Annex E - Bulk Procedure

1) It is necessary to obtain the density/specific gravity of the adhesive, through the manufacturer catalog.

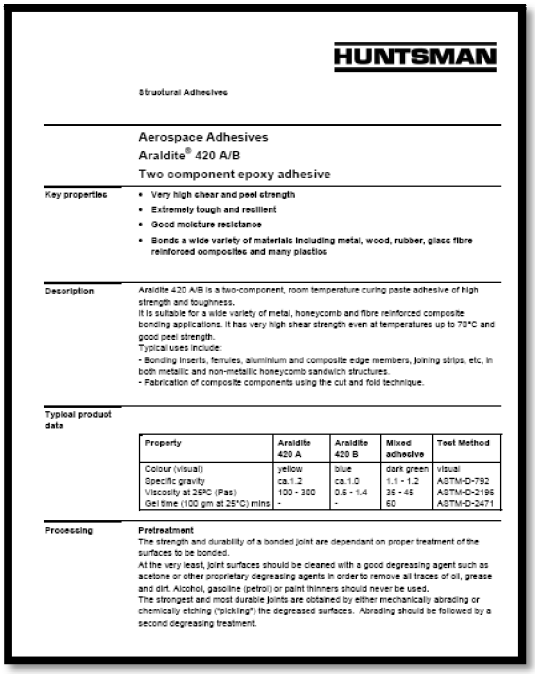

HUNTSMAN

Structural Adhesives

Aerospace Adhesives
Araldite® 420 A/B
Two component epoxy adhesive

Key properties

- Very high shear and peel strength
- Extremely tough and resilient
- Good moisture resistance
- Bonds a wide variety of materials including metal, wood, rubber, glass fibre reinforced composites and many plastics

Description

Araldite 420 A/B is a two-component, room temperature curing paste adhesive of high strength and toughness.
It is suitable for a wide variety of metal, honeycomb and fibre reinforced composite bonding applications. It has very high shear strength even at temperatures up to 79°C and good peel strength.
Typical uses include:
- Bonding inserts, ferrules, aluminium and composite edge members, joining strips, etc. in both metallic and non-metallic honeycomb sandwich structures.
- Fabrication of composite components using the cut and fold technique.

Typical product data

Property	Araldite 420 A	Araldite 420 B	Mixed adhesive	Test Method
Colour (visual)	yellow	blue	dark green	visual
Specific gravity	ca.1.2	ca.1.0	1.1 - 1.2	ASTM-D-792
Viscosity at 25ºC (Pas)	100 - 300	0.6 - 1.4	35 - 45	ASTM-D-2196
Gel time (100 gm at 25°C) mins	-	-	60	ASTM-D-2471

Processing

Pretreatment
The strength and durability of a bonded joint are dependant on proper treatment of the surfaces to be bonded.
At the very least, joint surfaces should be cleaned with a good degreasing agent such as acetone or other proprietary degreasing agents in order to remove all traces of oil, grease and dirt. Alcohol, gasoline (petrol) or paint thinners should never be used.
The strongest and most durable joints are obtained by either mechanically abrading or chemically etching ("pickling") the degreased surfaces. Abrading should be followed by a second degreasing treatment.

Figure E 1 – Manufacturer data sheet.

2) After the adhesive density is obtained, it is required to calculate the adhesive volume necessary to fill the mould.

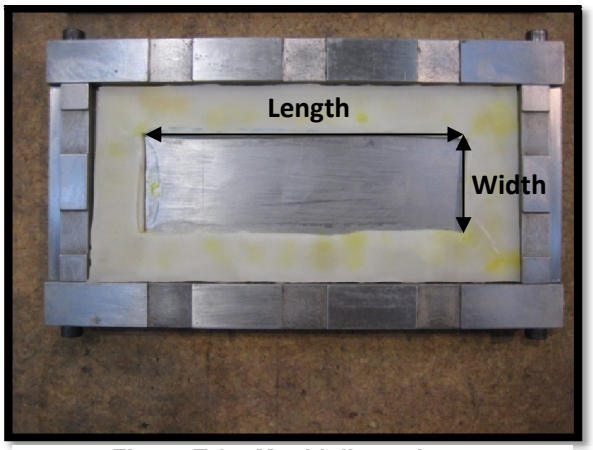

Figure E 2 – Mould dimensions.

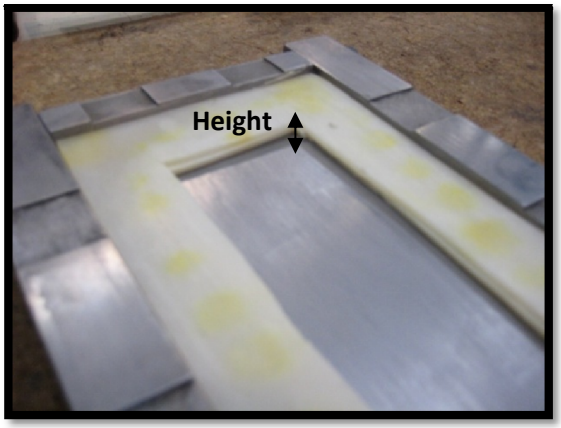

Figure E 3 - Mould height.

The volume is given by:

$$V_{mould} = Lenght * Width * Heigth \qquad [m^3]$$

3) With the volume known, the adhesive mass can be calculated by:

$$\rho_{adhesive} = \frac{m_{adhesive}}{V_{mould}} \ [kg/m^3]$$

Manipulating the expression we obtained:

$$m_{adhesive} = \rho_{adhesive} * V_{mould} \qquad [kg]$$

The adhesive mass has to be approximately 5% more that the calculated previous, due to measurement deviations.

4) Place in the scale a clock glass.

Figure E 4 – Clock glass in scale.

5) Tare the scale with the clock glass on.

Figure E 5 – Scale taring.

6) Slowly add the adhesive mass previously calculated using a spatula.

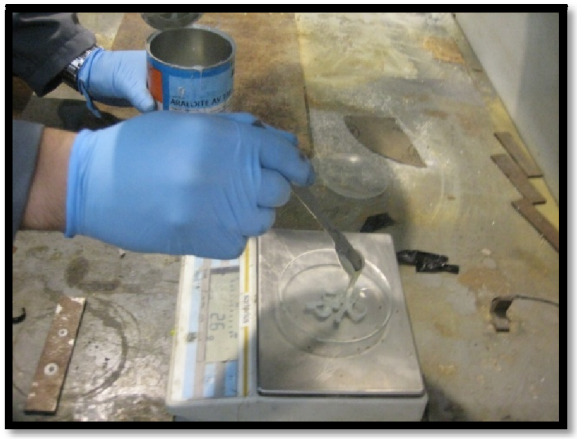

Figure E 6 – Adding adhesive to the scale.

Figure E 7 - Adhesive weighting.

7) Put the adhesive in the mould with a spatula, having in attention the amount of adhesive that is retained in the spatula and the clock glass.

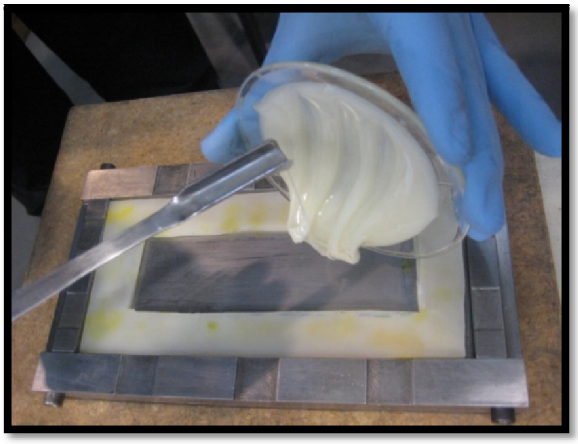

Figure E 8 –Adhesive application into the mould.

8) Place the top mould part carefully so that the adhesive remains in the mould.

Figure E 9 – Closed mould.

9) Place the mould in the press.

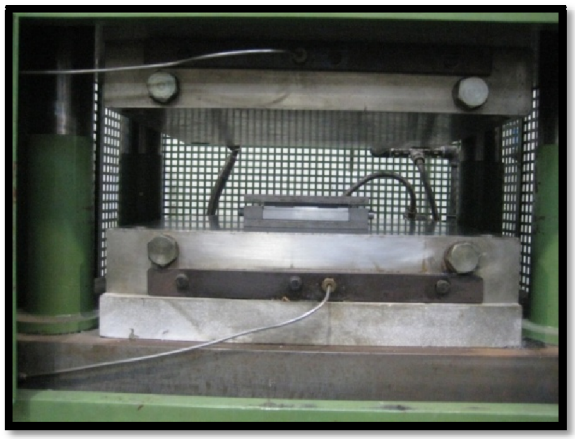

Figure E 10 – Mould in press.

10) Apply the adhesive cure cycle.

Figure E 11 – Adhesive tin.

11) After finishing the cure cycle, cool the mould with the use of water, opening the tap in the wall.

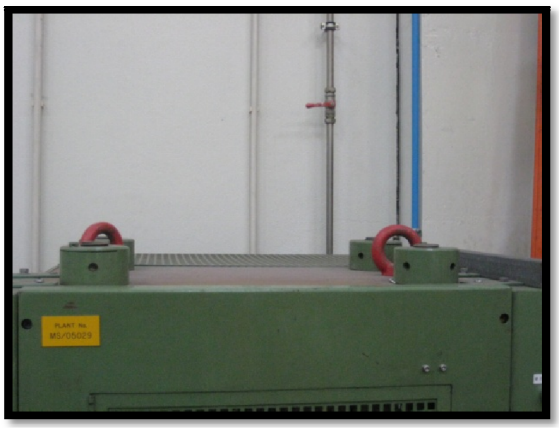

Figure E 12 – Cooling water tap.

12) Remove the mould from the press and with the help of a hexagonal key remove the top mould plate.

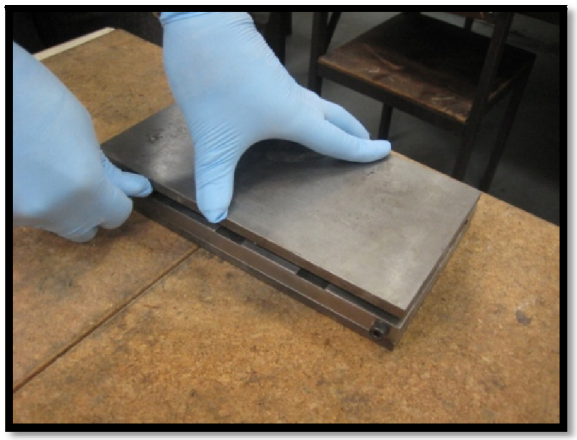

Figure E 13 – Opening of the mould.

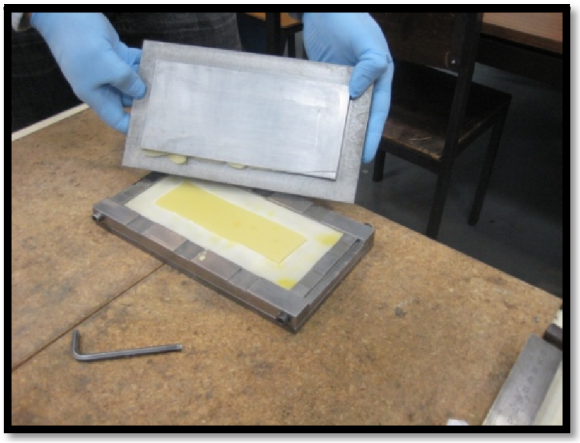

Figure E 14 – Removing the top plate.

13) Disassemble the mould with the help of a hexagonal key.

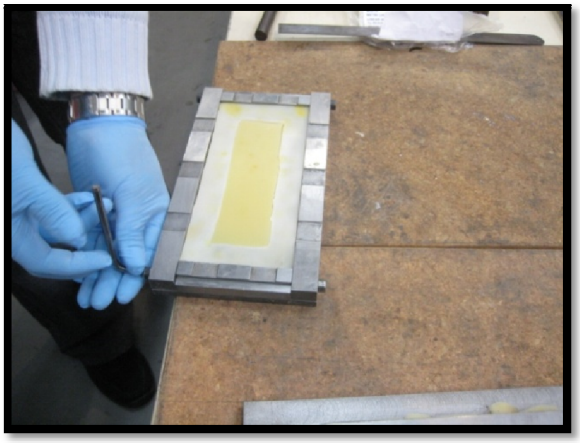

Figure E 15 – Mould disassembly.

14) Remove the silicone frame.

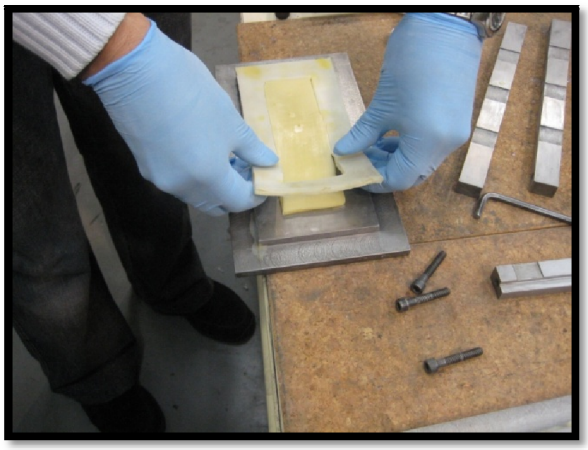

Figure E 16 –Silicone frame removal.

15) Remove the adhesive plate.

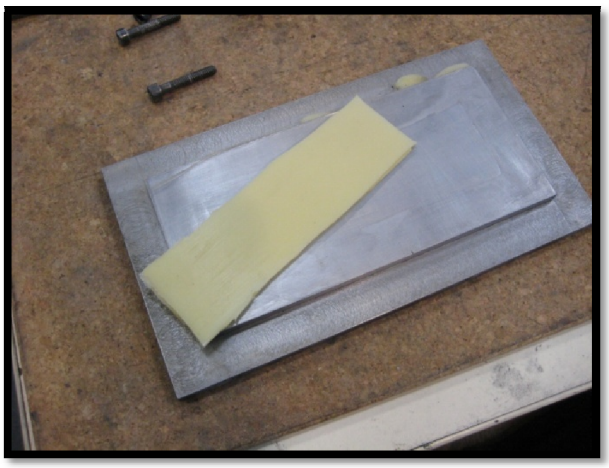

Figure E 17 – Completed adhesive plate removal.

16) Wrap the adhesive plate in aluminium foil and put the plate in the desiccator, avoiding that the adhesive properties change with the contact with the air humidity.

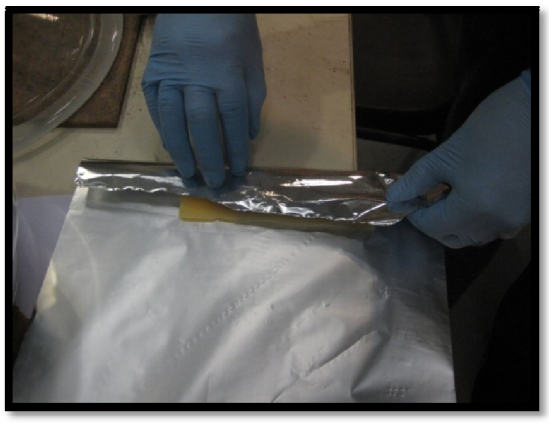

Figure E 18 –Wrapping the adhesive pate in aluminium foil.

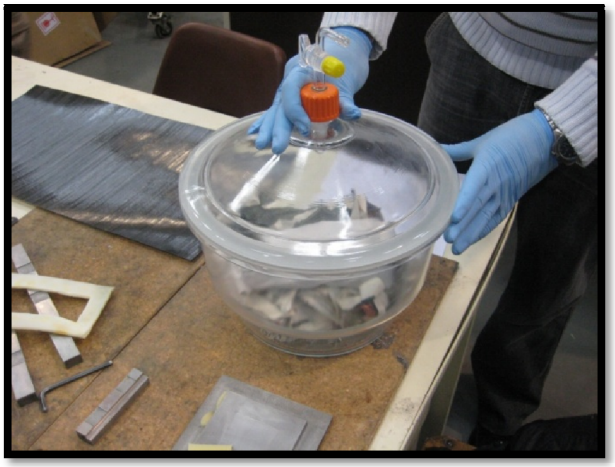

Figure E 19 - Storing the adhesive plate.

17) Finally the plate is sent to the workshop to be machined.

Figure E 20 - Bulk specimen completed.

Annex F - SLJ Procedure

1) Ensure that the mould has a mould release agent layer thick enough to avoid bonding between the specimen and the mould (glossy surfaces indicate that they no longer have mould release agent).

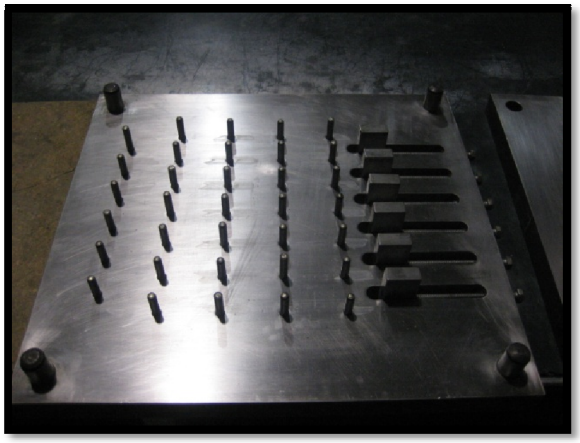

Figure F 1- SLJ bottom base.

2) Apply the surface treatment to the overlap length and wedges. This treatment can be sanding, etching or other.

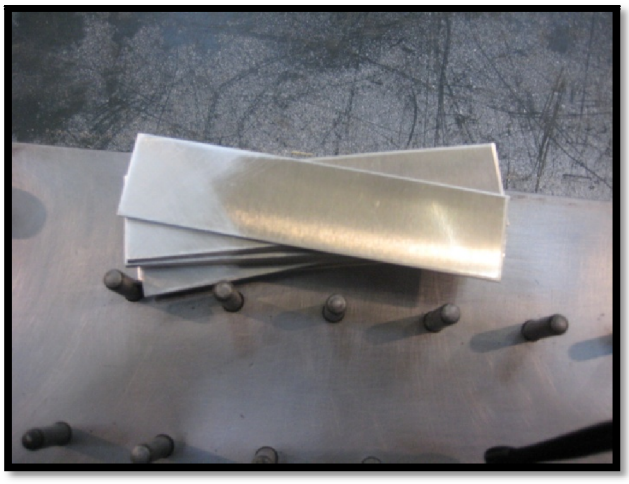

Figure F 2 – Sanded aluminium adherends.

Figure F 3 – Adherends etching process.

3) Place the tab ends, adherends and spacers in the mould.

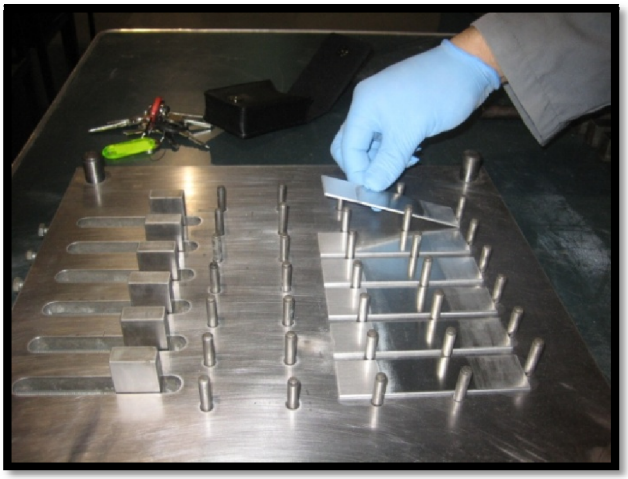

Figure F 4 – Adherends placement.

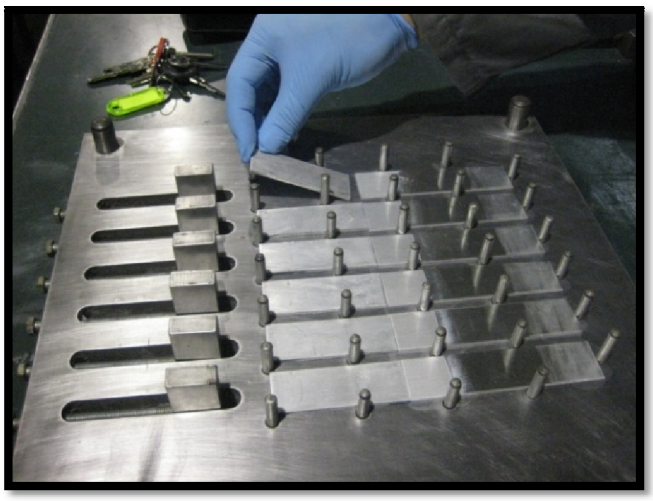

Figure F 5 – Spacers placement.

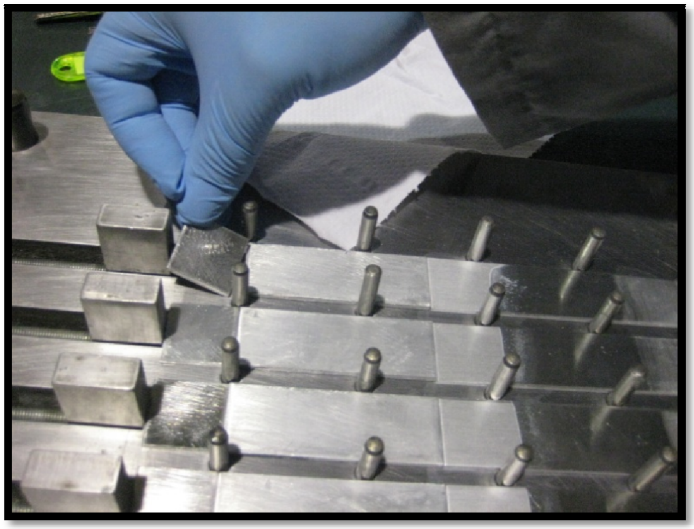

Figure F 6 – Tab ends placement.

4) Weight and mix the adhesive, if necessary.

Figure F 7 – Adhesive weighting.

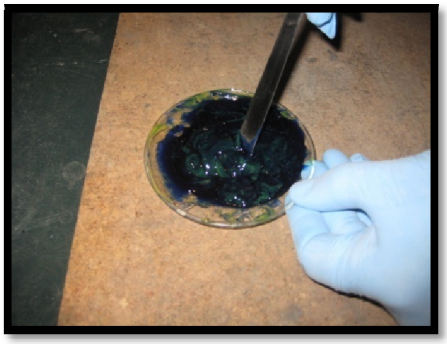

Figure F 8 –Adhesive mixture.

5) Place a generous adhesive quantity in the middle of the overlap length and in the middle of the tab ends bonding area. Do this with the help of a spatula.

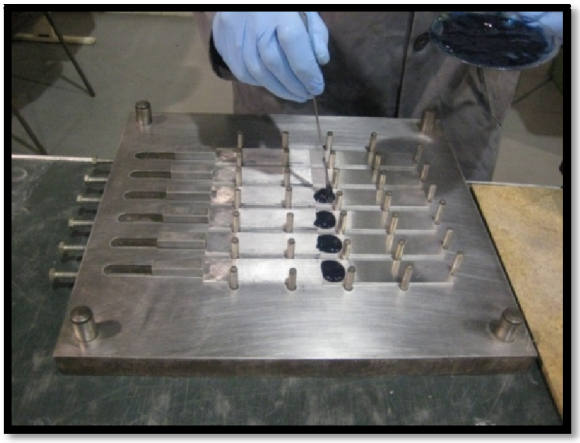

Figure F 9 – Adhesive application.

6) Place the remaining adherends, spacers and tab ends.

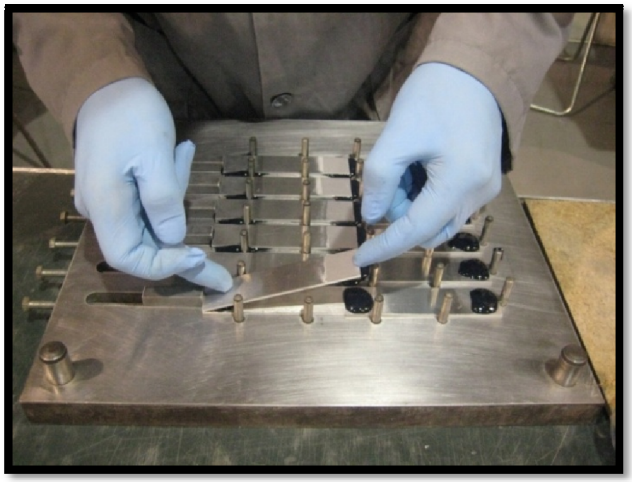

Figure F 10 – Adherends placement.

Figure F 11 - Tab ends placement.

7) Place the top mould base.

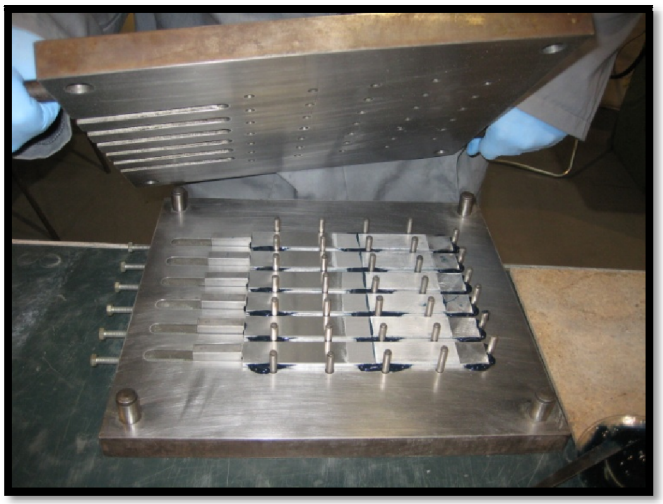

Figure F 12 – Top base placement.

8) After the adhesive cure cycle is completed, remove the top mould base and the pins from the bottom mould base to easily remove the specimens.

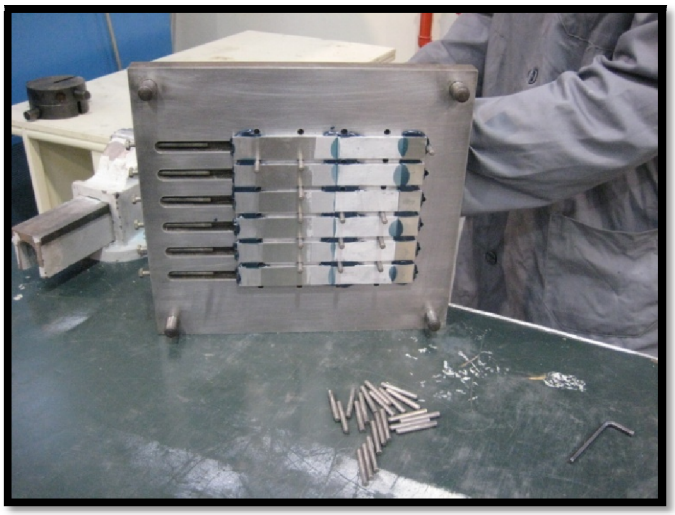

Figure F 13 – Mould pin removal.

9) After removing the specimens, put the pins back in the bottom base with the help of the hammer.

Figure F 14 –Mould pin replacement.

10) The specimens are generally bonded together. It is necessary to separate them with a fine saw.

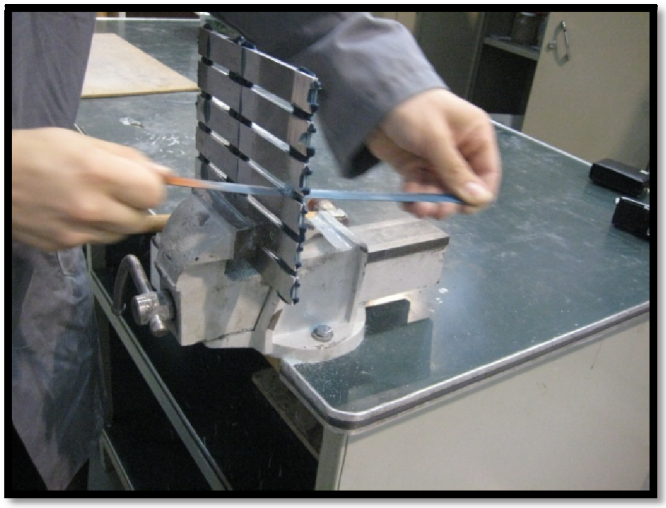

Figure F 15 – Specimens separation.

11) After all the specimens are separated, the adhesive excess must be removed. Remove most of the adhesive with a large woodworking file and when close to the adherends use a smaller woodworking file.

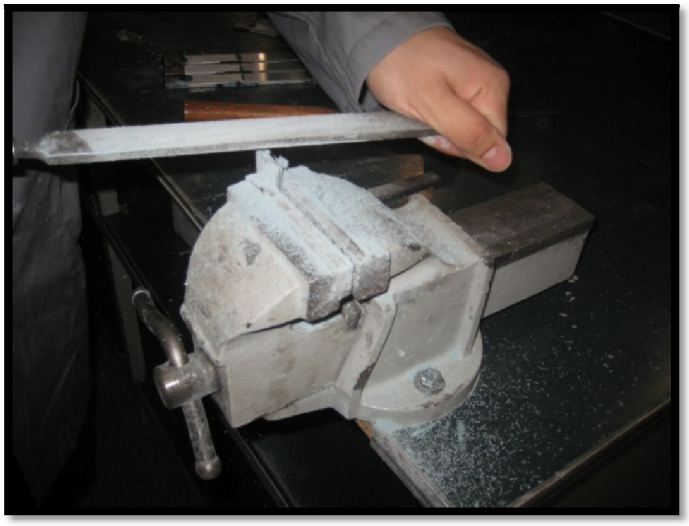

Figure F 16 – Adhesive removal with a large woodworking file.

Figure F 17 - Adhesive removal with a small woodworking file.

12) Remove the spacers.

Figure F 18 – Spacers removal.

13) Sand the areas were the test machine will hold.

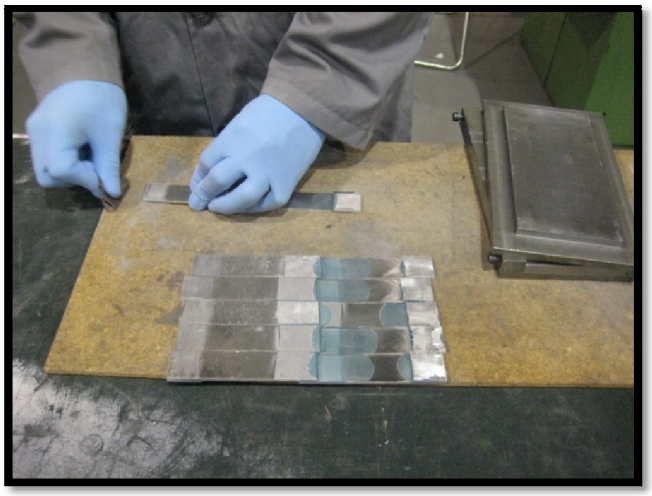

Figure F 19 – Tab ends sanding.

14) Wrap the adhesive plate in aluminium foil and put the plate in the desiccator, avoiding the change of adhesive properties from contact with air humidity.

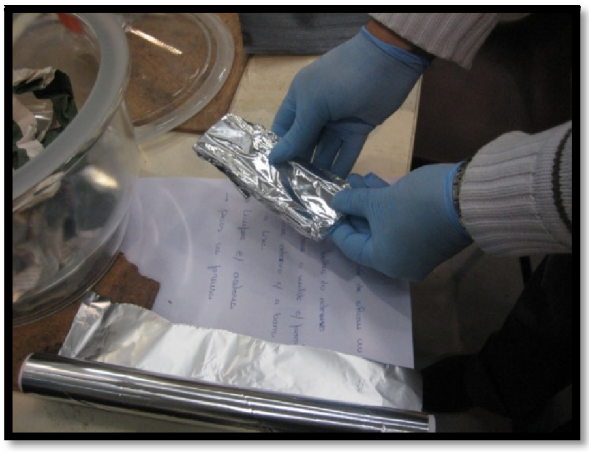

Figure F 20 – Specimens aluminium foil wrapping.

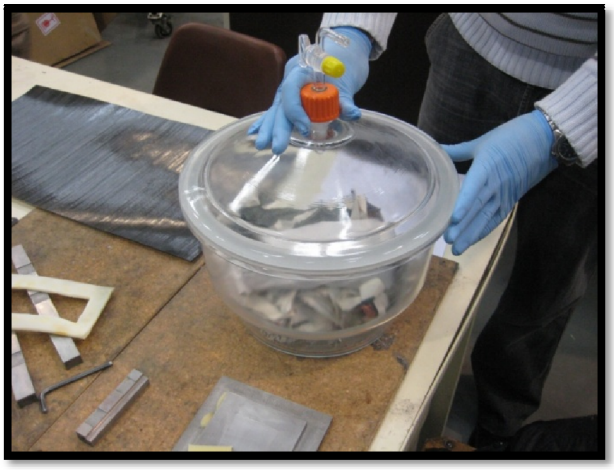

Figure F 21 - Desiccator

Annex G - Chromic acid etching procedure

1) Fill a glass vat with chromic acid.

Figure G 1 – Glass tin with chromic acid.

2) Heat the acid up to about 70 °C.

Figure G 2 – Acid heating process.

3) Make a support with adhesive tape and make a hole in the middle.

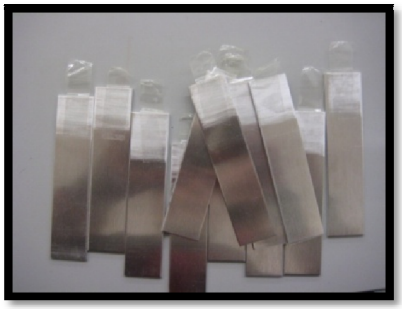

Figure G 3 – Adherends with adhesive support tape.

Figure G 4 – Hole making process for adhesive support.

4) Hang the adherends equally spaced in the support bar.

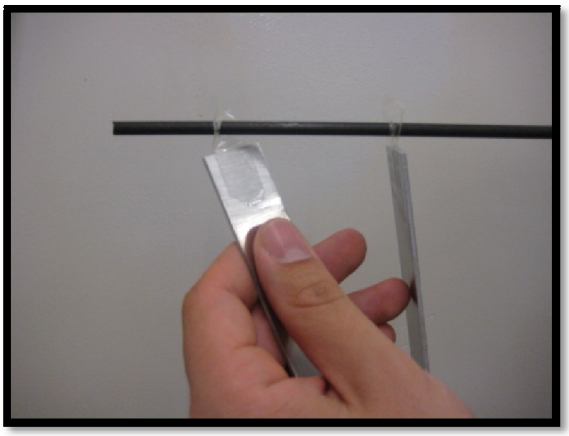

Figure G 5 – Adherends hanging.

5) Put the adherends in the acid for approximately 15 minutes.

Figure G 6 –Etching process.

6) Clean the acid from the adherends with tap water.

Figure G 7 – Adherends acid cleaning.

7) Remove the adhesive tape supports of the adherends.

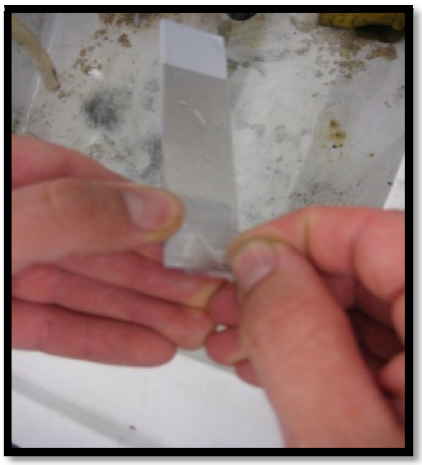

Figure G 8 – Adhesive tape removal.

8) Clean the adherends overlap length with distilled water, ensuring a complete cleaning of the adherends surfaces.

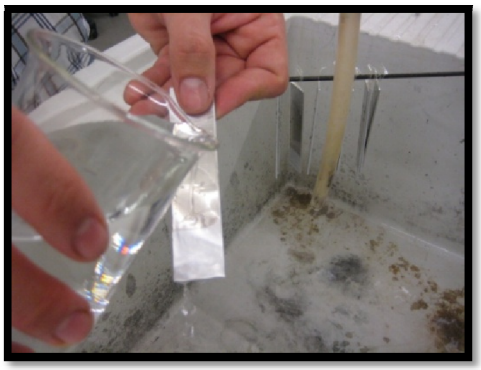

Figure G 9 – Adherends cleaning with distilled water.

9) Dry the adherends with a hair dryer to avoid contamination of the surfaces with paper or cloth remains.

Figure G 10 – Adherends drying.